CHAPTER 8
Geotechnical Observations

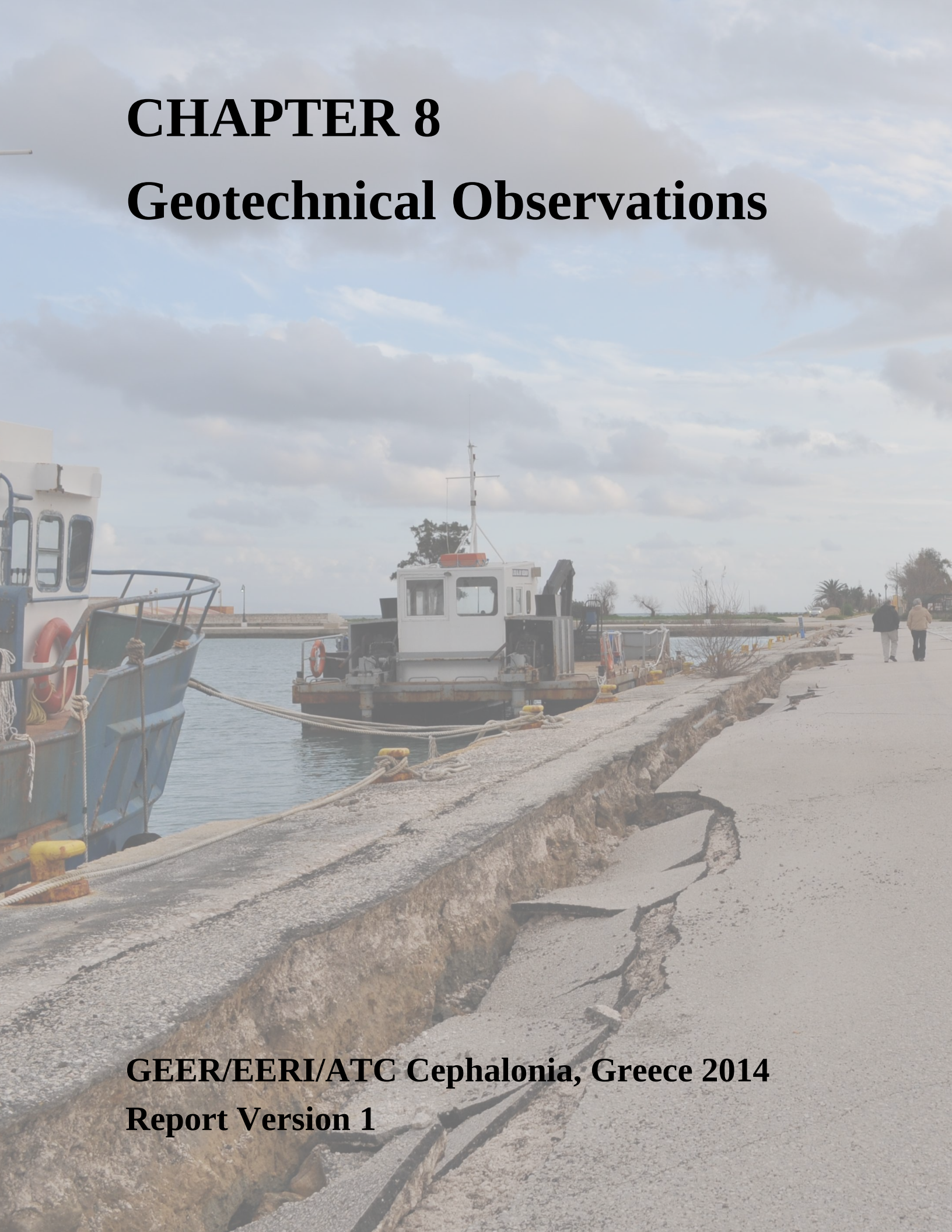

GEER/EERI/ATC Cephalonia, Greece 2014

Report Version 1

8.1 Site Effects

INTRODUCTION

Site effects, including both soil amplification and topography effects, are hypothesized to have played a significant role in the unusually high ground motion amplitudes recorded during the two main Cephalonia events of January 26th with magnitude M_w 6.1 and February 3rd with M_w 6.0. The exceptionally large recorded ground motion amplitudes and the concentration of earthquake-induced phenomena on both soils and structures in areas of thick young Holocene alluvial deposits of poor mechanical soil properties are indicative of ground motion amplification due to site effects. Moreover, the hypothesis of topographic amplification is consistent with the presence of pronounced irregular topographic features in the immediate vicinity of some stations. However, neither hypotheses can be verified at this point due to lack of geophysical site characterization data and high-resolution Digital Elevation Models (DEM).

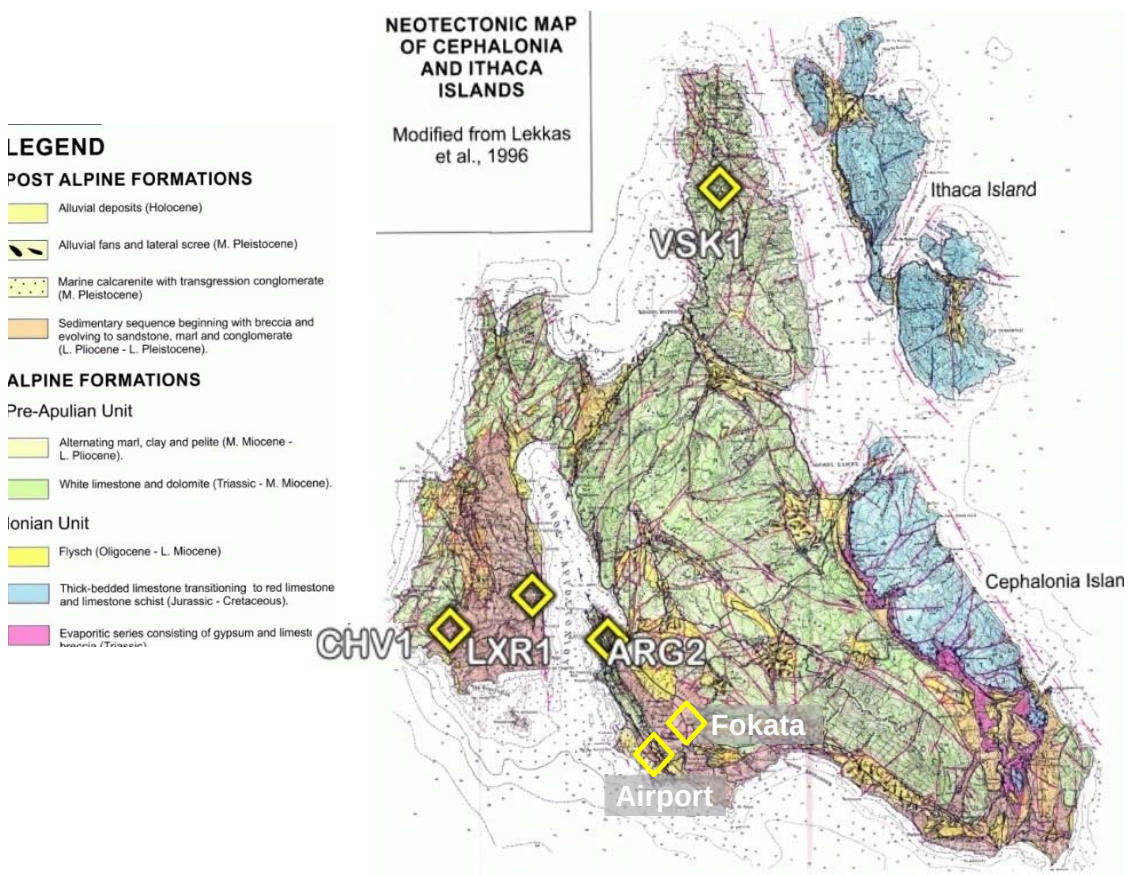

Figure 8.1.1 Strong motion stations referenced in this section (LXR1, ARG2 and CHV1) on the Cephalonia neotectonic map (modified from Lekkas et al., 1996).

Historically, site effects have played a significant role on losses caused by past earthquakes. As described in Papathanassiou et al. (2005), ground failures and liquefaction-induced port facility damages have repeatedly occurred in most of previous earthquakes. For example, the 1867 earthquake triggered liquefaction resulting in a subsidence of 1 m width and 100 m length along the waterfront of Lixouri. At the Kouvalata village, there were observations of sand craters and ejecta while in the village of Aghios Dimitrios, a sand crater with 1 m diameter and 0.5 m high was reported (Vergotis, 1867; Partsch, 1892). Liquefaction and lateral spreading were major factors in the destruction caused by the 1953 earthquake sequence at the ports of Lixouri and Argostoli (as described in Chapters 2 and 5), with similarities to the observations documented in the 2014 events (described in Section 8.2).

STRONG GROUND MOTION RECORDING STATIONS

Strong ground motion stations referenced in this section are depicted on the neotectonic map of Cephalonia of Fig. 8.1.1 and discussed in Chapter 7. Limited geotechnical information was available during reconnaissance in the immediate vicinity of the stations that could verify site effect observations and hypotheses. Therefore, discussions on site effects will mainly focus on the recording stations of LXR1, ARG2 and CHV1 of EPPO-ITSAK in the towns of Lixouri, Argostoli, and Chavriata. All three stations are within the same Triassic geologic zone (Fig. 8.1.1). As a result, their underlying profiles and site response characteristics may bare similarities indicative of site amplification effects. Additional recordings became available from UPATRAS and Prof. Pelekis of ASPETE that installed strong ground motion instruments following the 1st event at the Argostoli Port, Fokata, and Airport (Fig. 8.1.1). The few examples presented herein merit further studies incorporating in-situ subsurface investigations due to their significance in advancing our understanding of site effects.

SITE AMPLIFICATION

Despite their (misleading) moderate magnitudes on the order of $M_w \sim 6$ that could also indicate moderate ground motion levels, the Cephalonia events yielded exceptionally large amplitudes of ground motion. To illustrate this fact, Figure 8.1.2 compares response spectra of these recordings (LXR1 and CHV1) from the 2nd event with $M_w = 6$ and both at epicentral distances not more than 1 to 2 km away from the intersection of the fault with the ground surface, to those recorded by the Kobe 1995 (M_w 6.9) Takatori and the Northridge 1994 (M_w

6.7) Rinaldi stations (Gazetas, 1996). All four records have similar magnitude-distance (M-R) combination; yet, as shown on Fig. 8.1.2, their response spectra are quite different indicating possible influence of local site effects. Note that the Takatori and Rinaldi records are among the very few near-field 'impulsive-type' recordings (Garini et al., 2014), which are invaluable design-level motions for structural analyses and design of critical infrastructure.

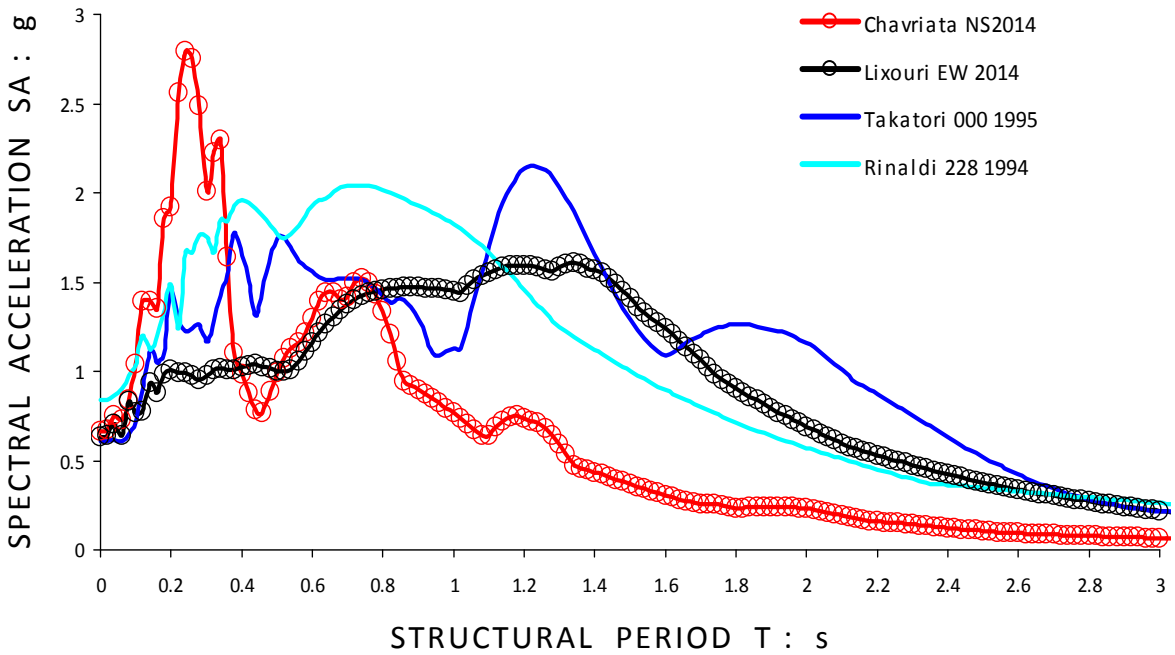

Figure 8.1.2 Response spectra (5% damping) of two of the strongest records obtained during the 2nd Cephalonia event, compared to two of the most widely referenced near-field strong motion records of Takatori and Rinaldi from the Kobe 1995 and Northridge 1994 earthquakes.

Available seismological and geological data that has been presented in preceding chapters indicates possible forward directivity effects on the fault normal (EW) component of the LXR1 station (in Lixouri) recorded 2nd event, with a Peak Ground Acceleration (PGA) of 0.68 g (Fig. 8.1.2) . The fault parallel (NS) component of the same recording, on the other hand, was not characterized by the same long period impulsive motion, although it had comparably large amplitude with PGA of 0.61 g.

Lixouri LXR1 Station Recordings

We examined the influence of local site effects from the LXR1 station recordings of the 2nd event using available nearby subsurface information, including: (i) a geotechnical investigation at the nearby Lixouri port conducted shortly after the 2nd earthquake to assist with the port repairs (Fig. 8.1.3) funded by the Ministry of Public Works, Port Division (Geosymvouloi EPE, 2014) and (ii) a shear wave velocity, V_s , profile (Fig. 8.1.4) measured previously in-situ by Spectral Analysis of Surface Waves (SASW) as part of a European research project (Pelekis, 2014). The generalized soil profile based on the port investigation consists of 5 to 20 m thick deposits of poor quality sandy silts and low plasticity clays. The representative V_s profile of Fig. 8.1.4 has an estimated elastic fundamental frequency of around 7 Hz, or 0.14 s (Fig. 8.1.5a).

Horizontal to Vertical Spectral Ratios (HVSR) of the LXR1 recordings were calculated based on the algorithm described by Theodulidis et al. (1996) and are shown on Figure 8.1.5b. The HVSR showed similar amplification characteristics in both the EW and NS components. The amplification observed through HVSR were at 1.2 Hz (0.83 s) and around 3~4 Hz (0.33~0.25 s) for the EW and NS components, respectively. However, these frequencies are significantly lower than the fundamental frequency of ~7 Hz (0.14 s) obtained from theoretical linear elastic transfer function of the SASW V_s profile (Fig. 8.1.5a). The discrepancy in fundamental frequencies indicates nonlinear soil behavior and can be also attributed to the fact that the LXR1 station was located near the north end of the port, which according to the cross-section in Figure 8.1.3b is characterized by shallow sediments. The SASW V_s profile used to derive the transfer function was obtained at the south end, where the same cross section reveals layers of low plasticity clay approximately 10 m thicker than the north end. The presence of thicker low plasticity clay layer might be shifting the fundamental frequency of the site to lower frequencies.

The significance of this large amplitude impulsive recording for predictions of near-field ground motions merits further site characterization studies complemented with in-situ measurements of dynamic soils properties and laboratory testing.

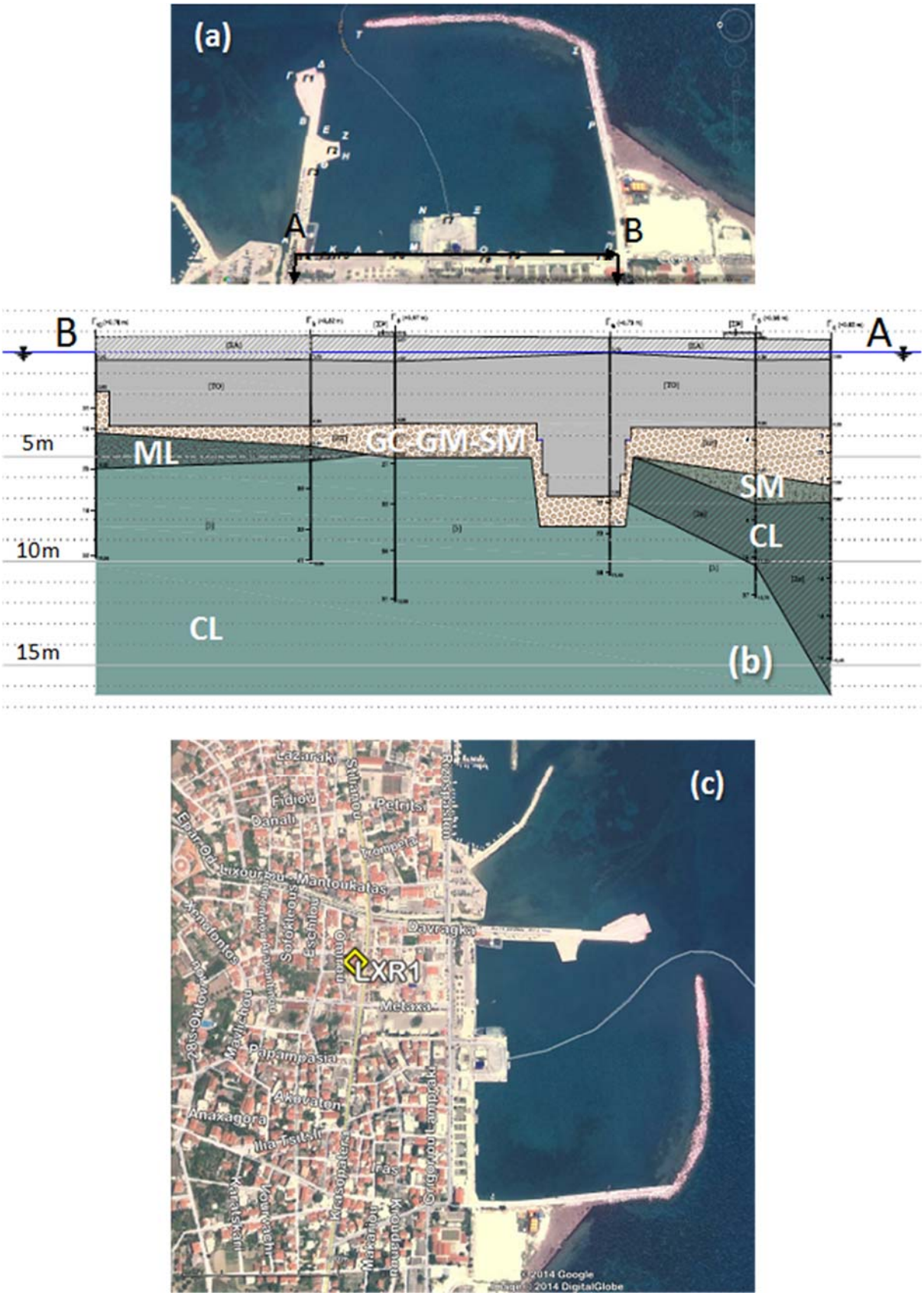

Figure 8.1.3 Geologic cross section at the port of Lixouri, revealing the low strength alluvial deposits (CL) which may have contributed to the high recorded accelerations (Geosymvouloi EPE, 2014).

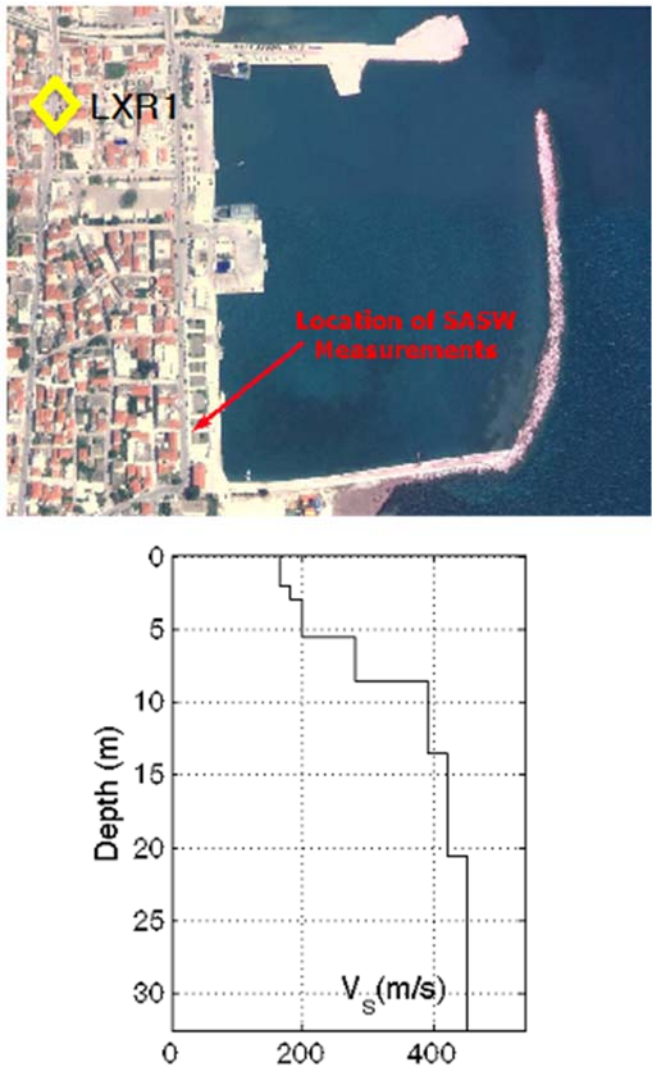

Figure 8.1.4 Spectral Analysis of Surface Waves (SASW) testing location (top) and generalized shear wave velocity, Vs, profile (bottom). Data from Pelekis (2014).

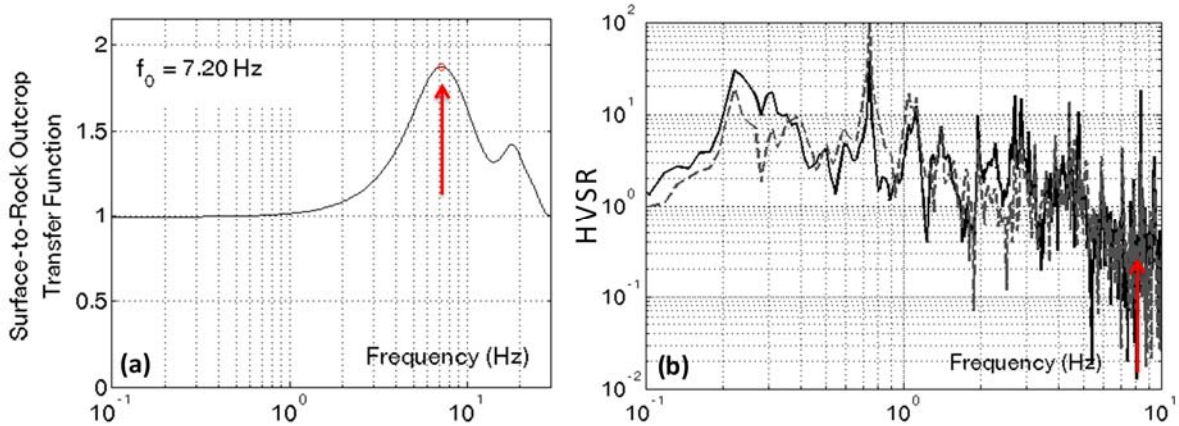

Figure 8.1.5 (a) Elastic transfer function from rock outcrop to ground surface using the generalized V_s profile of Fig. 8.1.4, and (b) Horizontal to Vertical Spectral Ratio (HVSR) of the LXR1 recording of the 2nd event

Argostoli ARG2 Station Recordings

The role of site amplification was also examined in the ground motions recorded at station ARG2, whose response spectrum of E-W component is shown in Fig. 8.1.6. A shear-wave velocity profile, obtained from the restoration study of the historical Debosset bridge (discussed in detail in Section 8.5), was used for site characterization of the ARG2 station (Fig. 8.1.7). The comparison of the theoretical linear elastic transfer function (surface to rock outcrop) based on the V_s profile of the site to the HVSR of ARG2 recordings from both events revealed almost identical fundamental mode at approximately 2 Hz (0.5 s). However, the comparison results are only indicative of nature of Argostoli due to the significantly large distance between the ARG2 station and Debosset Bridge.

The good agreement between HVSR and linear site amplification suggests that nonlinear response was not a dominant feature of the ground response at ARG2; in absence of dynamic soil properties, however, this hypothesis has not yet been verified. Moreover, the difference observed in the recordings of LXR1 and ARG2, with epicentral distances of 7 and 12 km, respectively; indicate the influence of local site effects on recorded ground motions.

Section 7.2 presents another recording of the 2nd event main shock at the Argostoli port by instruments that were installed by the UPatras. When compared to the response spectra of the ARG2 motions, recorded motions from both stations have similar response in terms of amplitude. Based on similar amplitude response recorded at both Argostoli stations, similar subsurface conditions with minor variability might be expected between the stations.

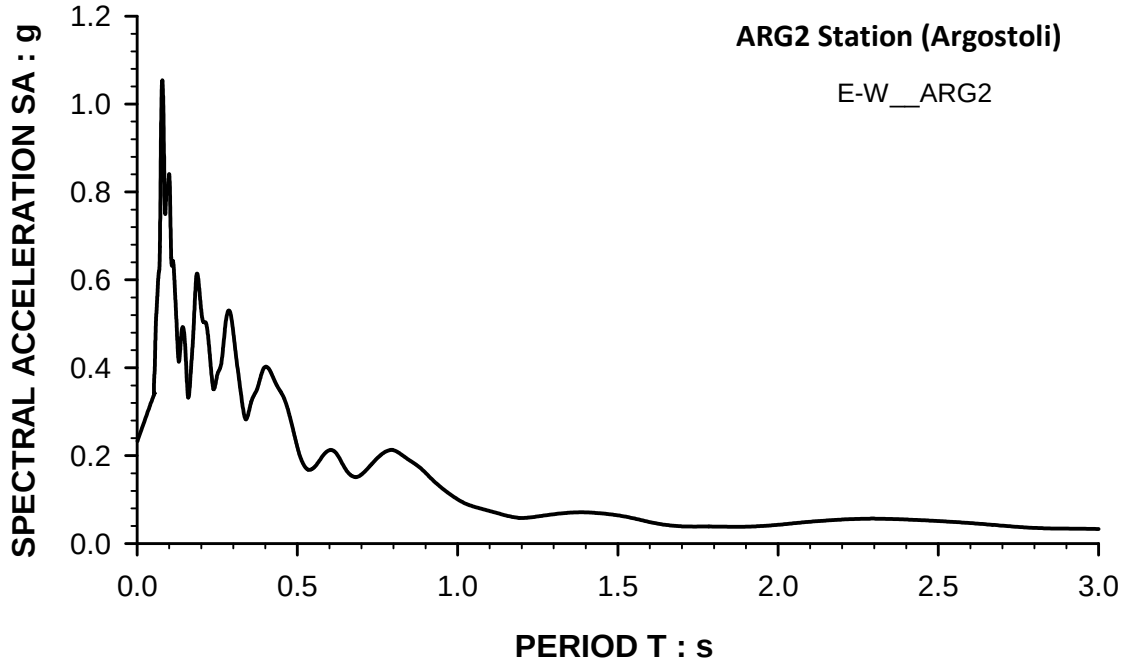

Figure 8.1.6. Acceleration response spectrum of E-W ground motion recording at ARG2 station of EPPO-ITSAK during the 2nd event for structural damping ξ of 5%.

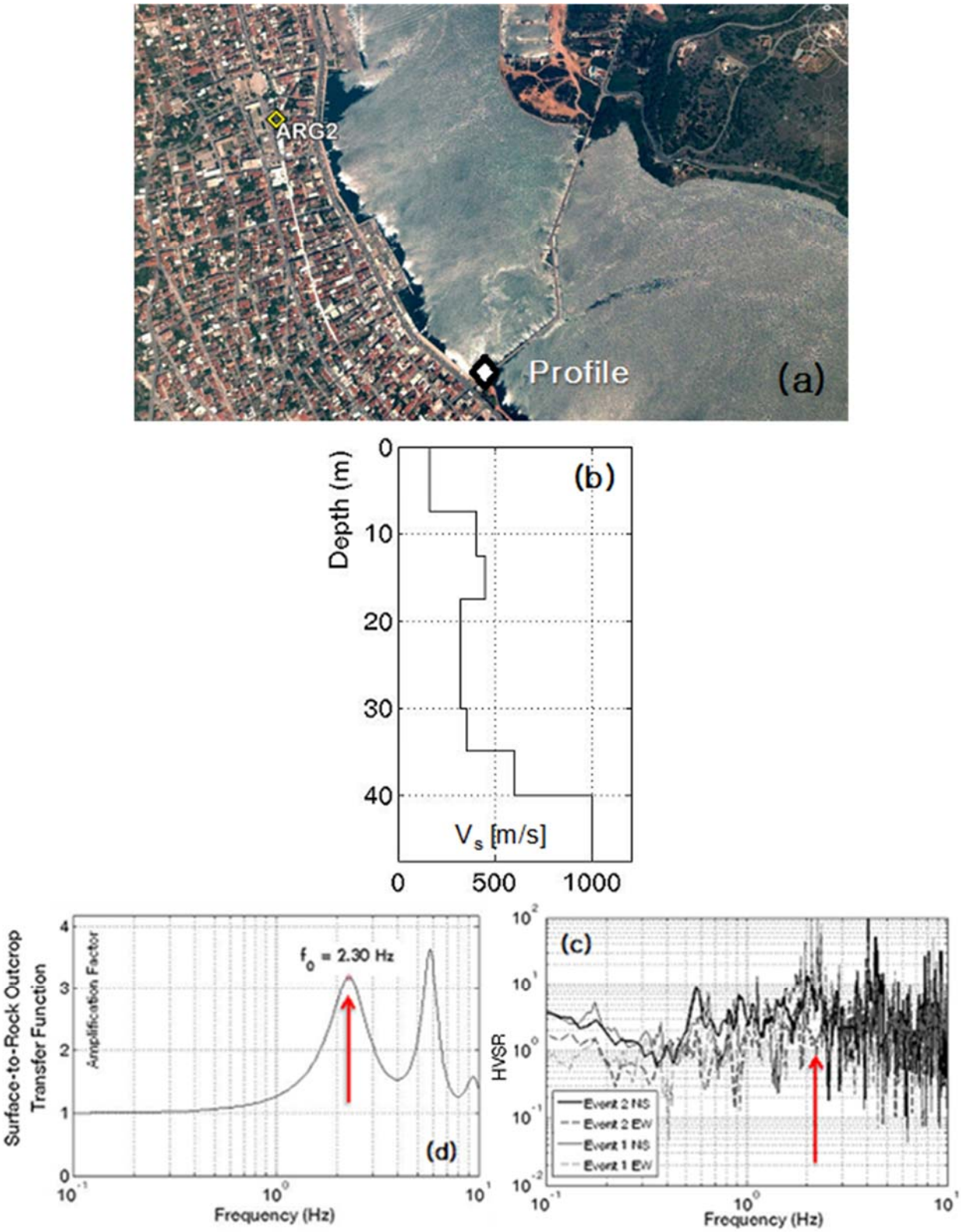

Figure 8.1.7. Site response at station ARG2: (a) shear wave velocity V_s profile at the adjacent Debosset bridge by Rovithis et al (see Section 8.5); (b) idealized V_s profile; (c) HVSR at station ARG2 from both events (4 components); and (d) theoretical linear elastic surface-to-rock outcrop transfer function at Debosset bridge SW embankment

3D SITE EFFECTS: TOPOGRAPHIC AMPLIFICATION COUPLED TO SITE RESPONSE

HVSR studies of the recordings at station CHV1 (at Chavriata, at an epicentral distance of 7 km) also revealed distinct peaks during the 2nd event. The geologic structure in the region (see also Figure 8.1.1) is characterized by 50 to 80 m thick sediments (interchangeable layers of weathered marls, limestone, and sandstone) overlying much stiffer Pre-Pliocene bedrock (Fig. 8.1.8a). For a 70 m thick soil column of average shear wave velocity 500 m/s the fundamental frequency would be around 1.78 Hz (0.56 s). It is therefore likely that the HVSR peaks in Figure 8.1.8 (b) are manifestations of 1D (one-dimensional) site response.

On the other hand, the CHV1 station is located in a region with very strong topographic relief as shown on the topographic map and ground surface topography of Figure 8.1.8 (c, d). Thus, topographic amplification may also have contributed to the large accelerations recorded at CHV1 with max PGA of 0.76g (see Fig. 8.1.2 and Chapter 7).

Recent studies on the relative contribution of site amplification and topography effects at sites with similar surface and subsurface geologic features as CHV1 suggest that the simultaneous triggering of site and topography effects (referred to as 3D site effects) can generate accelerations much higher than what would have been predicted by mere superposition of the effects of topography and 1D site response (Assimaki et al., 2005; Assimaki & Jeong, 2013). Moreover, several studies have shown that for ground motions levels above 0.5g recorded at sites with soft sediments such as CHV1, 1D nonlinear site response frequently fails to physically explain how the soil can sustain ground motion amplitudes that supersedes its strength in simple shear (Andrews et al., 2007).

The large accelerations at CHV1 provide a learning opportunity on 3D site effects and their complex mechanisms of ground motion amplification. This insight in turn can lead to improved predictions of extreme ground motions and their upper physical limits that can be applied to improve design ground motions for critical infrastructure and critical facilities.

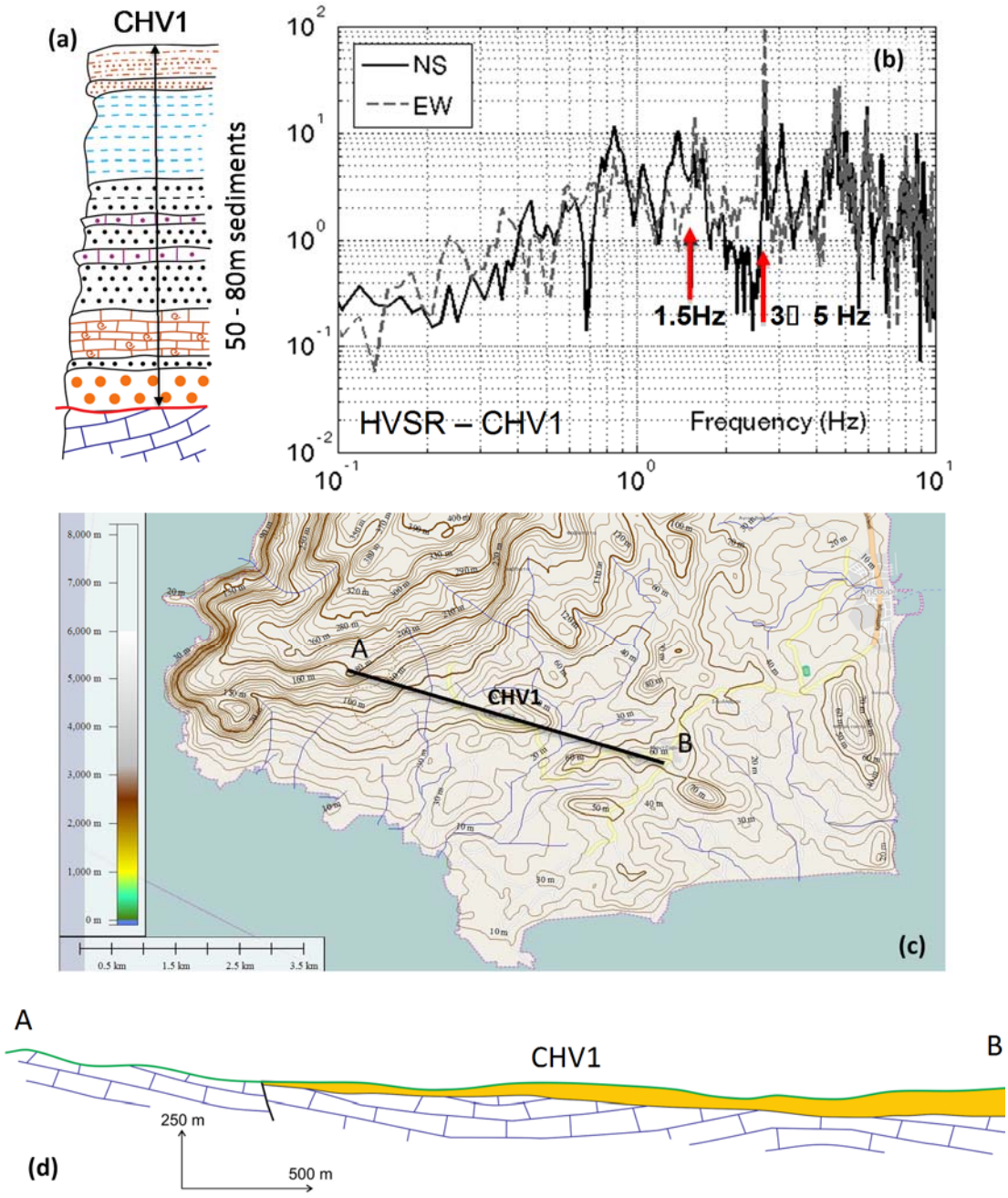

Figure 8.1.8. (a, b) HVSR at station CHV1 (Chavriata), revealing consistent site response modes with the 50-80m sedimentary structure underlying the region; (c, d) topographic map and cross section across Chavriata, clearly showing irregular surface and subsurface topography that may have contributed to the large recorded ground accelerations.

COMPARISONS WITH EUROPEAN AND USA CODE SPECTRA

The Eurocode 8 (EC-8, 2008) defines the seismic hazard at a site at the firm ground conditions (ground type A) based on seismic zonation of the local National Authorities of each country that uses EC-8 as their model code. The hazard is defined as a reference ground acceleration a_g on ground type A (rock with shear wave velocity V_s > 800 m/s) for an event with approximate return period of 2,500 years, and modified for site conditions based on the ground type. Table 8.1.1 presents the definition of ground types according to EC-8. Site factors, S, associated with each ground type and average shear wave velocity at the top 30 m ($V_{s,30}$) are applied to produce design spectra for the various ground types. In Greece, Cephalonia is on the highest zoning level of the national code EAK (2000) with zoned a_g of 0.36 g (Fig. 8.1.9). EC-8 code-based acceleration spectra for Cephalonia developed for rock, and dense and soft soil conditions are presented on Fig. 8.1.10.

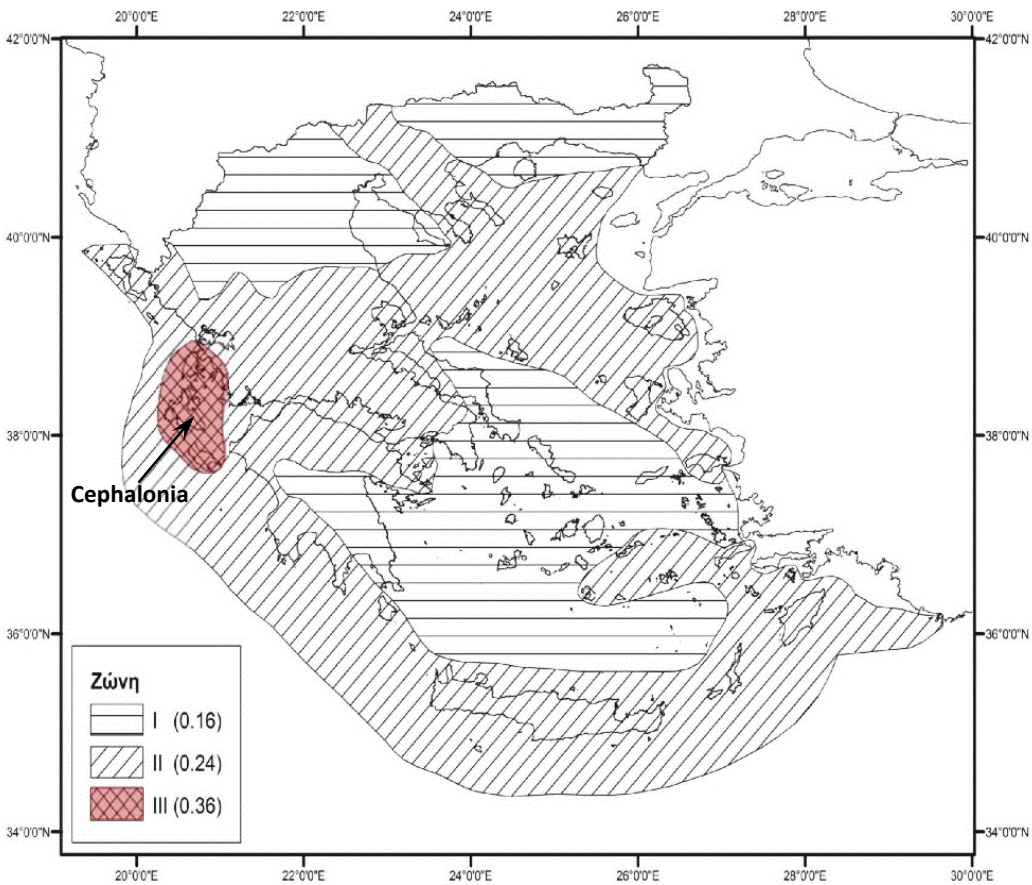

Figure 8.1.9. Seismic hazard mapping of Greece according to EAK (2000) for ground type A (rock). There are three zones I, II, III with reference ground acceleration a_g of 0.16, 0.24, and 0.36 g, respectively. Cephalonia belongs in Zone III with a_g = 0.36 g.

Table 8.1.1 Eurocode EC-8 and ASCE7-05 site classification.

EC-8			ASCE7-05		
Ground Type	Description	$V_{s,30}$ (m/s)	Site Class	Description	$V_{s,30}$ (m/s)
A	Rock	> 800	A	Hard Rock	> 1,500
B	Deep - Very Dense	360 – 800	B	Rock	760 – 1500
C	Deep - Dense to Medium	180 – 360	C	Very Dense Soil / Soft Rock	360 – 760
D	Loose to Medium Dense	< 180	D	Stiff Soil	180 – 360
E	5-20 m thick	–	E	Soft Soil	< 180
	V_{s30} same as Type C or D		F	Liquefiable Soil	–

ASCE 7-05 is the basis of the International Building Code (IBC 2009), currently used as model for most local state codes in the United States (US). The local seismicity is provided by the national USGS seismic hazard mapping for Maximum Considered Earthquake (MCE) hazard level and Rock B site conditions (V_s > 760 m/s). Mapping is provided for two Spectral Acceleration (SA) parameters: S_s for short-periods (0.2 s) and (S_1) for long periods (1 s). Site factors F_a and F_v modify S_s and S_1 respectively to produce MCE SA values adjusted for soil conditions (see Table 8.1.1 for ASCE7-05 site classes).

An analogy between EC-8 and ASCE 7-05 for Cephalonia can be made by identifying a US site in the US with the same level of reference acceleration a_g of 0.36 g (or $S_s = 2.5 \times a_g$ = 0.72 g). Based on the USGS seismic map of ASCE7-05, the city of Portland, Oregon has S_s = 0.72 g, and will be used for comparison. Figure 8.1.10 presents ASCE7-05 MCE response spectra for Portland and rock, dense and soft soil conditions. When two different code spectra are compared for Cephalonia and Portland, it appears EC-8 produces slightly higher SA values for rock and stiff sites, and is significantly higher for soft site conditions for T < 2.3 s).

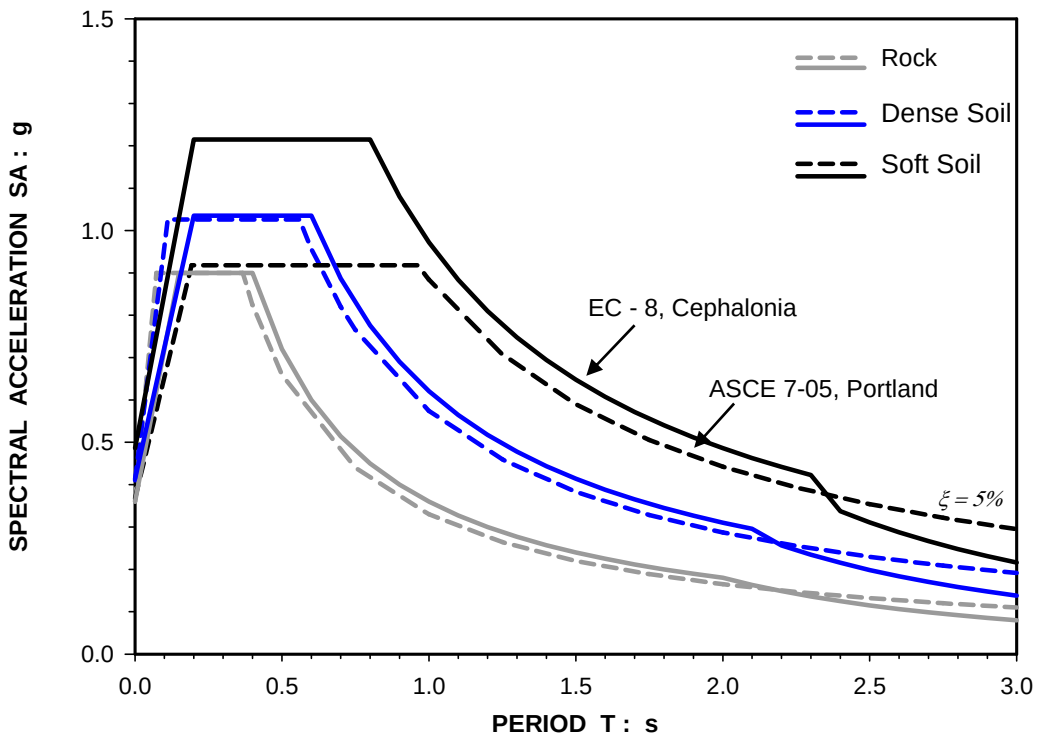

Figure 8.1.10. Comparison of design acceleration response spectra obtained based on EC-8 and ASCE 7-05 design event for Cephalonia and Portland that are on equivalent level of seismic hazard zoning.

Figure 8.1.11 compares acceleration response spectra of three records from the 2nd event at the stations of LXR1, CHV1, and ARG2 stations (at Lixouri, Chavriata, and Argostoli) to the EC-8 spectra for ground types A (rock) and D (soft soil). Both components of the CHV1 record and the EW component of the LXR1 record far exceed code-based spectra in the structural period range of less than 1 s (CHV1) and greater than 0.8 s (LXR1). As discussed earlier in this section, local site effects and directivity have likely contributed to these high amplification effects that need to be confirmed with pertinent in-situ testing. The ARG2 station response spectra are lower than the code-based spectra, which can be expected since this station is farther away from the epicenter and is on stiffer site conditions as compared to the other two stations.

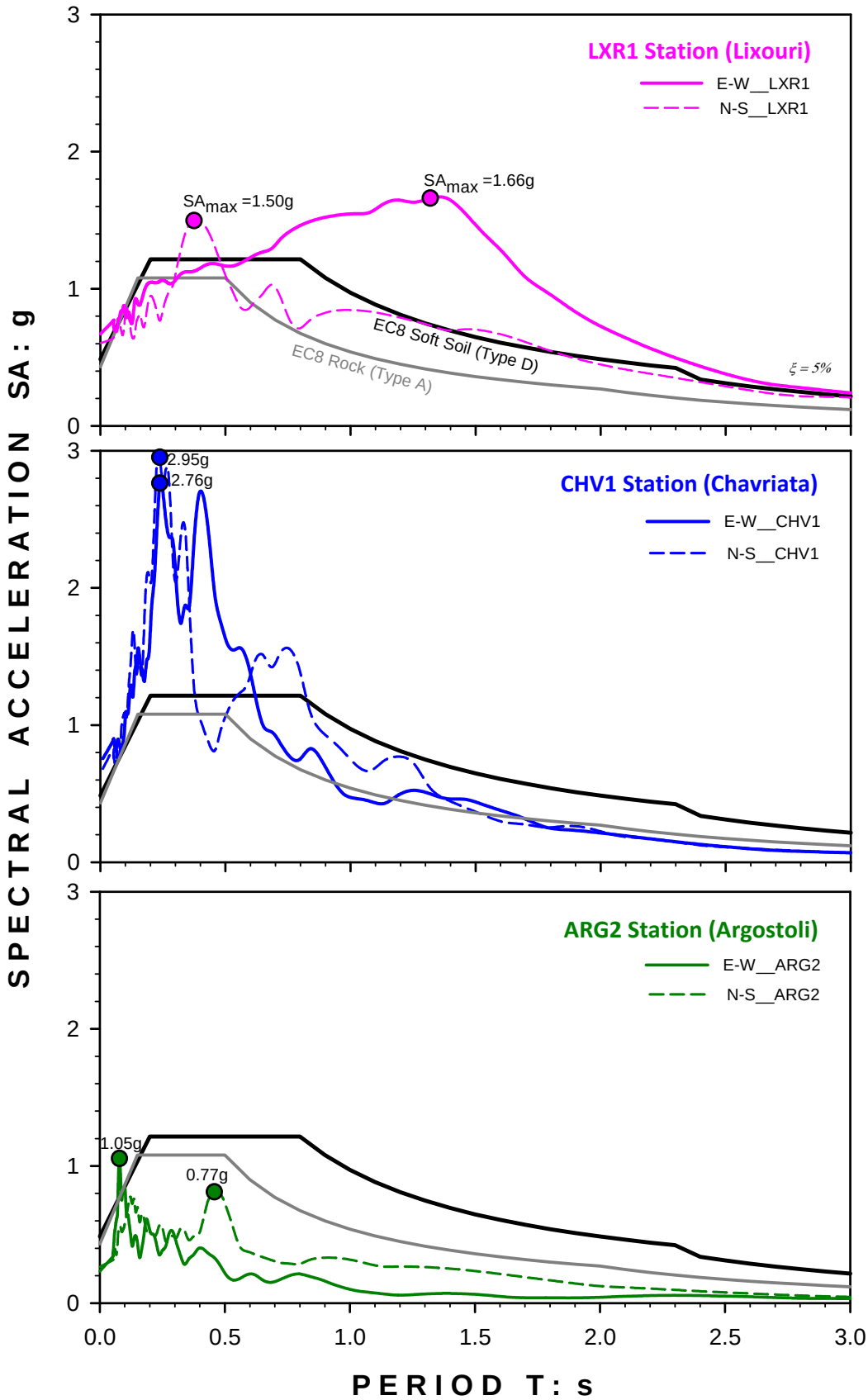

Figure 8.1.11. Comparison of acceleration response spectra of recorded Cephalonia motions at (a) LXR1, (b) CHV1, and (c) ARG2 stations with EC-8 design spectra.

CONCLUSIONS

Although analysis of Horizontal-to-Vertical Ratios (HVSR) of several ground motion records revealed features of 1D site amplification, geotechnical site investigation data are necessary for validation. Exceptions were the ground motions at station ARG2, which systematically showed HVSR peaks consistent with the fundamental mode of an adjacent site, for which shear wave velocity measurements were available. In addition, topography 3D effects coupled to site response have likely contributed to the PGA = 0.76 g recorded at station CHV1 and the large exceedance of its spectral acceleration values compared to code-based values. This station presents an opportunity for learning about the complex mechanisms of nonlinear 3D site response, and merits further investigation including site characterization and high resolution topography mapping (e.g., through LiDAR). Finally, the large acceleration and strikingly near-field features of the EW component recorded by station LXR1 during the 2nd event provide a unique case study that merits further investigation as an opportunity to better understand nonlinear site response from near-field motions.

8.2 Liquefaction, Ports and Waterfront

INTRODUCTION

The two main shocks of the Cephalonia 2014 earthquake sequence (Event 1 and Event 2) caused widespread liquefaction in the Lixouri and Argostoli ports (two of the four main ports) and in adjacent waterfronts. Figure 8.2.1 shows the location of the four ports: Argostoli, Lixouri, Sami, and Poros. Liquefaction was followed by lateral spreading, manifested by opening of large cracks, predominantly parallel to the coastline with movement towards the seafront. Marginal liquefaction and movement of pier blocks was also observed at the port of Sami. No damage was observed in the port of Poros, which is located the farthest away from the earthquake epicenters.

This section presents observations regarding the response of the waterfront in the former three ports. The information presented in this section was gathered by: (i) the UPatras reconnaissance team after the 1st and 2nd events, prior to the GEER/EERI/ATC team January 28-30 and February 5, (ii) collectively by the GEER/EERI/ATC team during February 8-10 (most data collected by UPatras, AUTH-LSDGEE, ITSAK, NTUA and UTH), and (iii) follow-up reconnaissance visit by UPatras on February 18-19.

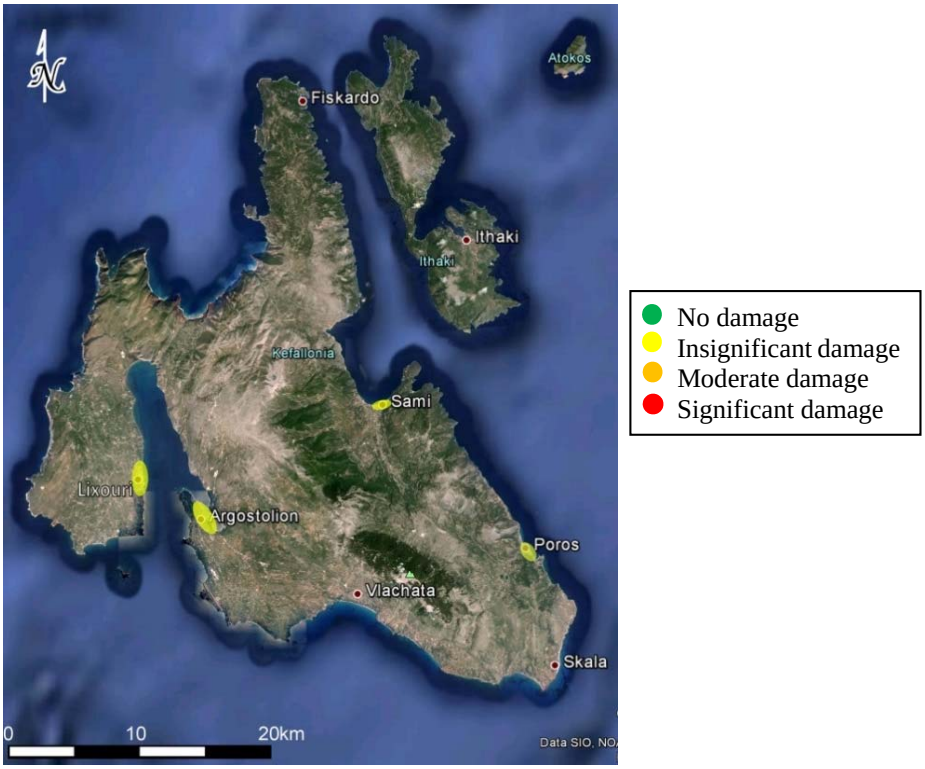

Figure 8.2.1. The four main ports in the island of Cephalonia: Argostoli, Lixouri, Sami, and Poros.

LIXOURI PORT

General Lixouri Port Area

The Lixouri port seafront is approximately 400 m long (Fig. 8.2.2). It was reportedly constructed by reclaiming part of the sea using debris generated following the destructive M7.2 earthquake of 1953.

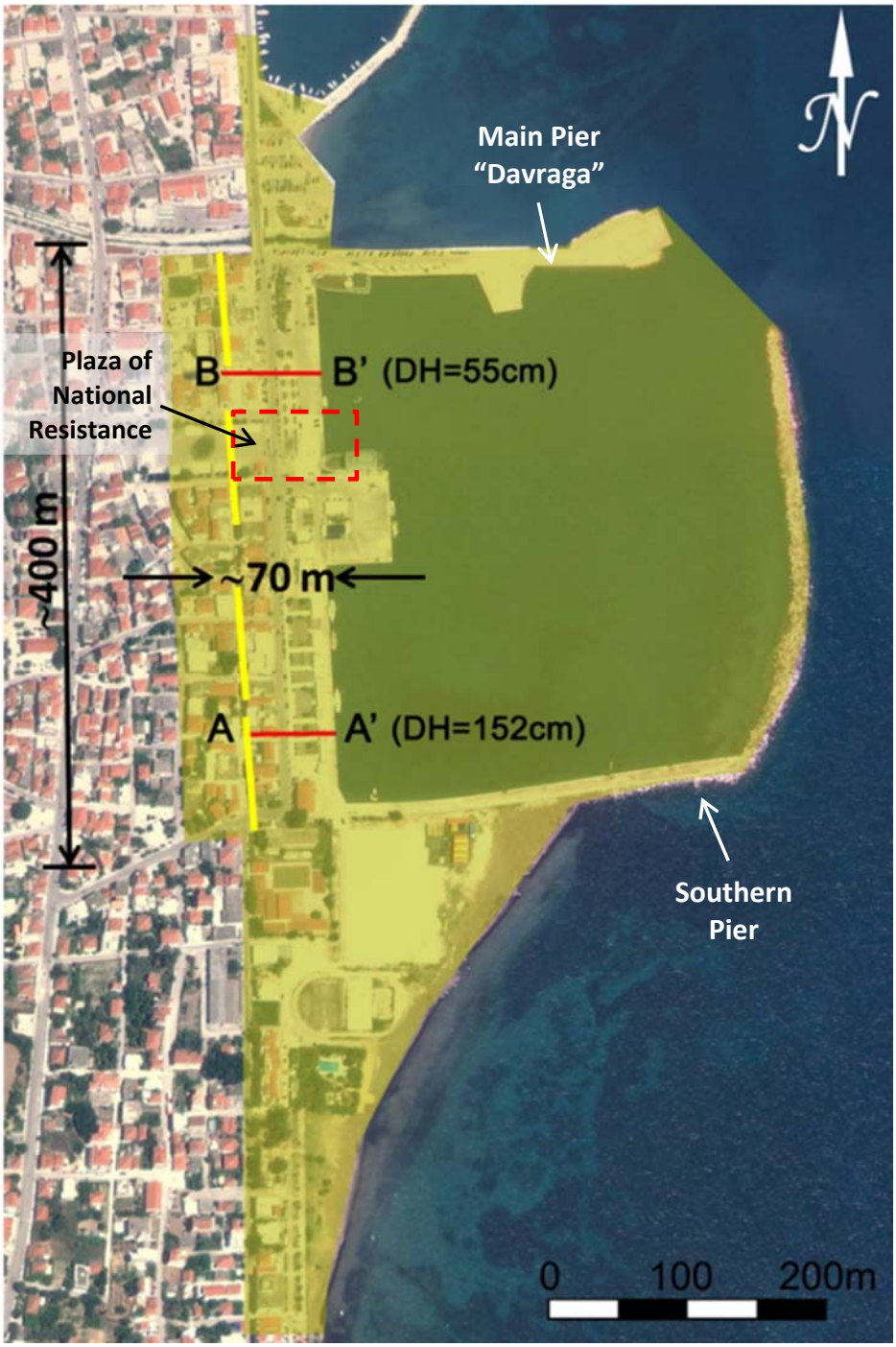

Figure 8.2.2. Google Earth photo of the Lixouri Port Area (GPS coordinates 38.20°, 20.44°).

The yellow line in Fig. 8.2.2 outlines the location of the first cracks based on reconnaissance after Event 2 that appears to coincide with the coastline prior to the 1953 earthquake. Liquefaction and lateral spreads in the Lixouri port and waterfront area were first observed during Event 1. Eye witnesses in the port area reported that during Event 1 ejected material reached a height of 1.5 m. Liquefaction and lateral spreads in the Lixouri port and waterfront area were more extensive during Event 2.

Figure 8.2.3 shows an example of damage due to liquefaction and lateral spreading in Lixouri's quay wall following Event 1 (Fig. 8.2.3a) and following Event 2 (Fig. 8.2.3b). As shown in Fig. 8.2.3, at this location the horizontal displacement was 9 cm and vertical displacement was 6 cm after Event 1 (Fig. 8.2.3a). After Event 2, horizontal and vertical displacements increased to 49 cm and 30 cm, respectively (Fig. 8.2.3b). Many sites that were liquefied in Event 1 re-liquefied during Event 2 along the Lixouri waterfront. Figure 8.2.4 illustrates an example from the Lixouri port's main pier, which was practically undamaged following Event 1 (Fig. 8.2.4a), but suffered significant damage in some sections following Event 2 (Fig 8.2.4b).

Lixouri Quay Wall

The quay wall of the Lixouri port is shown in Fig. 8.2.5. Soil ejecta found on the ground surface and lateral spreading towards the seafront observed during reconnaissance surveys were indicative of soil liquefaction along the Lixouri waterfront. Figures 8.2.6 through 8.2.13 present pictures of the soil ejecta and lateral spreading taken during reconnaissance surveys. In many cases, the liquefied material was brown in color and by inspection appeared to be silty sand or sandy silt. In some cases, grayey material was also observed (Fig. 8.2.7b). In several occasions, the ejecta included coarse material, including coarse gravels (Figs. 8.2.7c, 8, 9, 13). The gravel-size particles are part of the fill immediately below the ground surface. Samples of soil ejecta were collected for classification testing. The ejecta in Lixouri port is in some places coarser than the ejecta observed in the Argostoli port area, which may be indicative of higher pore water pressures developed in Lixouri area.

Figure 8.2.3. Lixouri port movement following (a) Event 1 and (b) Event 2. (GPS coordinates 38.198767°, 20.439533°). George Athanasopoulos of UPatras is on the photo.

Figure 8.2.4. Damage to the main pier of Lixouri port, Davraga, following: (a) Event 1 and (b) Event 2 at (GPS coordinates 38.201500^{o}, 20.441283^{o}).

Figure 8.2.5. Temporary Exhibit: Quay wall of Lixouri port from postcard mailed in 1919 (Poulaki-Katevati, 2009). To be replace by Google Earth view of the quay wall. (FIGURE PENDING, SO THAT IT CAN BE UPDATED ONCE THE REST OF PHOTOS AND TEXT IS FINALIZED).

Figure 8.2.6. Soil ejecta with gravel size particles along the Lixouri port waterfront after Event 2. Note gravel size particles in the ejecta (GPS coordinates 38.19873^{o}, 20.43934^{o}).

Figure 8.2.7 Typical liquefaction ejecta in Lixouri port [GPS coordinates: a-(38.197531°, 20.439784°), b-(38.19988°, 20.43969°), c-(38.19922°, 20.43928°), d-(38.19873°, 20.43934°), 2/8/2014].

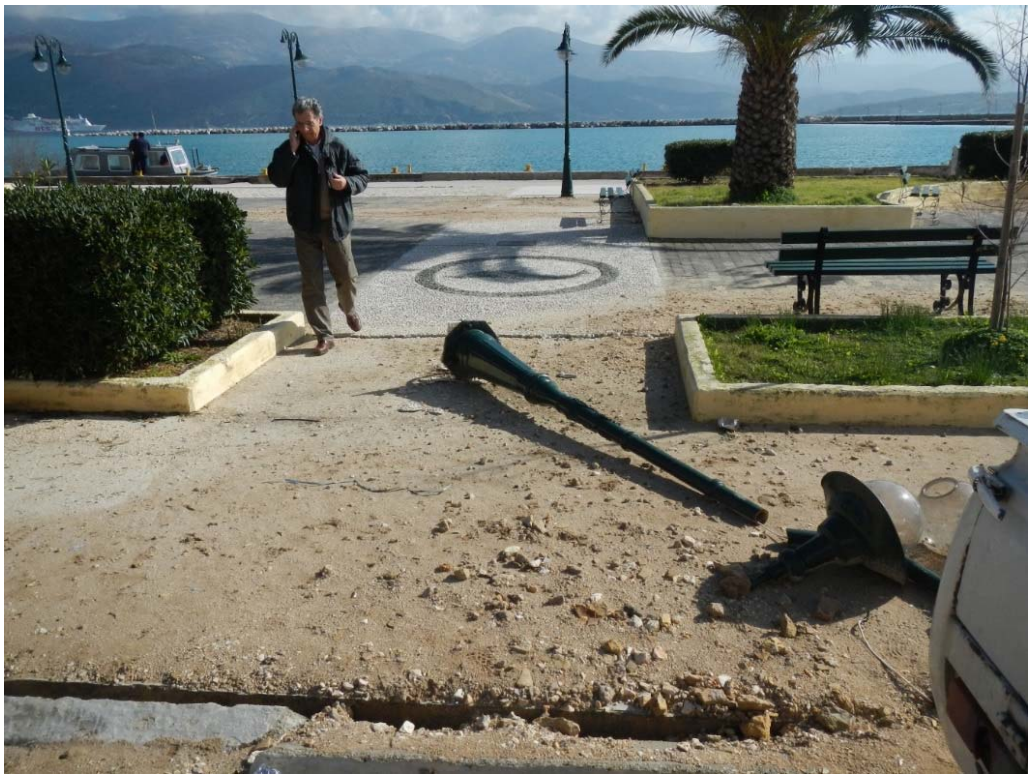

Figure 8.2.8. Example of seafront crack opening at the port of Lixouri. Note large particle size of the ejecta (38°11'55.38"N, 20°26'20.98"E).

Figure 8.2.9. Extensive evidence of coarse-grained ejecta in the area of Lixouri port: (a) at quay wall (38°12'0.02"N, 20°26'22.62"E), and (b) towards the first row of buildings parallel to the shoreline (38°11'59.82"N, 20°26'21.76"E).

Figure 8.2.10. Remnants of liquefaction on the Lixouri coastal sidewalk (GPS coordinates: 38.199444, 20.439166).

Figure 8.2.11. Ejecta on Lixouri coastal sidewalk tiles (GPS coordinates: 38.199166, 20.439166).

Figure 8.2.12. Evidence of liquefaction at Lixouri coastal sidewalk (GPS coordinates: 38.199166, 20.439166).

Figure 8.2.13. Evidence of liquefaction at a Lixouri coastal sidewalk (GPS coordinates: 38.199166, 20.439166).

Figures 8.2.14 through 8.2.33 present examples of displacement patterns observed at the Lixouri port seafront. Measurements of cumulative horizontal displacement were performed by the UPatras team along several cross-sections perpendicular to the shoreline, whose results are currently being analyzed. Figure 8.2.20 shows two example cross-sections with corresponding values of total horizontal displacement. Soil cracking observed in the Lixouri coastal zone extended inland from the Lixouri waterfront to a maximum of two to three blocks spanning about 100 m. Displacement measurements were made along cross-sections A-A' and B-B', presented in Figs 8.2.32 and 8.2.33, respectively. The locations of the cross sections are shown in Fig. 8.2.2. Cumulative horizontal displacement measured along these cross-sections from points A and B are shown in Figs. 8.2.34 and 8.2.35, respectively. Total horizontal displacement towards the sea estimated along cross-sections A-A' and B-B' were approximately 1.5 m and 0.55 m, respectively. Longitudinal cracks parallel to the seafront were observed as far as 100 m inland from the Lixouri waterline. However only small amount of these displacements are due to lateral ground spreading, they are mostly due to inertia sliding

of the blocks constituting the quay wall, as well as, the differential settlement at the base of the quay wall. Displacements due to lateral spreading were extending over a zone of about 15 m behind the quay wall (Fig. 8.2.34). Whereas, displacements that can be attributed to inertia-induced sliding and differential settlement (i.e. rotation) of the qual wall develop over a very short distance from the quay wall, as shown in Fig 8.2.34 and 8.2.35 by the steep increase observed in cumulative displacement near the quay wall.

Figure 8.2.14. 180 degrees panorama view of the displacement patterns at the Lixouri port in location: 38°11'53.53"N, 20°26'22.23"E.

Ejected material next to the displaced quay walls was not equally distributed in all locations. The liquefaction ejecta are not as abundant as in the foreground where the quay wall did not displace as much, due to the restraint provided by the small wharf located perpendicular to it. The ramps made for the access of cars into the ferries provided adequate restraint to lateral quay wall displacement as shown in Fig. 8.2.22a. Fig.8.2.26 shows that the displacement and rotation of external corner quay walls were significantly more severe compared to the other parts of the quay wall, showing the 3D geometry effects. Profound liquefaction ejecta evidence was observed in the foreground, for the cases where the wall was displaced and significantly damaged substantially as in Fig. 8.2.16. The outward horizontal displacement in Fig. 8.2.16 has been estimated from the sum of the widths of the cracks to be about 70 to 120 cm. This observation in the Lixouri Port is consistent with previous studies that demonstrated that lack of lateral outward displacement causes development of excess pore water pressures and ultimately liquefaction (Dakoulas & Gazetas, 2008).

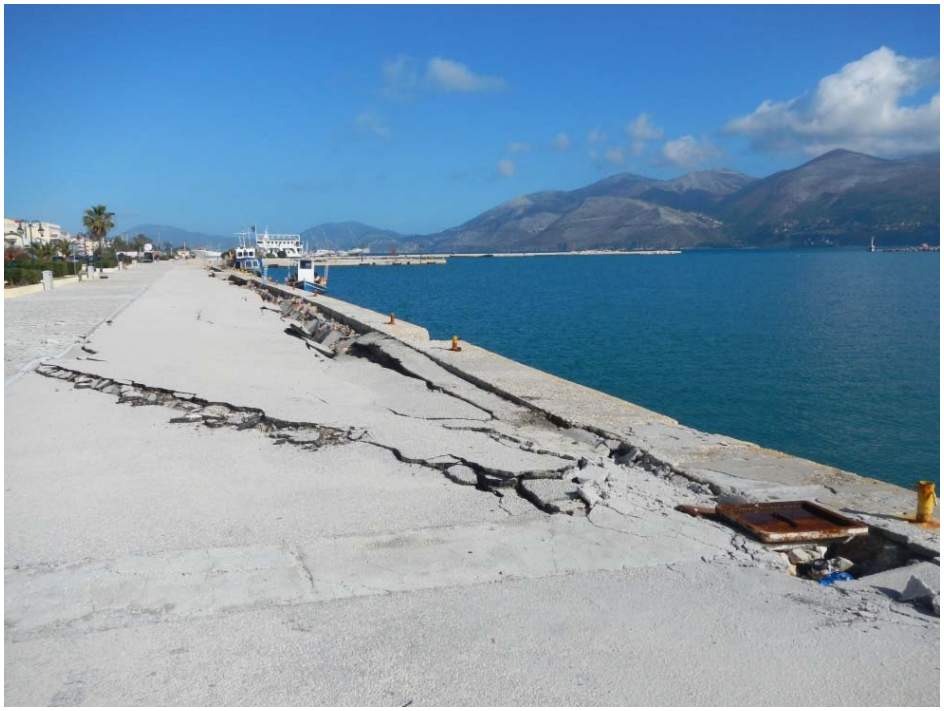

Figure 8.2.15. Example of the displacement patterns at the Lixouri quay wall (38°11'52.99"N, 20°26'22.48"E).

Figure 8.2.16. Lateral displacement of the quay wall, and ejected liquefied soil. This is abundant where the wall has not displaced horizontally due to the small perpendicular wharf restraining it. (GPS coordinates: 38.199444, 20.439166).

Figure 8.2.17. Vertical displacement observed behind the wavefront (marked with the yellow curve) and opening of a road-pavement joint (GPS coordinates: 38.199166, 20.439444).

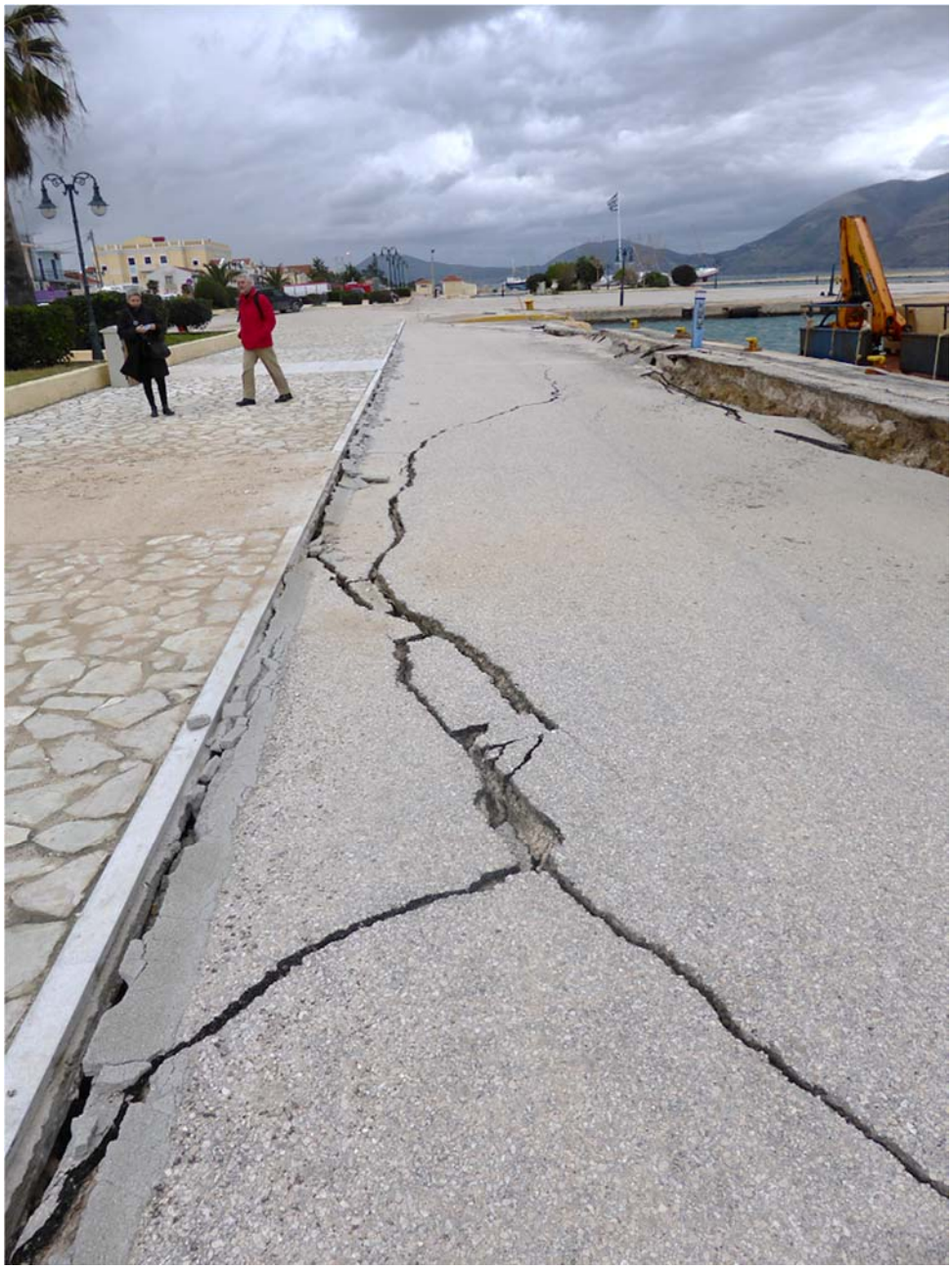

Figure 8.2.18. Cracks in the road behind the quay wall and liquefaction remnants on the sidewalk (GPS coordinates: 38.199166, 20.439444).

Figure 8.2.19. Vertical diaplacement behind quay wall exposing water network pipes (GPS coordinates: 38.199166, 20.439444).

Figure 8.2.20. Lateral displacement of the quay wall towards the sea (GPS coordinates: 38.199166, 20.439444).

Figure 8.2.21. Vertical settlement behind the quay wall reaching 70 cm (GPS coordinates: 38.199166, 20.439444).

Figure 8.2.22. Across the Plaza of National Resistance (shown in Fig. 8.2.2), damage consisted mainly of lateral quay wall displacement and road cracks (GPS coordinates: 38.199444, 20.439444).

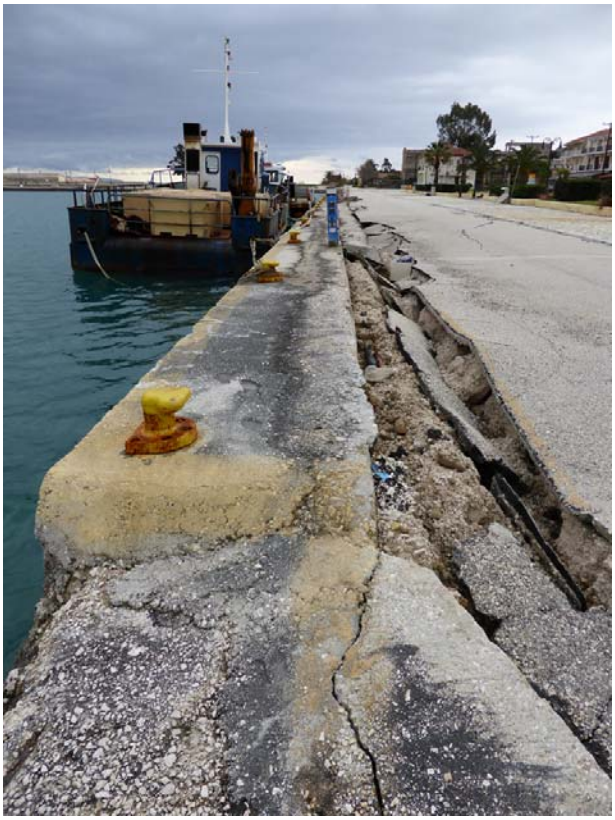

Figure 8.2.23. Lateral quay wall displacement and road cracks in the southern part of Lixouri port (GPS coordinates: 38.199444, 20.439444).

Figure 8.2.24. Settlement behind the quay wall (GPS coordinates: 38.199722, 20.439722).

Figure 8.2.25. Cracks in the southern part of the Lixouri port (GPS coordinates: 38.199722, 20.439722).

Figure 8.2.26. Settlement and cracks behind the quay wall (GPS coordinates: 38.199558, 20.439852).

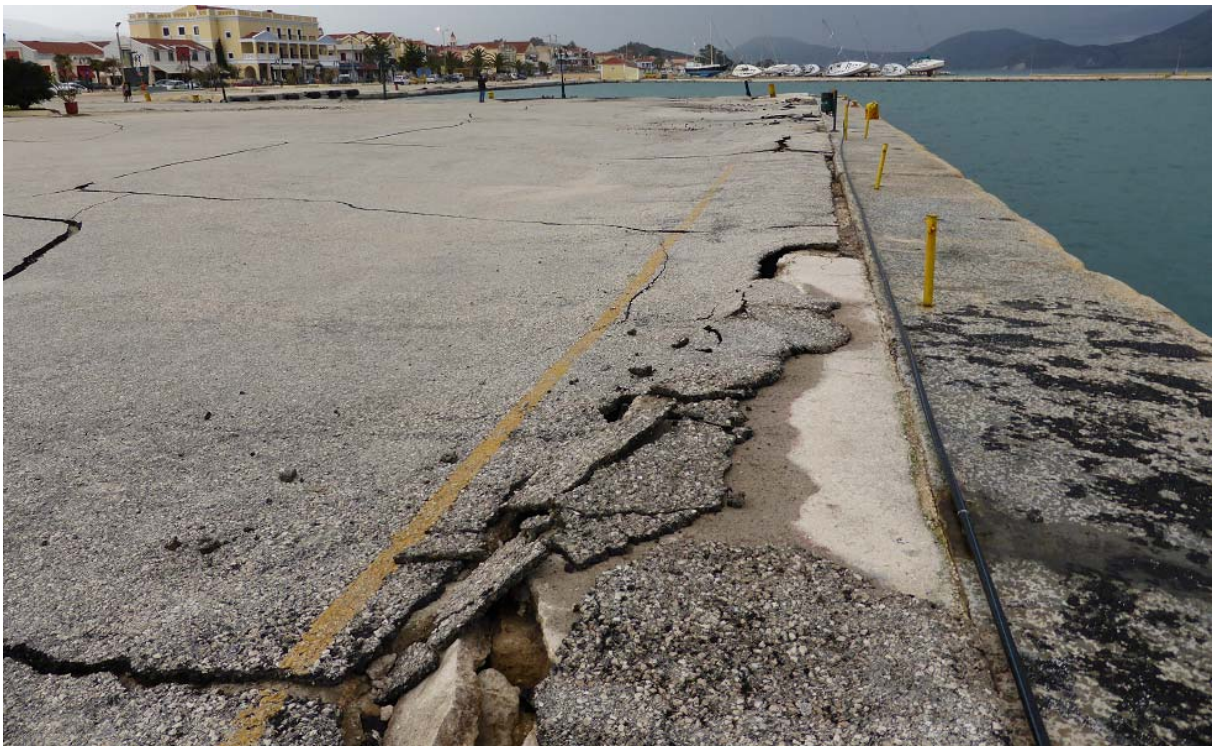

Figure 8.2.27. Uneven surface settlement due to lateral spreading and liquefaction of the wharf backfill (GPS coordinates: 38.199627, 20.440022).

Figure 8.2.28. Light brown color sand liquefaction ejecta (GPS coordinates: 38.200000, 20.440000).

Figure 8.2.29. Soil liquefaction remnants behind the quay wall and lateral displacement towards the sea front (GPS coordinates: 38.200277, 20.439383).

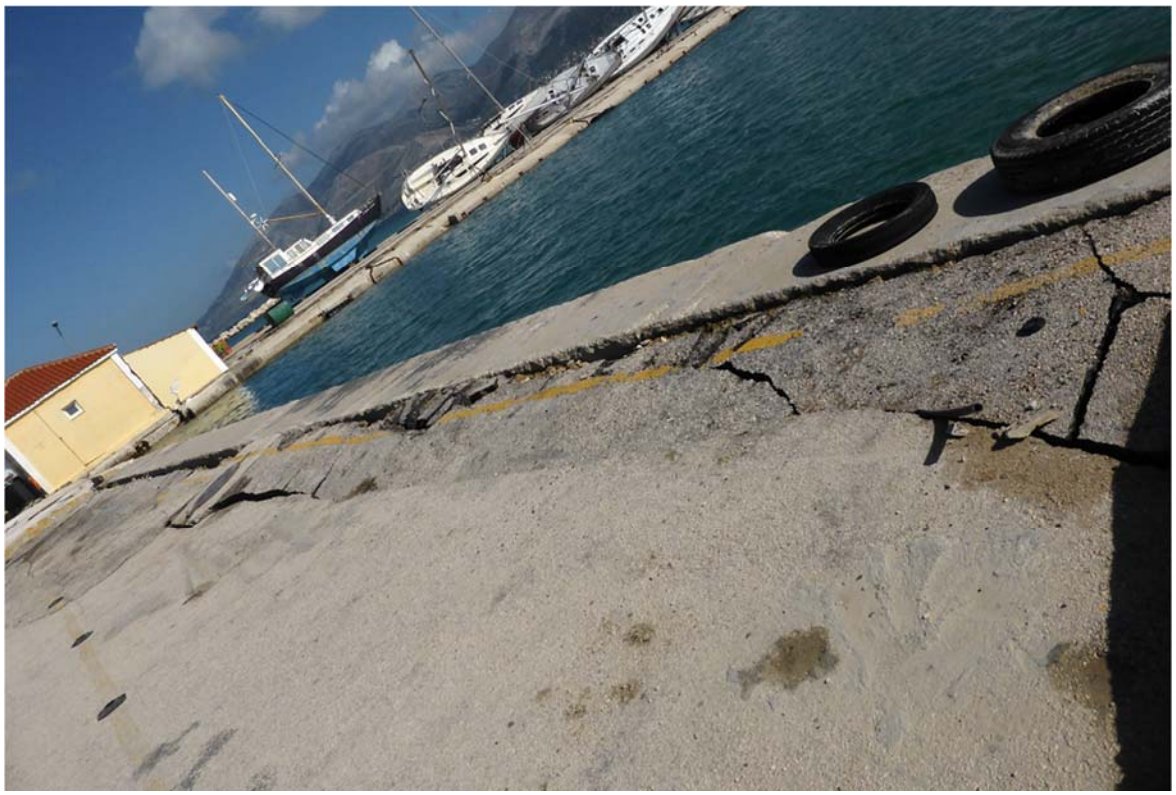

Figure 8.2.30. Cracks behind the wall and sand remnants of liquefaction ejecta (GPS coordinates: 38.201050, 20.439297).

Figure 8.2.31. Auxiliary dock on quay wall, located to the north of main dock in the port of Lixouri: (a) from 2011 archives {www.panoramio.com/photo/3072045?source=wapi&referrer=kh.google.com}; and after the 2nd event: (b) front and (c) back (38°12'1.39"N, 20°26'21.85"E).

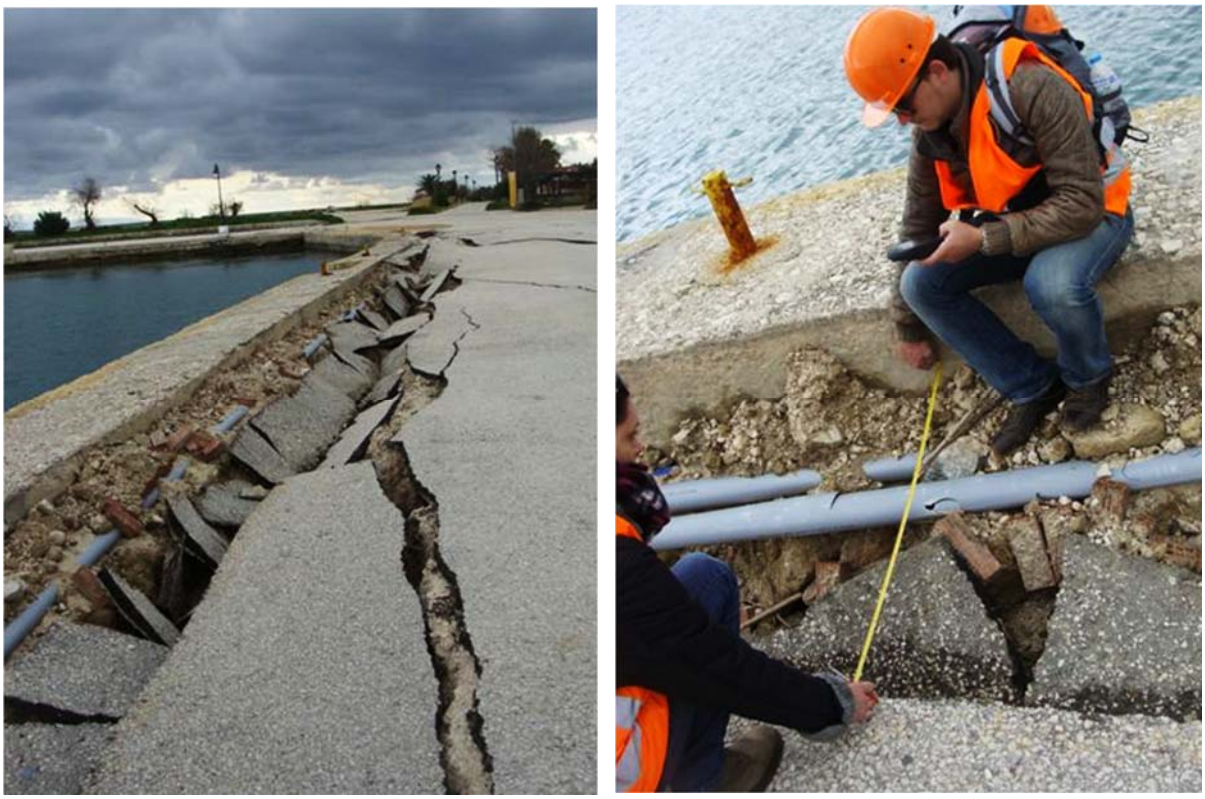

Figure 8.2.32. Lateral movement in Lixouri port along section A-A' of Fig. 8.2.2 being measured by Tasos Batilas and Xenia Karatzia of UPatras on 2/8/14 (GPS coordinates 38.19842 º, 20.43956 º).

Figure 8.2.33. (a) Lateral spread in Lixouri port along section B-B' and (b) movement of quay walls (GPS coordinates: a-(38.20072°, 20.43920 °), b-(38.20077 °, 20.43940 °), 2/8/14).

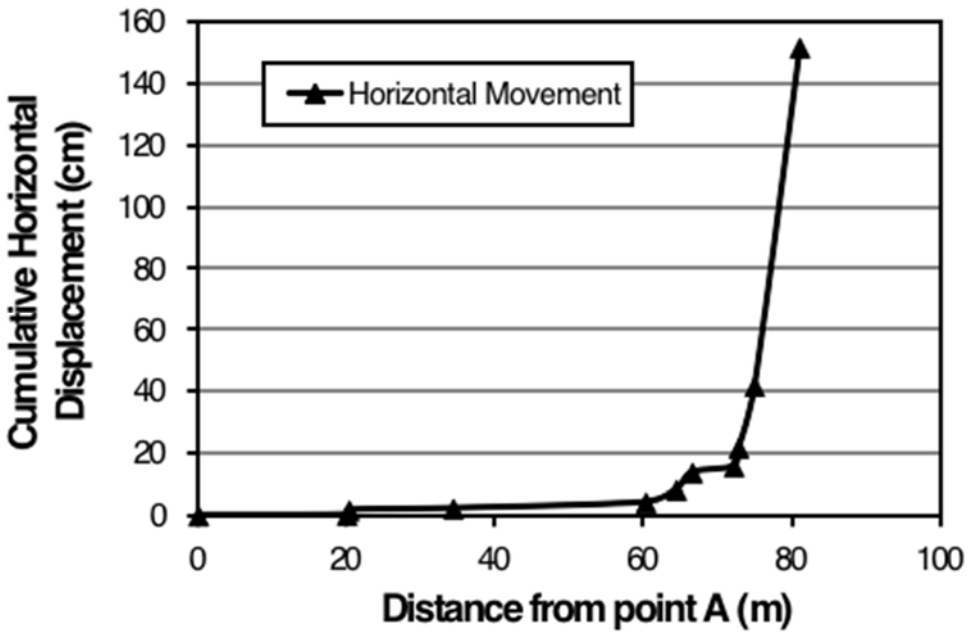

Figure 8.2.34. Plot of cumulative horizontal displacement vs. distance from point A (as shown in Fig. 8.2.2) at Lixouri port.

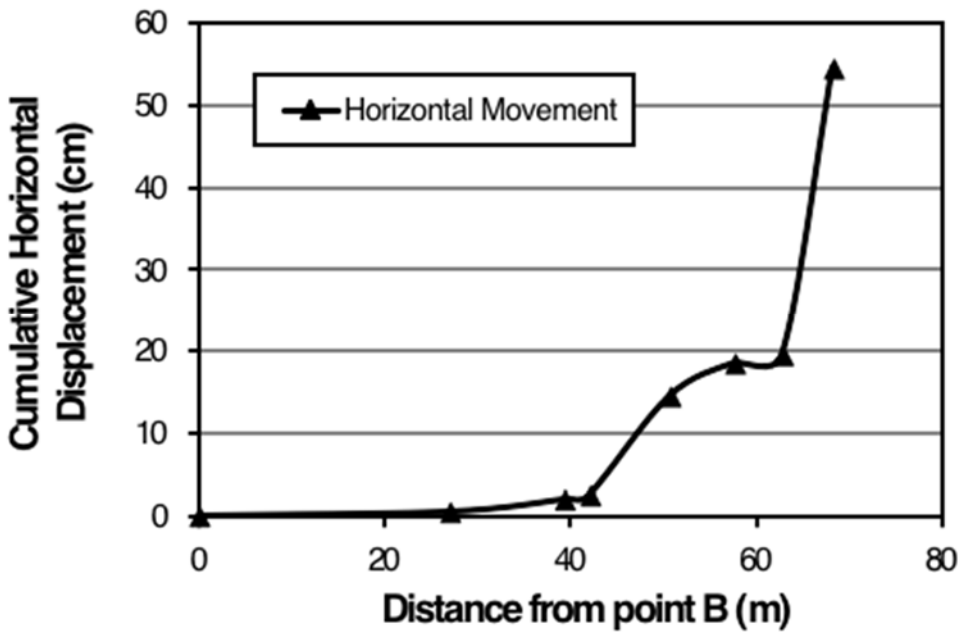

Figure 8.2.35. Plot of cumulative horizontal displacement vs. distance from point B (as shown in Fig. 8.2.2) at Lixouri port.

Lixouri Main (North) Pier Davraga

The performance of the main pier at the north of the Lixouri port of Davgara (Fig. 8.2.2) varied from excellent to poor. Figure 8.2.36 illustrates the main pier and has annotated the regions that exhibited significant damage.

Figure 8.2.36. Temporary Exhibit to be replace with Google Earth view of the Davraga Main pier [to be added after text and remaining photos are finalized).

Images such as the one shown on Fig. 8.2.37 caught significant media attention. The main pier appeared to be largely undamaged following Event 1, but in some places suffered heavy damage during Event 2. The pier has been constructed in phases. As a result, different sections suffered variable levels of damage (Fig. 8.2.38 to 40), depending on the construction and geometric aspects of the pier. Surveying measurements have been performed and results are currently being processed by the UPatras team.

The largest outward displacement was observed in the main pier Davraga (Fig. 8.2.41 through Fig. 8.2.52). The initial portion of the pier, of about 50 m in length, exhibited the largest displacement of about 1.5 m. The following 50 m portion displaced much less, perhaps less than 0.5 m, apparently due to the much greater width of its blocks. Damage of this portion took place only on the south side, since the north side, which serves as breakwater, had a very shallow water depth and was supported by huge rock blocks (monoliths) playing the role of the tripods that are used in major breakwaters.

Given the large displacements observed at the surface, exceeding 1 m in several locations, and the large friction angles between blocks, it is likely that the base block translated horizontally and rotated away from the backfill by a significant amount. This mechanism is

consistent with observations of quay wall behavior under strong seismic shaking during previous events (Iai 2001, Dakoulas & Gazetas 2008). Whereas currently the relative amounts of translation and rotation cannot be precisely determined, an assumed rotation of the base block by about 10 degrees is considered sufficient to produce the observed displacement at the top. The rubble fill behind the wall certainly liquefied, but the contribution of the liquefied soil to the horizontal displacement of the quay wall is not clear, since the wall may have moved simply due to its substantial mass, and the potential for significant compliance/limited strength of the base material. Detailed measurements are required to assess the contribution of the various mechanisms to the observed response. It is noted that no simple design recommendations exist to date to limit the deformations of this particular type of structure to high levels of seismic shaking experienced during the recent events.

Cross-sections through the eastern-most (Fig. 8.2.50) and most recently constructed (in 2007) part of the main pier, whose locations are shown in Fig. 8.2.36, are shown in Figs. 8.2.53 to 8.2.56 (data provided by Kostas Rouchotas of NTUA and sketches developed by Adam Dyer of MRCE). The pier wall body consists of four blocks having total height of 7 m and width ranging between 5 and 6.25 m. The design incorporated standard features such as drainage, geotextile interfaces, rubble fill, etc.

Few years ago, the protection slab at the foot of the pier at its easternmost section was accidentally damaged by a jack up drilling vessel that penetrated 2 m under the slab and ruptured the geotextile, in an effort to keep the vessel stable during rough weather. The edge column in that location fell during the earthquake, but it is unknown to what extent failure is associated with this specific damage. Overall, however, this portion of the main pier has moved much less than the other sections of the pier.

Figure 8.2.37. Example of liquefaction damage and lateral spreading at the most damaged section of the main pier (38°12'5.12"N, 20°26'22.40"E).

Figure 8.2.38. Most damaged section of the main pier (38°12'3.32"N, 20°26'22.92"E).

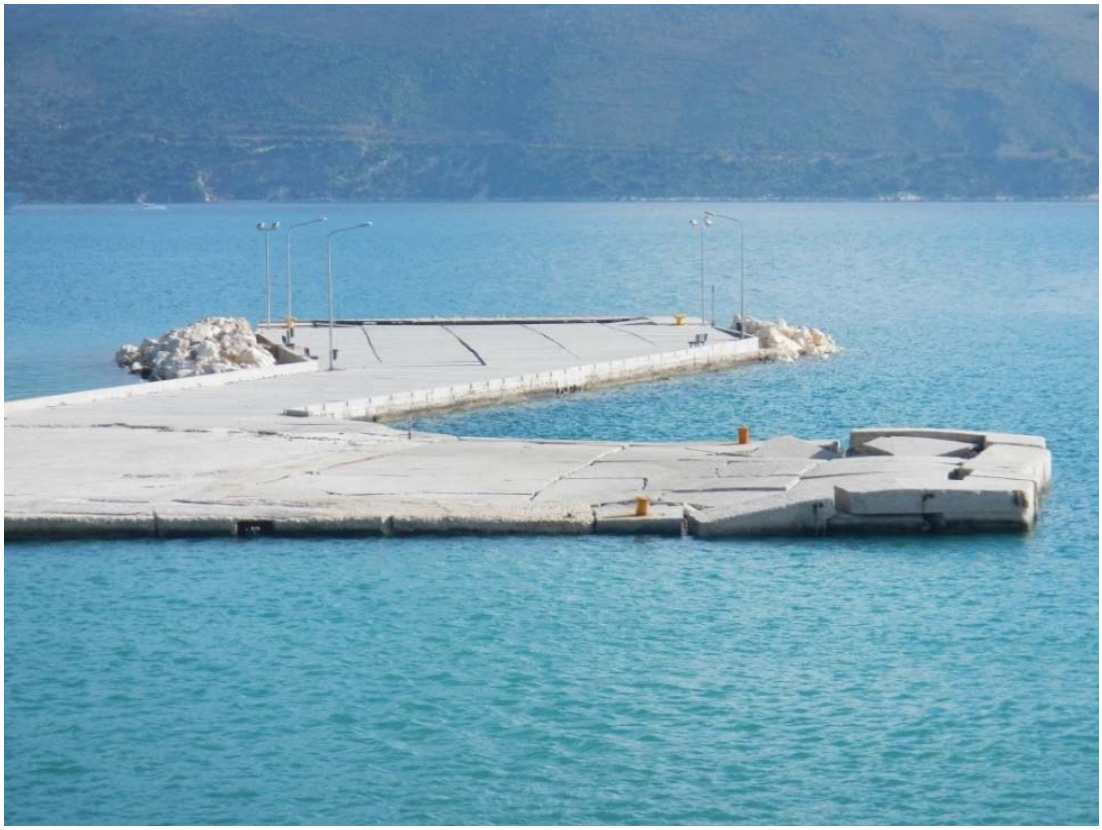

Figure 8.2.39. Another section of the damaged main pier (38°12'3.30"N, 20°26'23.02"E).

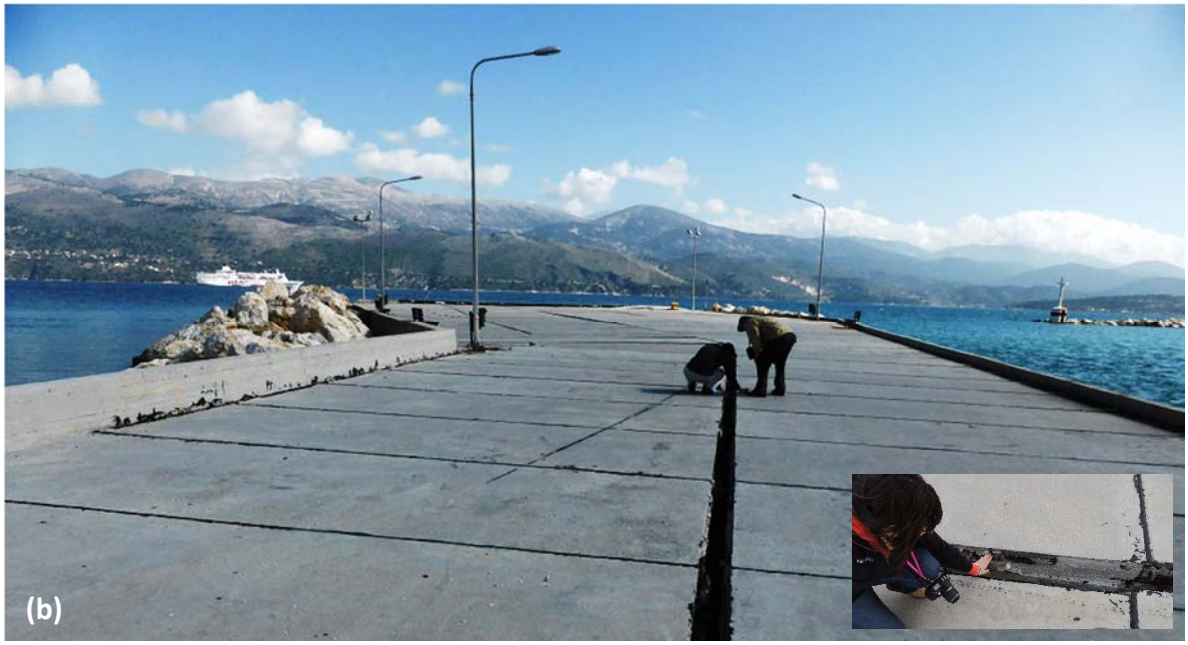

Figure 8.2.40. State of the main (Davraga) pier in Lixouri port): (a) Before the 2 events, from 2011 archives {www.panoramio.com/photo/59409701?source=wapi&referrer=kh.google.com}; (b) after the 2nd event (38°12'5.02"N, 20°26'21.73"E).

Figure 8.2.41. Damage of quay wall in Davraga pier. Sailboats overturned (GPS coordinates: 38.201050, 20.439297).

Figure 8.2.42. Lateral spreading and differential horizontal displacement along Davraga main pier wall. Note the different wall width shown with white arrows (GPS coordinates: 38.201436, 20.440202).

Figure 8.2.43. Horizontal displacement and rotation of wall of main pier (GPS coordinates: 38.201483, 20.439452).

Figure 8.2.44. Vertical settlement behind the wall of photo 8.2.43 (GPS coordinates: 38.201397, 20.439511).

Figure 8.2.45. Southern side of main pier, the only side where damage was observed. Presence of large monoliths at the northern side had a positive effect by restricting lateral movement (GPS coordinates: 38.201666, 20.440000).

Figure 8.2.46. Lateral movement is greater behind the narrower wall of the main Lixouri pier (GPS coordinates: 38.201466, 20.440158).

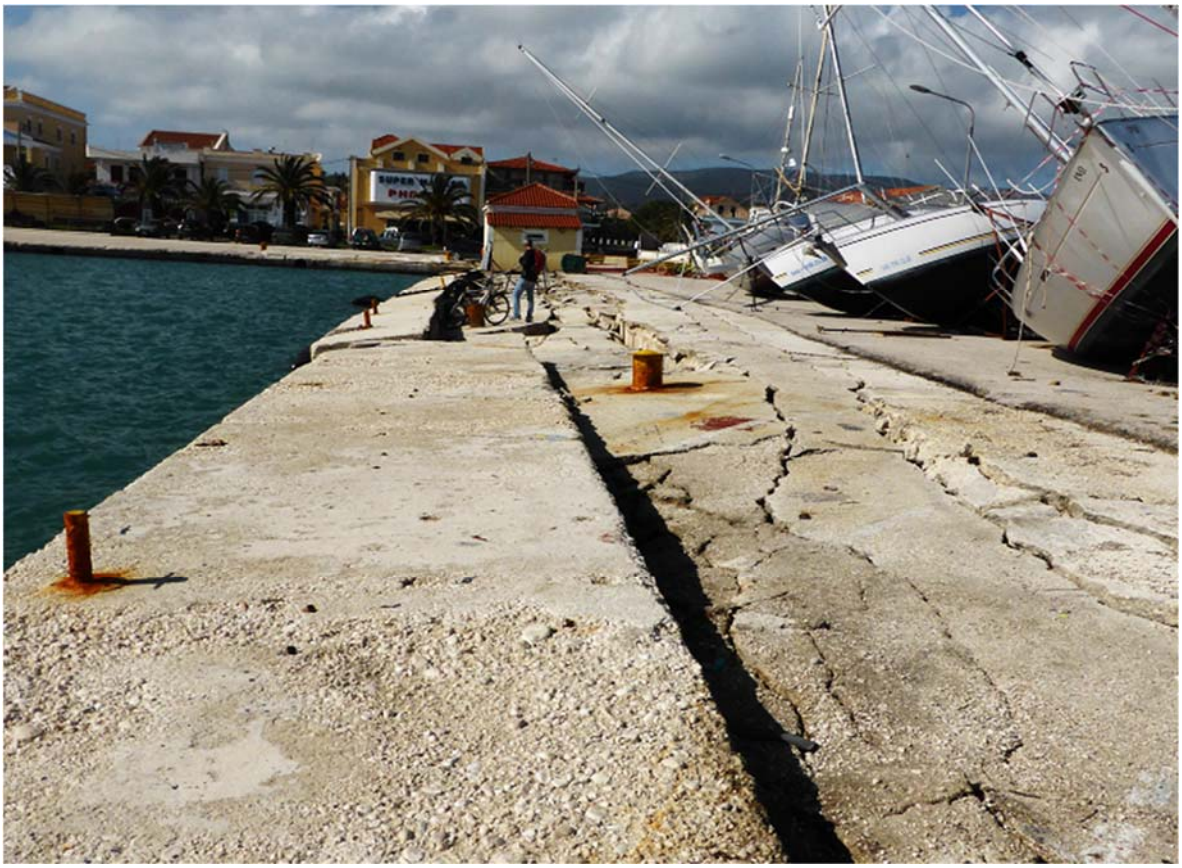

Figure 8.2.47. Cracks along main Lixouri pier dock surface (GPS coordinates: 38.201486, 20.441266).

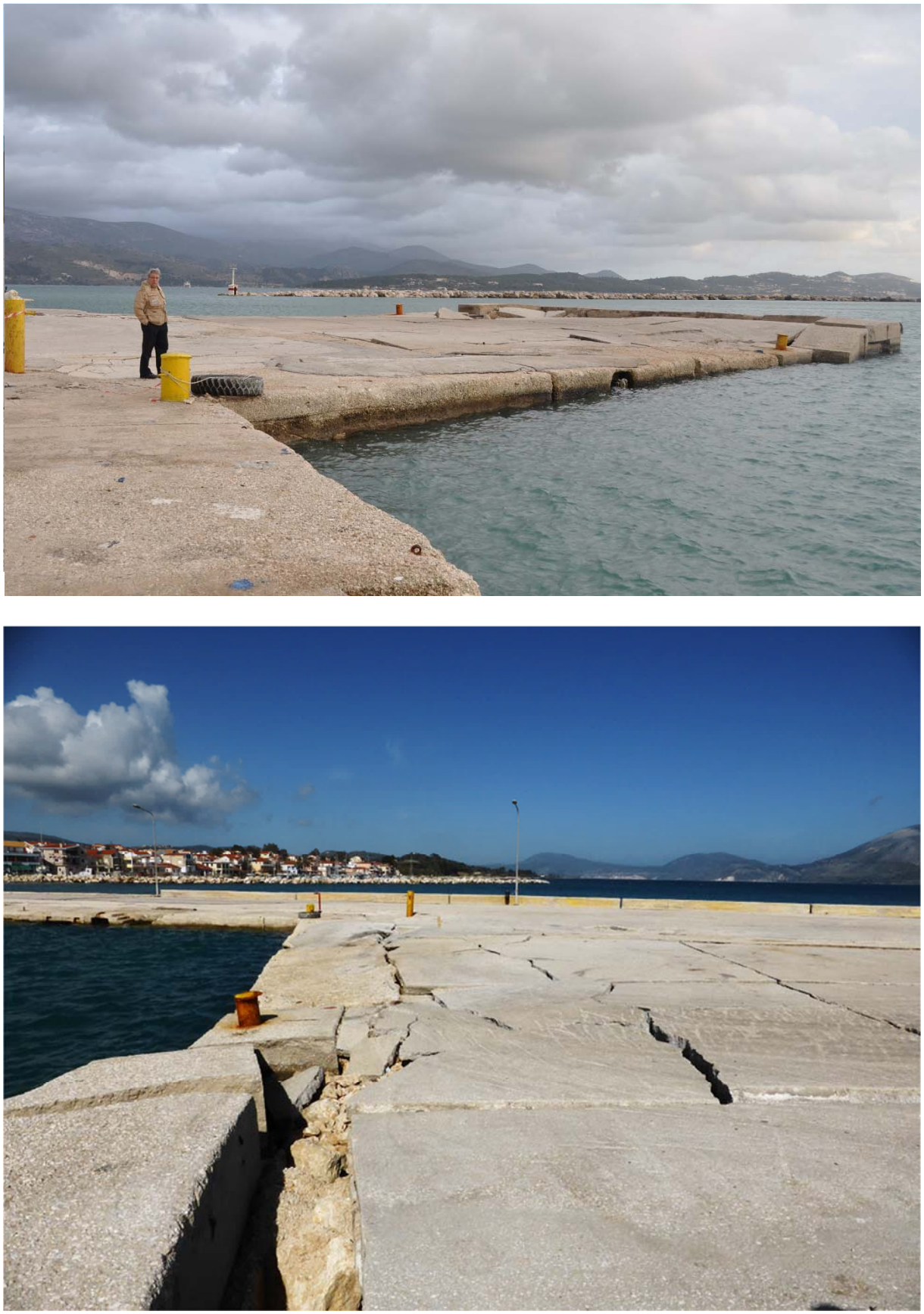

Figure 8.2.48. Rotation and lateral movement of main pier. Prof. G. Gazetas of NTUA shown on top photo (GPS coordinates: 38.201269, 20.440977).

Figure 8.2.49. Vertical displacement of main pier marked with yellow arrow (GPS coordinates: 38.201269, 20.440977).

Figure 8.2.50. Panoramic views of the eastern-most section of Davraga pier.

Figure 8.2.51. Main pier: (a) opening of horizontal joint; (b) monolith breakers constraining lateral movement; (c) concrete slabs settlement; and (d) detail of vertical settlement in yellow arrows (GPS coordinates: 38.201611, 20.442094).

Figure 8.2.52. State of eastern most section of main pier of Lixouri port: (a) from 2011 archives, {www.panoramio.com/photo/49466386?source=wapi&referrer=kh.google.com} with jack up drilling vessel that reportedly caused pier damage, and (b) after the 2nd event (38°12'6.14"N, 20°26'32.08"E).

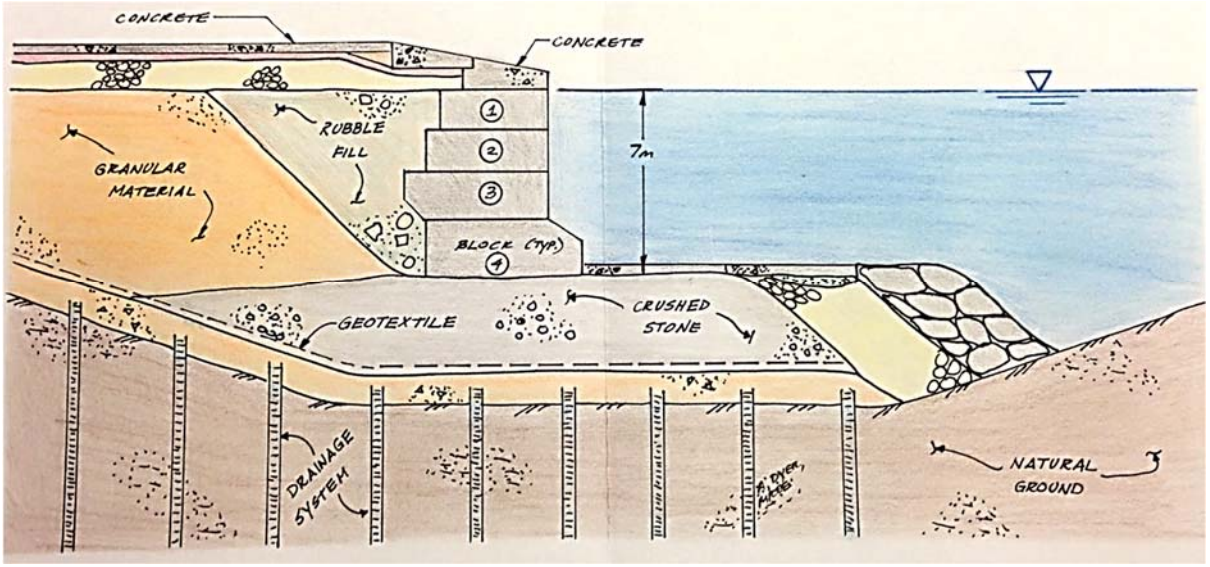

Figure 8.2.53. E-W cross section of eastern-most section of main pier of Lixouri Port. Data collected by Kostas Rouchotas of NTUA team. Sketch by Adam Dyer of MRCE.

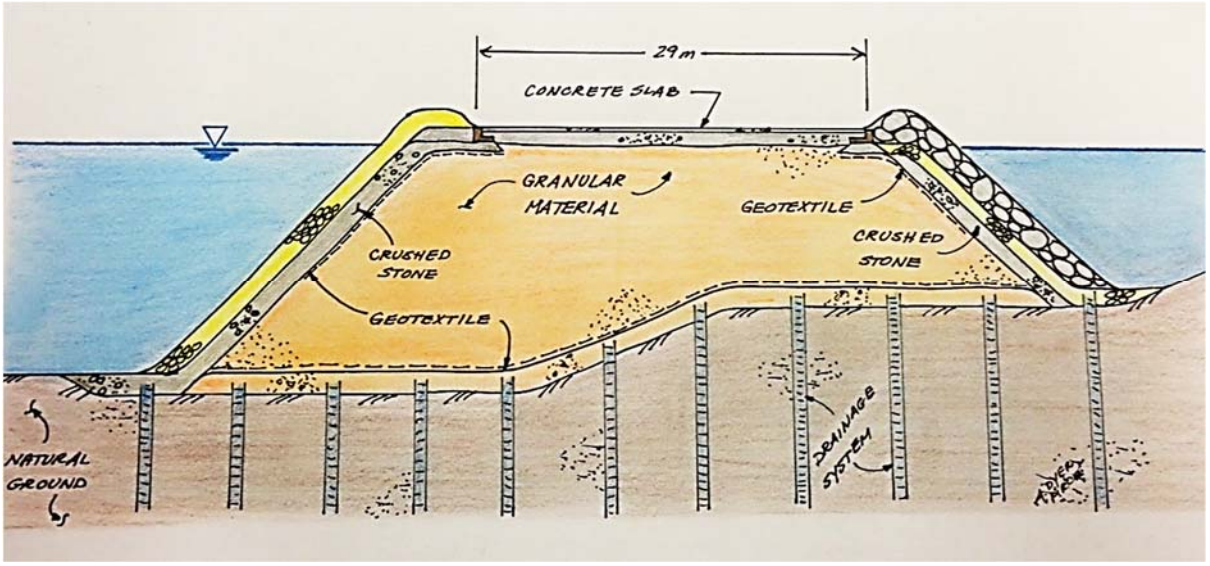

Figure 8.2.54. N-S cross section of eastern-most section of main pier in Lixouri Port. Data collected by Kostas Rouchotas of NTUA team. Sketch by Adam Dyer of MRCE.

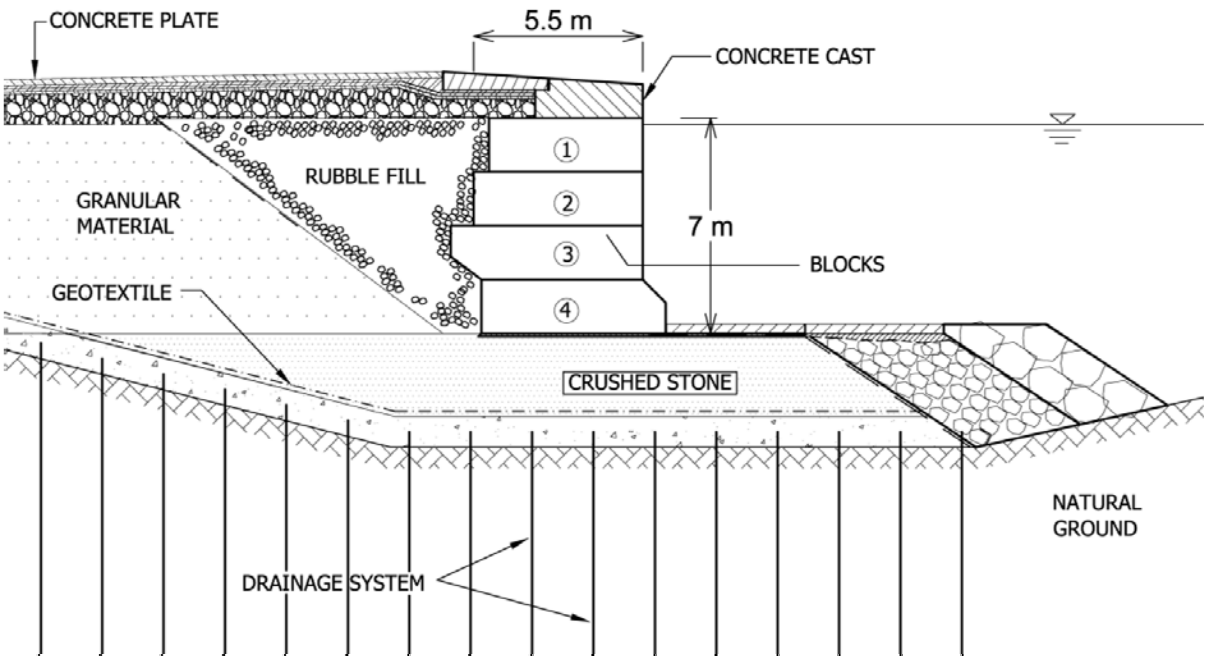

Figure 8.2.55. Detailed drawing of the sketch of Fig. 8.2.53 developed from data by Kostas Rouchotas of NTUA team showing E-W cross section of eastern-most section of main pier of Lixouri Port.

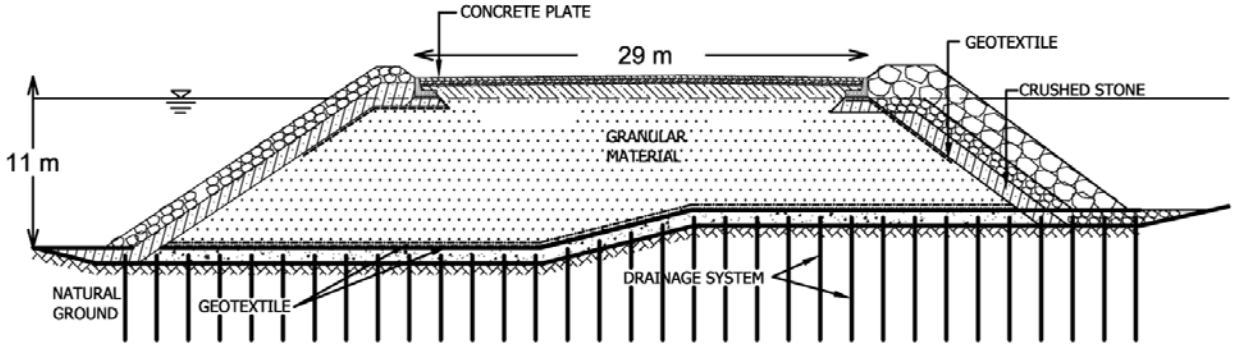

Figure 8.2.56. Detailed drawing of the sketch of Fig. 8.2.54 developed from data by Kostas Rouchotas of NTUA team showing N-S cross section of eastern-most section of main pier in Lixouri Port.

Lixouri South Pier and Lighthouse

The seismic settlement of the breakwater and lighthouse at the south entrance of the Lixouri port is also of interest. As shown in Figs. 8.2.57 to 8.2.60, the lighthouse and the supporting rip-rap appear to have settled. Discussions with the lighthouse operator, photos prior to the earthquakes, and measurements indicate that: (a) the lighthouse had been settling since its construction and (b) additional (currently unquantified) settlement took place during Event 2.

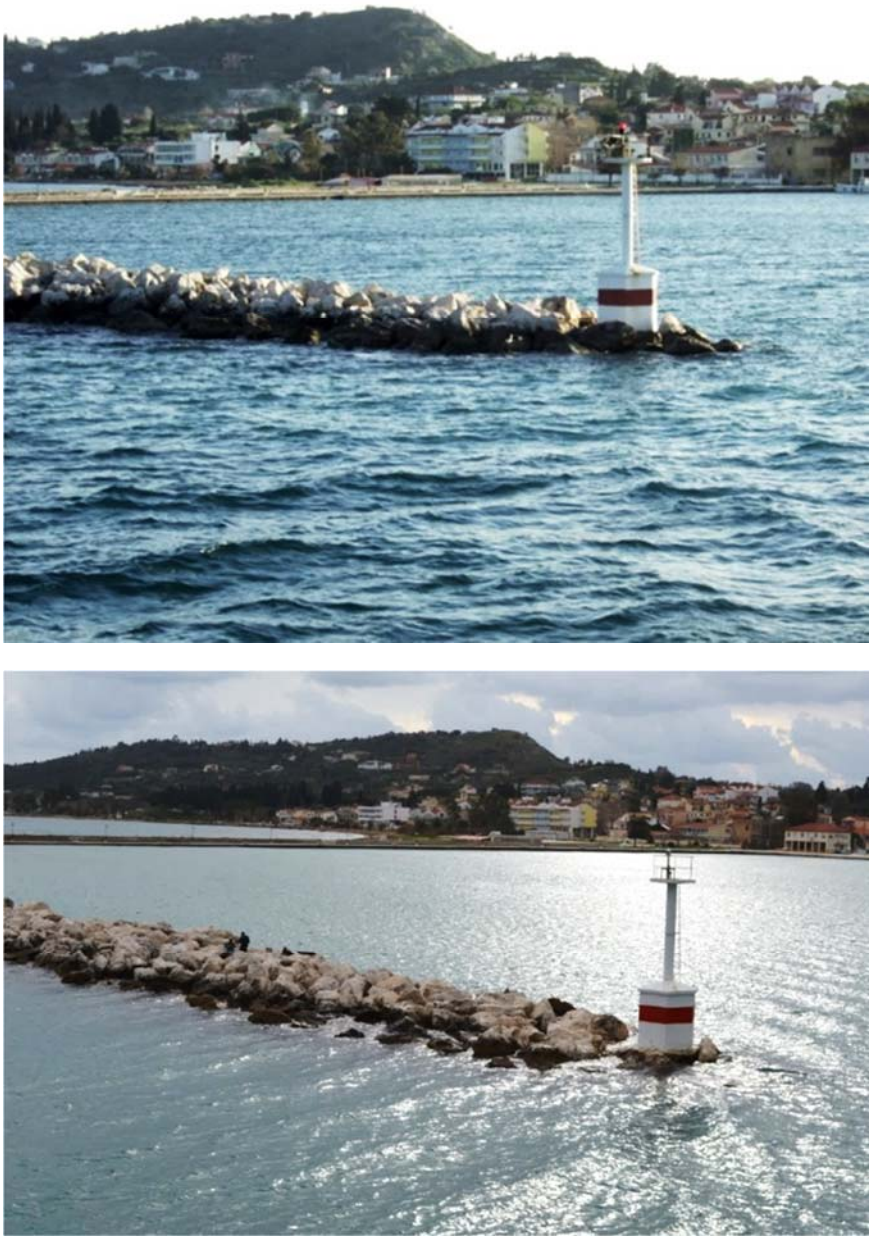

Figure 8.2.57. State of lighthouse at Lixouri breakwater tip: (a) from 2011 archive photo {www.panoramio.com/photo/50853069?source=wapi&referrer=kh.google.com}, and (b) after the 2nd event (38°12'3.70"N, 20°26'35.41"E).

Figure 8.2.58. View of breakwater with the lighthouse (left: 38°11'53.97"N, 20°26'22.06"E; right: 38°12'4.90"N, 20°26'37.09"E).

Figure 8.2.59. Detailed view of the light-house's settlement (a) From an online picture dated 5/8/09; and (b) after the 2nd event (GPS coordinates: 38.200897, 20.443222).

Figure 8.2.60. Light house settlement views (GPS coordinates: 38.200897, 20.443222).

The southern arm of the port serves as a small-boat marina and experienced from negligible to minor damage. As shown in Figs. 8.2.61 and 8.2.62, in the first part of this marina, the quay wall had neither cracks nor seaward displacement, apparently as a result of shallow water depth of less than 2 m. In the most damaged section part of the marina (Figs. 8.2.63 and 8.2.64), cracks appeared accompanying a 20 to 30 cm seaward displacement of the quay wall. The displaced main quay wall and the liquefaction of the fill over a substantial distance from it contributed to lateral spreading, and was demonstrated with cracks in the pavement and the sidewalks over a distance of 2 blocks (Fig. 8.2.65).

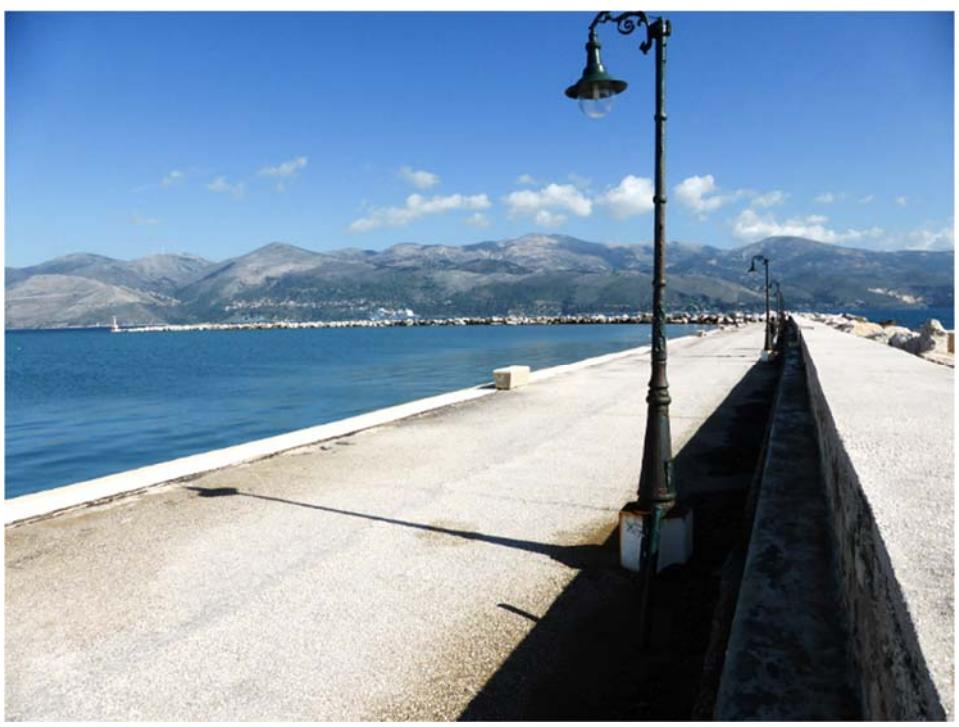

Figure 8.2.61. Southern part of Lixouri port that experienced only minor cracks (GPS coordinates: 38.197944, 20.441044).

Figure 8.2.62. Land reclamation on the outer side of the southern marina prevented lateral displacements of the shallow quay wall. The ejected liquefied soil on the reclaimed land is abundant (GPS coordinates: 38.197944, 20.441044).

Figure 8.2.63. Settlement of the coastal road and cracks on road surface (GPS coordinates: 38.198372, 20.439483).

Figure 8.2.64. Detailed views of the south part of Lixouri port: (a) and (b) minor cracks behind the wall, (c) shallow water level (GPS coordinates: 38.198158, 20.442222).

Figure 8.2.65. Sidewalk, pavement cracks and road settlement (GPS coordinates: 38.201102, 20.438855).

Some evidence of liquefaction was observed to the south of the port of Lixouri (Fig. 8.2.66), but is more limited. The limited number of liquefaction evidence may be attributed to a number of rainfall events that might have "washed away" the soil ejecta.

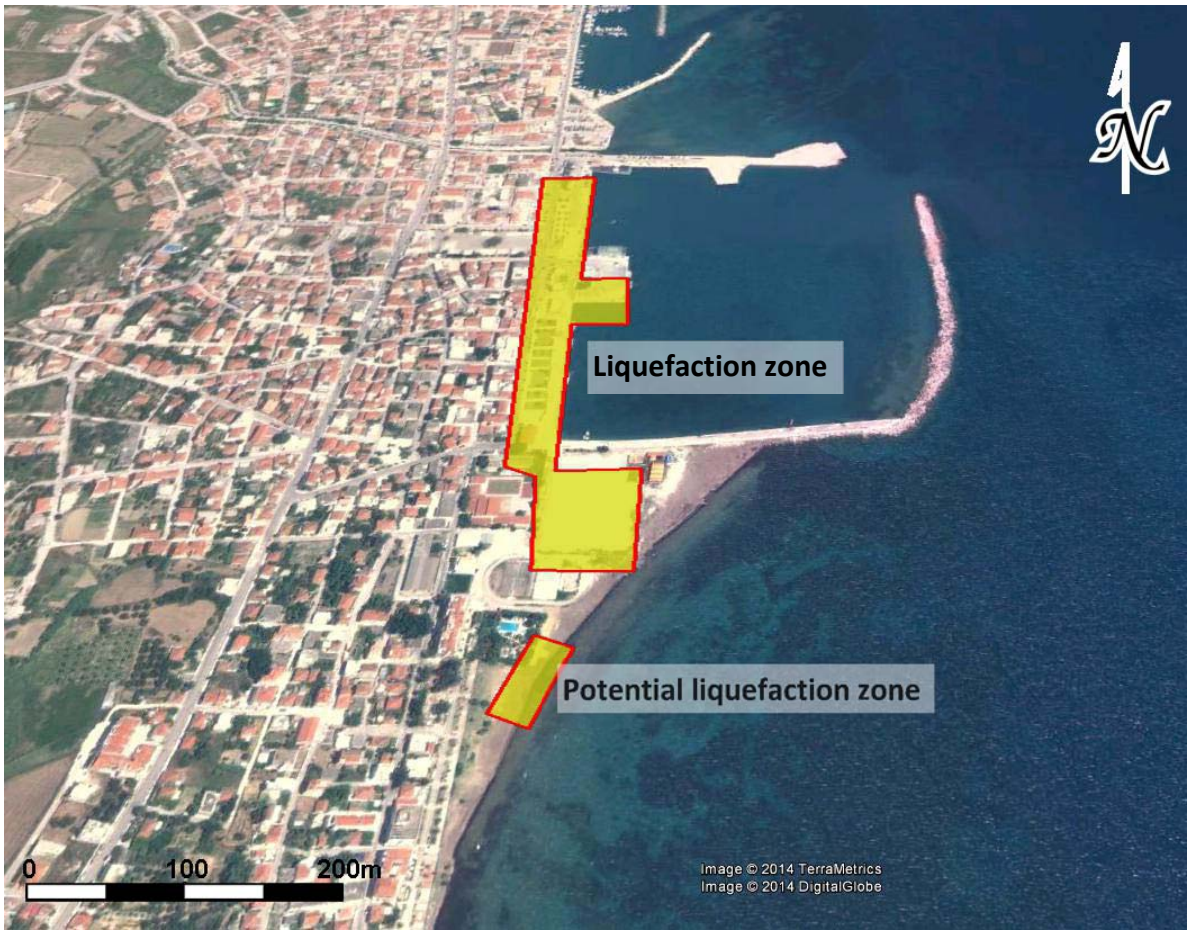

Figure 8.2.66. Liquefaction zones observed along Lixouri port (GPS coordinates 38.20^{o}, 20.44^{o}).

ARGOSTOLI PORT

Historical Information

Argostoli is Cephalonia's capital since 1757 (Fig. 8.2.67) with a population of 8,000 people, one-third of the island's inhabitants. Historically, it has been reported that the entire coastal area of Argostoli was destroyed (Figs. 8.2.68 and 8.2.69) following the catastrophic series of the 1953 earthquake events with magnitude M_s of 7.3 and modified Mercalli intensity of IX-X (Stiros et al., 1994, and Papagiannopoulos et al., 2012.)

Figure 8.2.67. Old painting of Argostoli port, ca. 1757 (ref: Wikipedia).

Figure 8.2.68. Argostoli port after the 1953 earthquake, looking west from above the town bridge (Bittlestone, 2005).

Figure 8.2.69. Argostoli quay wall damage after the 1953 event (Papathanassiou & Pavlides, 2011).

The port was rebuild through reclamation of the sea using fill materials that were, to a large extent, debris of collapsed or demolished masonry buildings (Fig. 8.2.67). New construction on the reclaimed land zone used mostly reinforced concrete mat foundations (thickness ~ 0.60 m) with a foundation depth of probably not more than 1.5 m.

Liquefaction Observations

Following the 2014 earthquake events, the Argostoli port (Fig. 8.2.70) and adjacent coastline experienced liquefaction and lateral spreading. The town's waterfront is approximately 1.1 km in length. Soil liquefaction was observed throughout the Argostoli waterfront, most evident in particular areas. In general, the damage in the Argostoli port was less severe than the damage in the Lixouri port, which was closer to the earthquake epicenter. Liquefaction was manifested by soil craters and ejecta, and cracks in paved surfaces surrounded by large amounts of ejecta (Fig. 8.2.71). No signs of liquefaction were observed beyond an inland distance of 100 m from the waterfront.

Figure 8.2.70. Panoramic view of the Argostoli port following the two 2014 seismic events.

Figure 8.2.71. Examples of soil craters and ejecta along the waterfront of Argostoli port GPS coordinates a-(38.18105°, 20.48955°), b-(38.118118°, 20.48954°), c-(38.180752°, 20.489990°), d-(38.17118°, 20.49600°)].

Photos of liquefaction manifestation surrounding the customs building in the Argostoli port is shown in Fig. 8.2.72 through Fig. 8.2.75. One of the accelerograph stations installed after the 1st event, on January 30th 2014, in the region by the Geotechnical Engineering Laboratory of UPatras was placed inside the Customs Building of Argostoli, in close proximity to observed liquefaction triggered by the 1st event. This instrument recorded the 2nd event, which caused more extensive soil liquefaction at the same location (Fig. 8.2.72). This location represents an interesting case of re-liquefaction, similar to the cases described in the 2010-11 New Zealand earthquakes (GEER, 2011). The availability of recorded horizontal surface acceleration in the vicinity of soil liquefaction, combined with site characterization data, has the potential to generate another well-documented case history of soil liquefaction (Batilas et al., 2014).

Figure 8.2.72. Ejecta material outside the Customs Building of Argostoli where the UPatras Geotechnical Engineering Laboratory strong motion station is located [GPS coordinates: a: (38.18010°, 20.48993°), b: (38.17998°, 20.48996°)].

Figure 8.2.73 presents evidence of ejecta in the area of the Port Authority complex of Argostoli, where the abundance of gravel and the existence of even small cobbles (maximum diameter of 3 cm) was observed. This is not typical for ejecta, which usually consist of finer particles. However, it is not clear at this point, whether the gravelly soil did indeed liquefy or if the gravelly particles were ejected out under the high water pressure. In any case, these particle sizes are very uncommon for ejected material.

Figure 8.2.74 presents evidence of the maximum height of ejected soil-water mixtures in the perimeter of one the Port Authority complex buildings at Argostoli. The measurement reads clearly a height of 35 cm of ejecta, with finer soil mark evidence reaching a height of 50 cm, indicative of the high pore water pressures.

Figure 8.2.73. Evidence of ejecta in the Port Authority building area at Argostoli (38°10'47.85"N, 20°29'24.42"E).

Structural Settlements

Evidence of rigid body rotation due to differential liquefaction-induced settlements is presented in Fig. 8.2.75 for a single story R/C frame building at the Port Authority complex in Argostoli. The settlement is greater towards the sea (i.e., to the east), and led to rigid body rotation of about 1° without causing structural damage. Additional settlement observations are discussed in the Settlement and Soil-Structure Interaction section of this chapter.

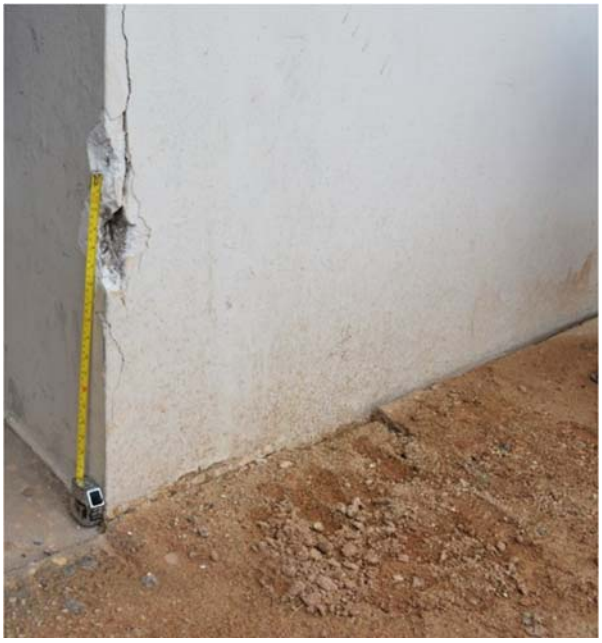

Figure 8.2.74. Evidence of maximum height of ejected soil-water mixtures against the wall of a Port Authority building at Argostoli (38°10'47.50"N, 20°29'23.43"E).

Figure 8.2.75. Rigid body rotation of a single story R/C frame building (at left) due to differential liquefaction-induced settlements at Port Authority complex in Argostoli (38°10'47.91"N, 20°29'23.47"E): (a) view towards the south, (b) view towards the north.

Lateral Movements

As a result of soil liquefaction and the presence of a free face, large cracks opened in the port area of Argostoli as well as along the asphalt-paved coastal street of the town. The cracks were, in general, parallel to the waterfront and their widths decreasing with increasing inland distance from the waterfront. No signs of surface cracking were observed beyond the first row of buildings adjacent to the coastal street. Measurements of crack widths were performed along several cross-sections, perpendicular to the waterfront and the total displacement was recorded.

Significant lateral movements, extensive cracking and joint openings were observed especially in the large dock of Argostoli port (38.181°, 20.489°), as shown in Fig. 8.2.76. The length and the width of dock are approximately 210 m and 80 m, respectively. The maximum lateral displacements was observed along line A-A' and was about 9 cm. At the north side of the dock, the lateral displacement was approximately 6 cm while at the south was about 16 cm. Fig. 8.2.77 through Fig. 8.2.80 illustrate the damage, and the measurements performed.

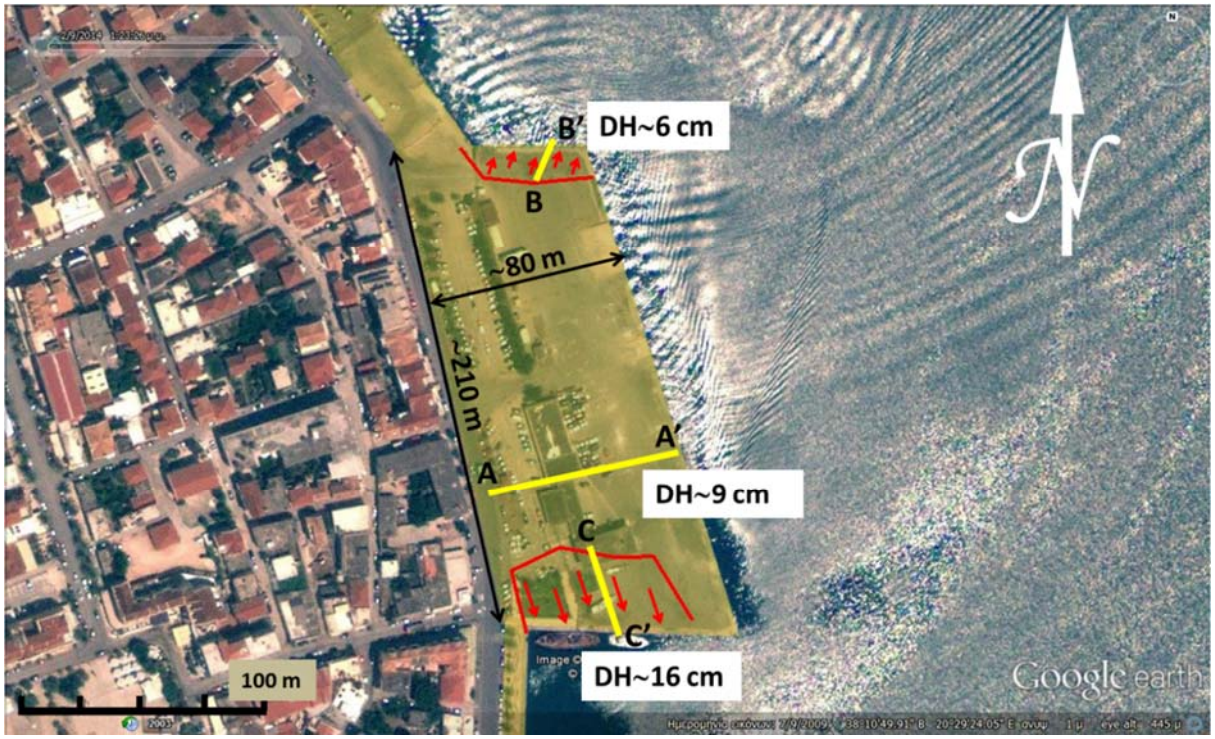

Figure 8.2.76. Google Earth photo of the central dock of Argostoli port. Red arrows indicate development of excessive cracking and lateral spreading.

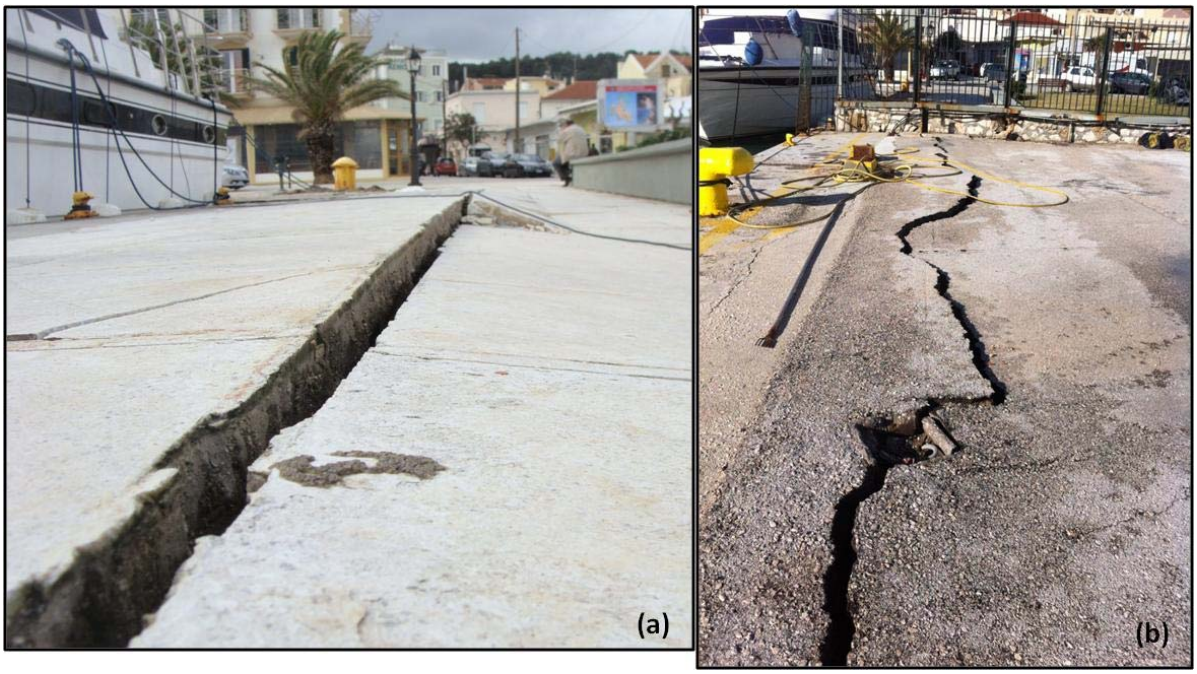

Figure 8.2.77. Quay wall at dock of Argostoli port: (a) wall outward movement and (b) cracks due to lateral spreading dated 2/9/14. GPS coordinates: a-(38.17955°, 20.48987°), b-(38.17955°, 20.49011°).

Figure 8.2.78. Outward movement of quay wall and vertical displacement in front of the main Argostoli port dock measured by Tasos Batilas of UPatras (GPS coordinates 38.18024°, 20.49034°, 9/2/2014).

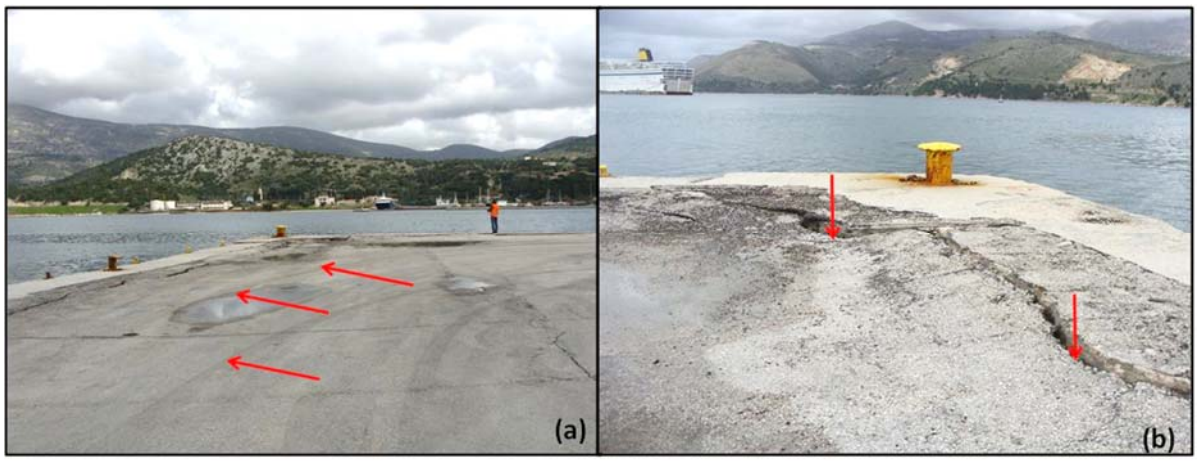

Figure 8.2.79. (a) Photograph of lateral movement and (b) settlement of ground behind the quay wall (GPS coordinates 38.18137°, 20.48980°, 9/2/2014)

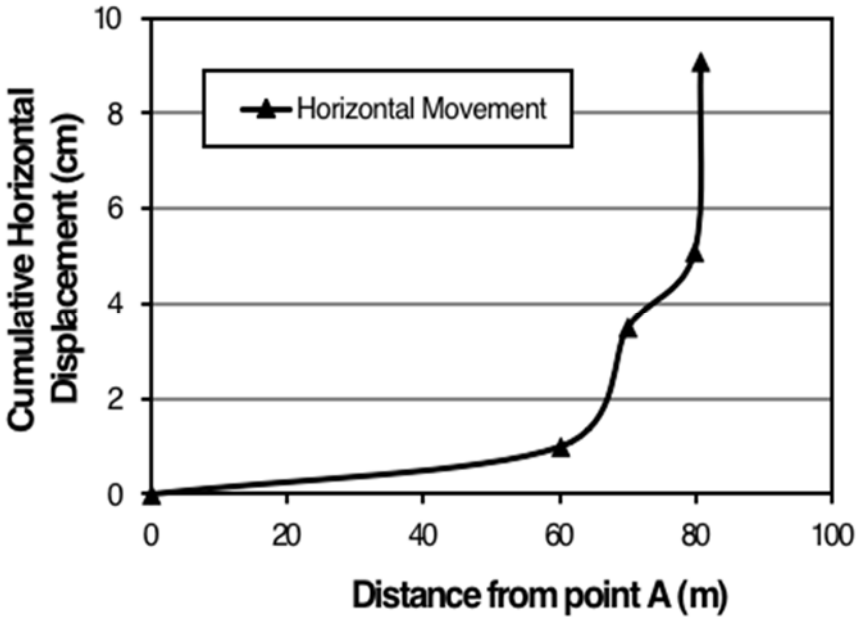

Figure 8.2.80. Argostoli port cumulative horizontal displacement vs. distance from A (see Fig. 8.2.75).

Liquefaction and damage associated with lateral movement of the seafront was also observed beyond the central dock, as shown in Fig. 8.2.81, and measurements have been collected. The port quay wall displaced about 10 cm on average, creating a gap and separating from the sidewalk, as shown in Figs. 8.2.82 through 8.2.84. The performance of the port quay wall can be considered satisfactory given the PGA (Peak Ground Acceleration) levels in excess of 0.35g that was recorded at the Customs building of the port.

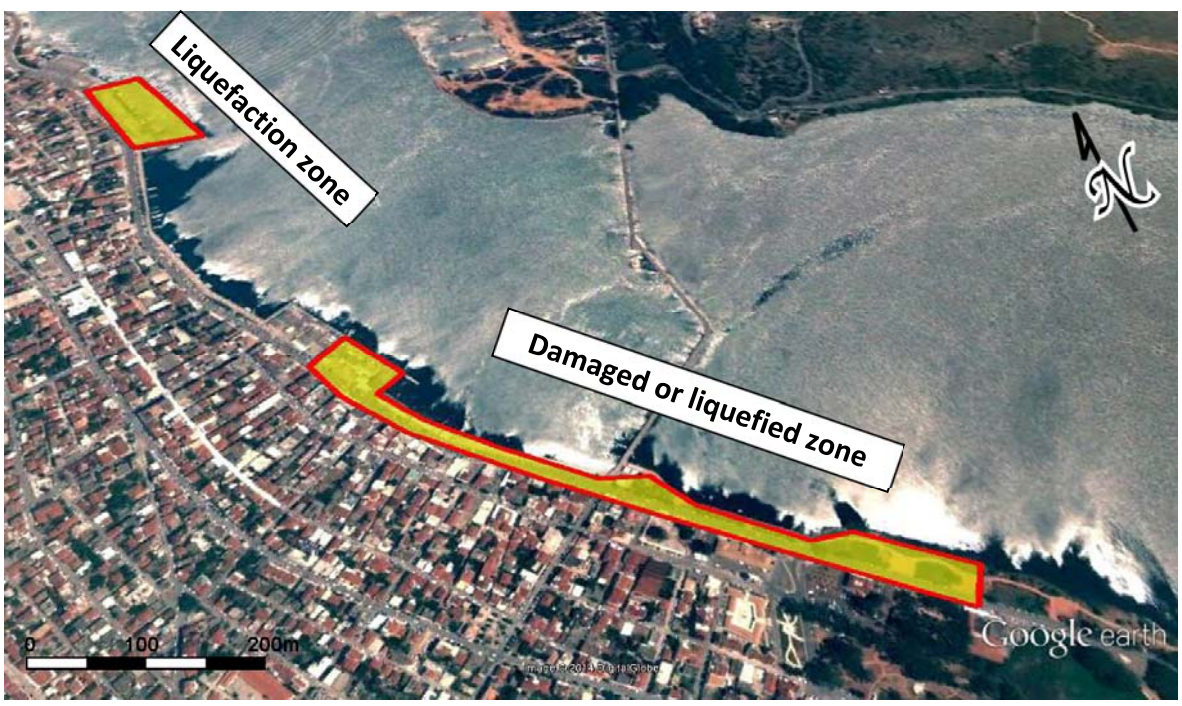

Figure 8.2.81. Liquefaction observations at Argostoli coastal area (GPS coordinates 38.17°, 24.49°).

Figure 8.2.82. Quay wall view south of the Argostoli Port Authority building complex: (a) from 2011 archives {www.panoramio.com/photo/57109645?source=wapi&referrer=kh.google.com} and (b) after the 2nd event (38°10'45.96"N, 20°29'22.51"E).

Figure 8.2.83. Minor displacement of quay wall (GPS coordinates: 38.176938, 20.490008).

Figure 8.2.84. (a) Vertical settlement of the backfill soil and (b) signs of liquefaction on the road surface (GPS coordinates: 38.179525, 20.489597).

Underwater Surveying

An underwater camera survey conducted following the earthquakes in the Lixouri and Argostoli ports (provided by team member Kostas Rouchotas of NTUA), identified that the quay wall blocks were as far as 30 cm apart (see Figs. 8.2.85 and 8.2.86), significantly higher than the general acceptable range for seismic design between 2 and 5 cm.

Figure 8.2.85. Underwater view of a 30-cm gap between blocks in Argostoli quay wall.

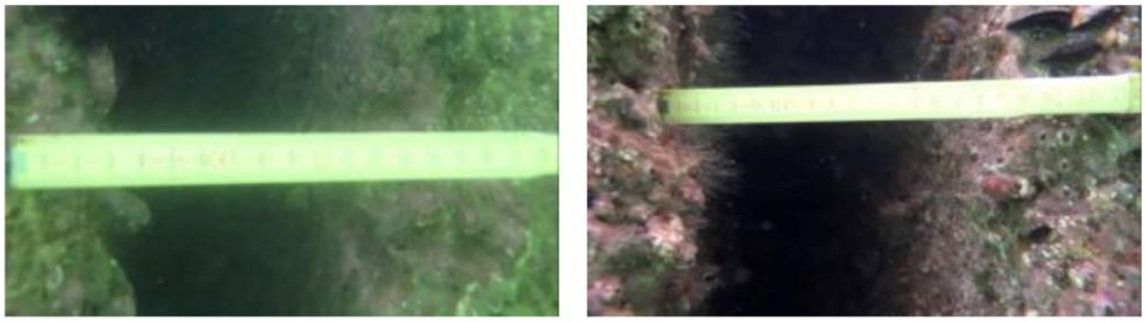

Figure 8.2.86. Underwater view of 20-cm gaps between blocks in Argostoli quay wall.

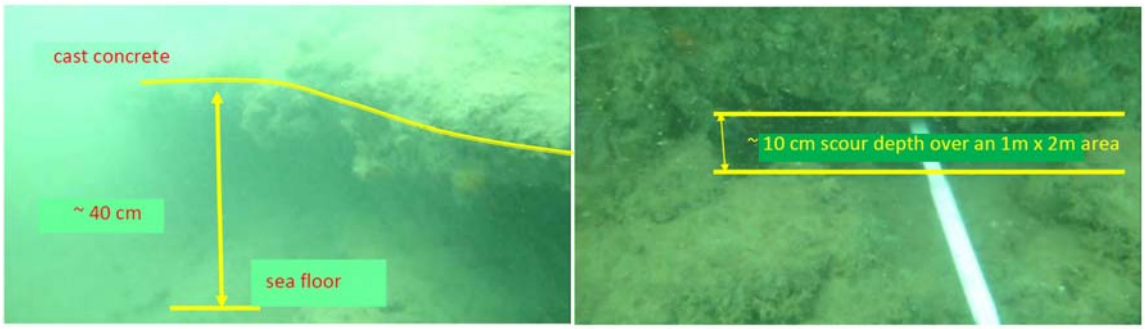

Figure 8.2.87. Underwater view of scour under base block in Argostoli quay wall.

Granular material from the backfill may have passed through these gaps and gradually washed out, generating cavities in the retained mass that were stable under static conditions possibly due to soil arching, but collapsed during earthquake shaking. It is also likely that during the earthquake shaking, the high pore pressures generated in the liquefied soil backfill were released through these openings. This mechanism would explain the settlement of the backfill immediately adjacent to these blocks and the lack of sand boils on the ground surface. In addition, block movements in the two ports were apparently aggravated due to the surveyed scour depth of 10 to 20 cm, extending as far as 1 m under the base blocks (Fig. 8.2.87).

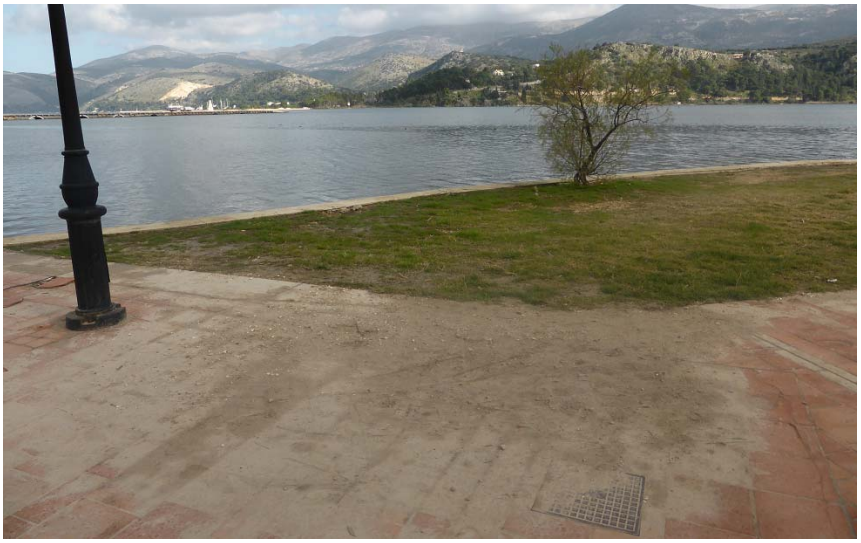

Figure 8.2.88. Visible evidence of soil liquefaction at southeast part of Argostoli port (GPS coordinates: 38.171197, 20.495725]

Liquefaction was also evident on the ground surface on the south coast where the water depth is of the order of 1 m, and the wall hardly displaced at all. The consequences were not significant (Figs. 8.2.88 through 8.2.90).

Figure 8.2.89. Sand boils on the free surface, southeast part of Argostoli port (GPS coordinates: 38.171100, 20.495930).

Figure 8.2.90. Sand boils on the free surface in the southeast part of Argostoli port (GPS coordinates: 38.171166, 20.496000).

PORT OF SAMI

The effects of earthquake shaking during both events in Sami port, at an epicentral distances greater than 25 km, were less severe to those observed at the Lixouri and Argostoli ports that were closer to the epicenters (less than 10 km). Minor damage was observed in the yellow-shaded areas of Figure 8.2.91.

Figure 8.2.91. Port of Sami. Detailed damage shown on Fig. 8.2.92 for the area in lower annotated circle, and in subsequent figures for the upper circle area which experienced more significant damage.

Figure 8.2.92. Post-earthquake damage observation in the lower annotated circle area of Fig. 8.2.91 at the Sami port.

Liquefaction-induced phenomena were not clearly observed in the port area of Sami. Only minor displacements, opening of joints between concrete pier blocks and formation of new cracks associated with settlement of pier blocks were observed and traces of what appeared to be minor soil liquefaction (Figs. 8.2.91 to 8.2.94). Possible evidence of ejecta may have been washed out due to significant rainfall in the days preceding the reconnaissance in this area.

Figure 8.2.93. Crack following the 2nd event at Sami port main pier (38°15'14.97"N, 20°38'50.56"E).

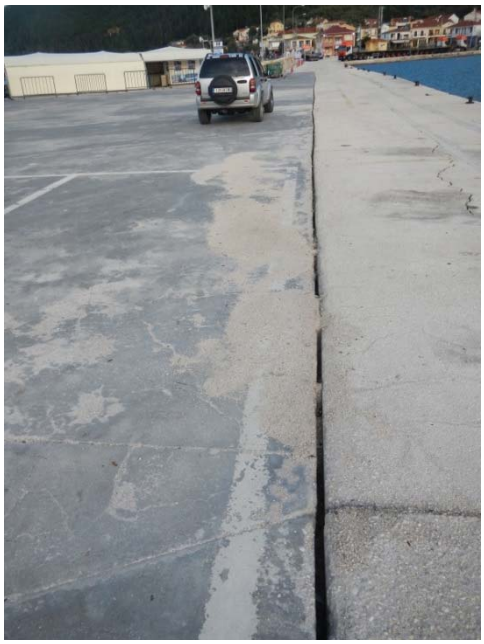

Figure 8.2.94. Joint opening between blocks at Sami port pier with possible ejected sandy soil material at the deepest water area of the pier. This was the only location where these questionable sandy ejecta were identified (38°15'14.93"N, 20°38'51.60"E).

BROADER PALIKI PENINSULA

Scattered limited liquefaction phenomena were identified at three locations of Paliki peninsula:: (i) a sand crater with diameter less than 5 cm in a stream bank that crosses plio-pleistocene sediments was observed in Soulari (Fig. 8.2.95); (ii) brown coarse sandy material ejected through a crack at the edge of a paved road in Kounopetra of south Paliki peninsula (Fig. 8.2.96a); and (iii) a small amount of coarse sandy material ejected through a fissure with width less than 2 cm inside a field between the villages of Atheras and Livadi (Fig. 8.2.96b).

Figure 8.2.95. Evidence of liquefaction in Soulari (38,18996; 20,41198).

Figure 8.2.96. (a) Evidence of liquefaction in Kounopetra (38,15726; 20,38534). (b) Ground cracking with limited evidence of sand boils in a field between Atheras and Livadi (38,298547; 20,418600).

CONCLUSIONS

Widespread soil liquefaction and re-liquefaction occurred in the coastal zones and ports of Lixouri and Argostoli, as a result of earthquake shaking in both events 1 and 2, and was documented by the reconnaissance teams in this section. Damage in the port of Lixouri was more severe than the damage in the port of Argostoli. The observed difference in performance can be partially attributed to the distance from the epicenters and the shaking intensity. Liquefaction in the Lixouri port was abundant in the top backfill, which is made of sand with gravels and occasionally, boulders. Liquefaction contributed to the quay wall displacement and was accompanied by lateral spreading. Lateral spreading towards the sea direction together with the inertia sliding of the blocks constituting the quay wall and the differential settlement at the base of the quay wall resulted in a total seaward displacement exceeding 1.5 m in Lixouri. The outward differential displacement of the quay wall in Argostoli was significantly lower. The other two ports of Sami and Poros did not suffer significant damage. Very minor damage was observed in the port of Sami, located about 25 km from the epicenter of the 2nd event, and no damage in the port of Poros, which was located 35 km from the epicenter. Liquefaction boils and ground failure probably associated with liquefaction was also observed away from Lixouri in three locations in the Paliki peninsula.

8.3 Earth Retaining Structures

INTRODUCTION

The response of earth retaining structures subjected to strong ground motions has been the subject of several case studies and growing evidence of good performance has lately accumulated (Lew et al. 2010). In addition, recent experimental and numerical parametric studies (Al-Homoud and Whitman 1999, Gazetas et al. 2005, Lee 2005, Al Atik and Sitar, 2010, Athanasopoulos-Zekkos et al. 2013) have demonstrated that, at least in the case of yielding retaining walls, the large phase difference developed between the wall inertial force and dynamic increment of earth pressure, may be the main factor contributing to their satisfactory field response.

OVERVIEW OF RETAINING WALLS IN CEPHALONIA

The majority of earth retaining structures in Cephalonia is masonry, or even dry-stacked, retaining walls ranging in height from 1.0 m to 5.0 m and used to support roadway cuts and backfills adjacent to commercial or residential buildings. A smaller number of concrete walls (of gravity or cantilever type) have also been used in newer construction. Retaining walls of both types were subjected to strong ground motions during the two main earthquake events of January 26 and February 3, 2014. Their response varied based on their distance from the epicentral area and type. Stone masonry walls were in general more vulnerable compared to concrete walls with a typical damage pattern being out-of-plane collapse, away from the backfill. The stone masonry walls were typically made of limestone blocks with varying quality of construction. In some cases the limestone blocks were simply dry-stacked, whereas in other cases, different amounts of cement was used. Thus, besides the significant earthquake-induced earth pressures and accelerations imposed on these walls, possible structural deficiencies and poor condition of cement should be considered in interpreting the observed damages. Some characteristic case histories of performance are presented in detail in the following.

This section summarizes reconnaissance observations made by the UPATRAS, NTUA, ITSAK, DUTH, AUTH-LSDGEE and UTH teams during the periods of 27-30 January, 4-5, 8-12, 18-20 and 22-23 February of 2014. A total of 36 seismically-induced failures on retaining walls were recorded mainly in the Paliki peninsula after the 1st event (EPPO-ITSAK, 2014) and the 2nd event. The spatial distribution of recorded failures is shown on Fig. 8.3.1.

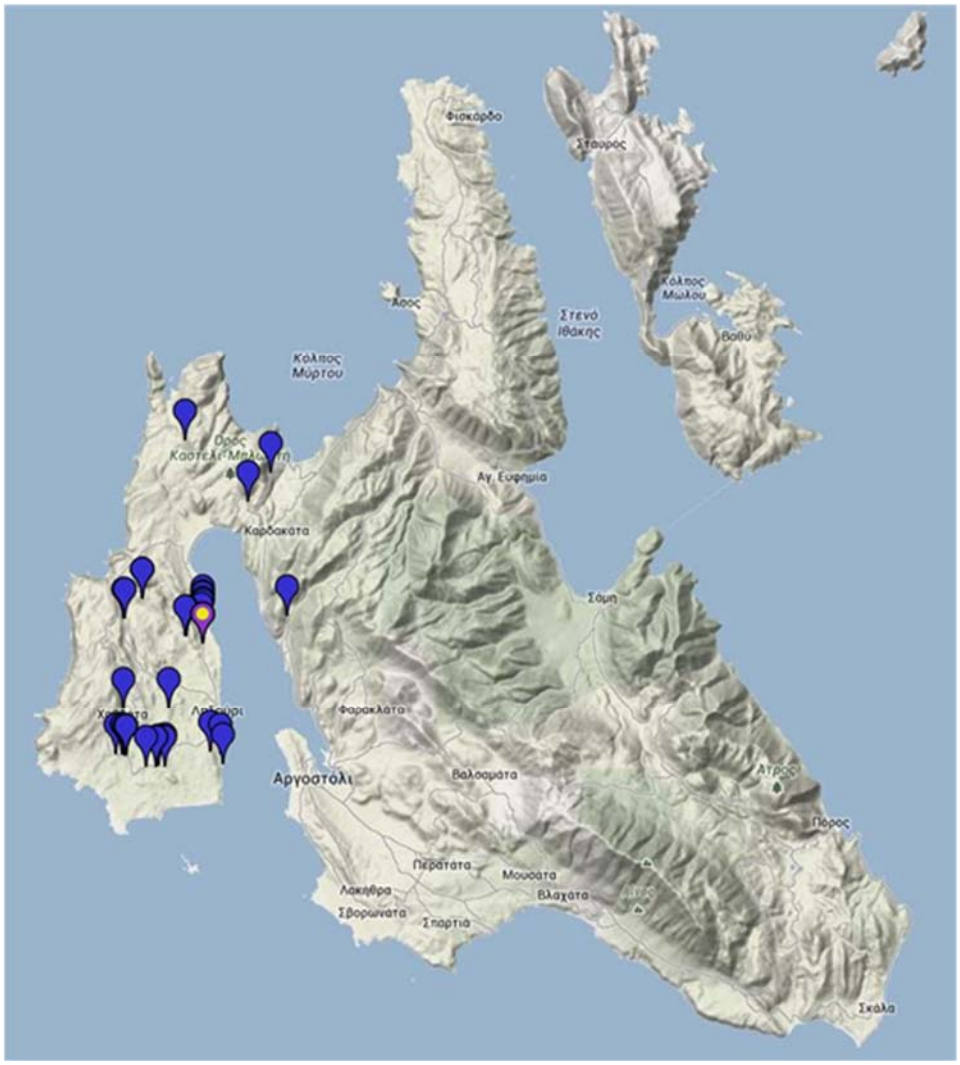

Figure 8.3.1. Geographical distribution of 36 retaining wall failures following the 1st and 2nd events. Original figure shows stone masonry retaining walls *(to be updated in next version).*

MASONRY EARTH RETAINING WALLS

A multi-tiered wall supporting a backfill in Chavriata village is shown in Fig. 8.3.2 with a schematic in Fig. 8.3.3. The Panayia Agriliotissa church was partially supported by the backfill. Fig. 8.3.2a depicts the condition of the wall prior to the 2014 earthquakes from a 2007 archive. The three-tiered wall sustained some damage during the 1st event (Fig. 8.3.2b) and was significantly damaged and actually collapsed during the 2nd event (Fig. 8.3.2c). As a result, lateral displacement and settlement of the backfill retained by the wall resulted in heavy damage of the church. This retaining wall is in close proximity (about 200 m) to a strong motion instrument that recorded a peak horizontal ground acceleration PGA of ~0.74 g during the 2nd event. Fig. 8.3.4 and 8.3.5 are close-up views from the southwest and south, respectively.

Figure 8.3.2. Retaining wall and historical church at Chavriata village: (a) before the 2 events, (b) following the 1st event; and (c) following the 2nd event; (38°10'57.52"N, 20°23'13.61"E). Photo (a) is from 2007 archives: www.panoramio.com/photo/50007113?source=wapi&referrer=kh.google.com

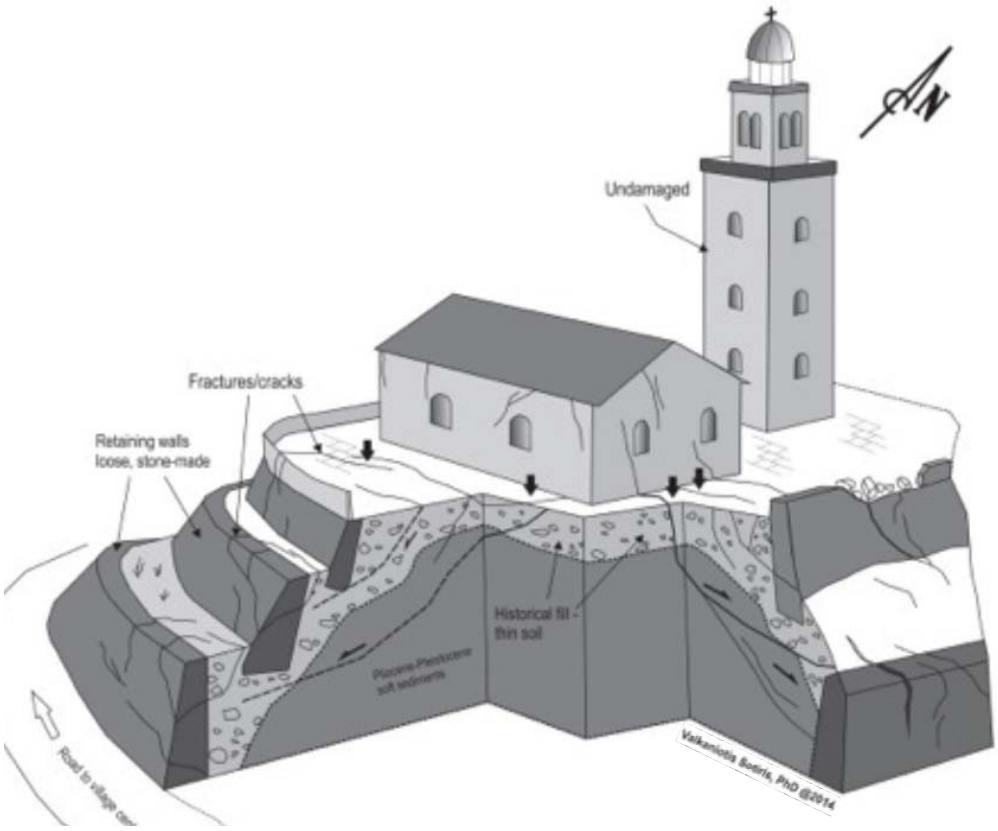

Fig. 8.3.3. Schematic of the Panayia Agriliotissa Church, prepared by S. Valkaniotis (modified from Papathanasiou et al., 2014).

Of interest is also that immediately downhill of the failed multi-tiered masonry wall of Figures 8.3.2 to 8.3.5 are two approximately 5-m high masonry walls with significant cement between blocks that responded much better to the two events, despite being subjected to the same intense shaking (Fig. 8.3.6).

As shown in Figure 8.3.6b, the first wall, in the foreground, is directly downhill the failed multi-tiered masonry wall (note its debris to the right), while the second one, in the background, starts at this location and is running towards the west, in parallel, but further to the west of the wall in the foreground. The second wall displaced horizontally and as a result a longitudinal crack to the pavement was observed. This wall is quite long, and its behavior further to the west of the church is presented in the section of concrete retaining walls below. The longitudinal crack also continued behind the first wall with smaller dimensions.

Figure 8.3.4. View of the retaining wall and church (a) from the southwest; and (b) from the south following the 2nd event (38°10'57.52"N, 20°23'13.61"E).

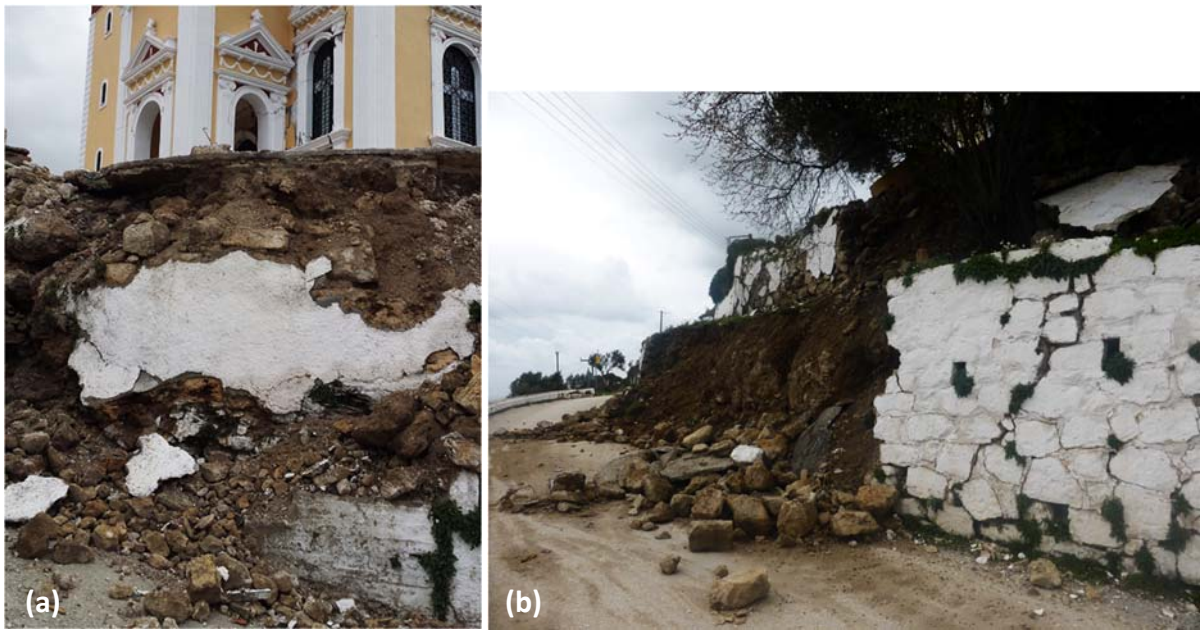

Figure 8.3.5. Closer views of the damaged wall (GPS coordinates: 38.182500, 20.387222).

Figure 8.3.6. View of the masonry retaining wall, just downhill of the three-tiered plastered masonry wall in Chavriata (38°10'57.52"N, 20°23'13.61"E).

Another example of out-of-plane collapse of a stone masonry retaining wall was also responsible for the closure of the road connecting the Vouni and Chavriata villages (38.177692° N, 20.397458° E) as shown in Figure 8.3.7. Adjacent to the failed stone masonry wall, a reinforced concrete retaining wall responded in a very satisfactory manner with no obvious damage observed following the two strong earthquakes.

Figure 8.3.7. Extensive failure of stone masonry retaining wall followed by road embankment sliding failure with horizontal and vertical displacement. This major failure is on the roadway connecting the villages of Vouni and Chavriata (38.177692°N, 20.397458°E). The reinforced concrete retaining wall shown in yellow dotted circle suffered no damage although adjacent to the collapsed one.

In the church of Vouni village (38.177578ºN ,20.403477ºE) a multi-tiered, 4.7 m high (in total), stone masonry retaining wall collapsed after the 2nd event of 2/3/14, as shown on Figure 8.3.8a. The tiers, starting from the lower one had a height of 1.2, 1.2, and 2.3 m. The length of the failed section was approximately 20 m and engaged the lower two tiers. Partial collapse of the wall had taken place during the 1st event of 1/26/14 (Figure 8.3.8b).

Figure 8.3.8: (a) Collapse of lower two levels of a three-level stone retaining wall supporting the bearing soil of a Vouni village church (38.177578° N, 20.403477° E) after the 2nd event, and (b) partial collapse of the same wall following the 1st event.

Figure 8.3.9. Single-story building close to Kouvalata village (38.234484° N, 20.419554° E): (a) failure of stone masonry retaining wall followed by local landslide of the supporting bearing soil after the 1st event, and (b) progression of failure after the 2nd event.

Failure of masonry wall was recorded following the 1st event near the Kouvalata village (38.234484° N, 20.419554°E). The wall retained a natural slope upon which a single-story structure was founded (Figure 8.3.9). The failure of the wall was accompanied with settlement of the retained backfill that became more pronounced following the 2nd event. The heavy rainfall that occurred during that period probably contributed to the evolution of this failure.

Another interesting case of masonry earth retaining wall involves a 3.3-m high wall supporting the yard ("perivolos") of Aghios Ioannis Chrysostomos church on steep ground in Kourouklata village. The location of Kourouklata is approximately 10 km east of the epicenters of the two events. The bell tower of this church was heavily damaged. Fig. 8.3.10 depicts the yard of the church which underwent settlement and lateral displacement.

The church's yard is retained by the masonry wall, which is flanked by concrete retaining walls. It appears that the entire masonry wall moved and the backfill movement occurred only behind the section retained by the masonry wall (Figs. 8.3.10, 11). The cracked ground parallel to the wall was 24 m long. The cumulative vertical displacement of the ground was 20 cm in the vertical direction (Fig. 8.3.12) and 21 cm in the horizontal direction. Interestingly, next to the church lies a cemetery that is almost entirely destroyed by the earthquakes with toppling observed in almost two thirds of the tombs.

On the road towards the Kourouklata village, there were also a few additional interesting failures of stone masonry walls. A pair of failures is shown in 8.3.13 and 8.3.14. One was located on the uphill side of the road, whereas the second one is located in the downhill side of the road just a few meters apart from each other. Fig. 8.3.13 shows a view of the uphill wall, which is 4.20 m high and has collapsed leaving the road pavement cantilevered. Fig. 8.3.4 shows a side view of the downhill wall. The natural stones were cemented. The wall has a maximum height of 2.8 m and a thickness of 45 cm. A series of additional failures of short retaining walls are shown also in Fig. 8.3.15 and 8.3.16.

Figure 8.3.10. Damage at Kourouklata village church. (a) cracked ground in foreground with wall to the right and church in background; (b) ground deformations taken by Prof. G. Athanasopoulos, V. Kitsis and O. Theofilopoulou; (c) damage at cemetery behind the church; (d) concrete wall adjacent to masonry wall from lower elevation; and (e) view of wall damage (38°14'31.72"N, 20°28'25.40"E).

Figure 8.3.11. Lateral soil movement, at Kourouklata's church front yard (38.242113, 20.473955).

Figure 8.3.12. Vertical settlement of 20 cm behind the retaining wall (38.242113, 20.473955).

Figure 8.3.13. Masonry wall damage towards Kourouklata village. (38°14'26.29"N, 20°28'35.14"E)

Figure 8.3.14. Another masonry wall damage towards Kourouklata village (38°14'26.29"N, 20°28'35.14"E).

Figure 8.3.15. Retaining wall failures at several locations in Kourouklata village (38.241075N, 20.475602E).

Figure 8.3.16. Collapse of stone retaining wall in Kourouklata village. (38.241797, 20.473677).

Stone masonry retaining wall failures supporting roadways were also identified on the road between Lixouri and Argostoli. Out-of-plane collapse was recorded in two successive locations following the 1st event with an estimated failure length of 10 m and 20 m, respectively (Figure 8.3.17a). These failures progressed following the 2nd event that also caused failure at an additional, third location (Figure 8.3.2b). In contrast, the adjacent reinforced concrete sections remained essentially intact.


10 m
20 m
28/01/2014
(a)


(b)


(c)
5 m


(d)

Figure 8.3.17. (a) Extensive failure of stone masonry retaining wall followed by road embankment settlement close to Atheras Village (38.293224°N, 20.45217°E) after 1st event; (b) failure at 3rd wall location after 2nd event with adjacent concrete sections undamaged; (c), (d), (e) failure details.

A case of a relatively short, 1.2-m high, wall is shown on Fig. 8.3.18 near Argostoli. Despite its low height, this wall was damaged as a result of earthquake shaking. However, it is not known which of the two events caused the failure.

Figure 8.3.18. Failure of a short masonry wall near Argostoli (38°10'50.76"N, 20°29'54.01"E).

Another example of masonry wall failure near Lixouri is shown on Figure 8.3.19. A stone/masonry wall failure in a cemetery in Livadi village is shown on Figure 8.3.20 and two retaining wall failures in the cemetery of Lixouri are shown on Figures 8.3.21 and 8.3.22. Another small wall failure at the Theotokos Kipouraion Monastery is shown on Figure 8.3.23 and a few failures in Aghia Thekla village, as shown on Figures 8.3.24 to 8.3.27.

Figure 8.3.19. Failure of masonry wall supporting roadway outside of Lixouri (38°12'21.05"N; 20°24'54.89"E).

Figure 8.3.20. (a) View of stone/masonry retaining wall failure at the cemetery of Livadi village. (b) Close-up photo showing rotation of the wall face and tension cracks in the backfill (GPS coordinates: 38.255833, 20.420833).

Figure 8.3.21. Collapsed retaining wall at cemetery of Lixouri with close up (b-c) side views (GPS coordinates: 38.192400, 20.438725); (d-e) top views (38.192433, 20.438725).

Figure 8.3.22. Failure of a small retaining wall at the back yard of the Lixouri cemetery's church (GPS coordinates: 38.192911, 20.438625).

Figure 8.3.23. Partially failed small retaining wall in the backyard of the Theotokos Kipouraion Monastery (38.203194, 20.348219); (b, c): View from the backyard: collapse of retaining wall marked with red circle. (38.203327, 20.347747).

Figure 8.3.24. Retaining wall collapse in front of the "new" Aghia Thekla church (GPS coordinates: 38.245202, 20.384422).

Figure 8.3.25. Damage of stone walls in Aghia Thekla village (GPS: 38.245202, 20.384422).

Figure 8.3.26. The old Aghia Thekla church (GPS coordinates: 38.244894, 20.386097).

Figure 8.3.27. A small retaining wall failure at the old Aghia Thekla church cemetery (GPS coordinates: 38.244944, 20.386433).

Note that related structural damage to churches is presented extensively in Chapter 11 of this report.

CONCRETE RETAINING WALLS

A number of concrete walls (gravity or cantilever types) were damaged as a result of the strong motions induced by the two earthquake events. An interesting case of a gravity wall that was heavily damaged during the 2nd event, in the town of Chavriata, shown on Fig. 8.3.28. This wall is located in the vicinity of the strong motion station that recorded a peak value of horizontal ground acceleration PGA equal to 0.74 g. The lower part of the wall is 2.1 m tall and the upper part has a height of 1.8 m. The two portions appear to have been built at different times as there is a cold joint between them with no tie-in steel reinforcement. The upper portion of the wall appears to have been simply pushed and toppled.

Figure 8.3.28. Failure of concrete retaining wall along a cold joint. The upper and lower portions of the wall appear to have been built at different times (38°11'0.07"N; 20°22'54.18"E); (a, b) side views; (c, d) top view with tensile cracks of soil surface at hill top where the strong motion station is located.

At the same location, another reinforced concrete wall with a length of approximately 250 m and a height ranging from 3.2 m to 3.9 m retains the main paved road of the town (Fig. 8.3.29). The axis of the wall is curved in plan and has a general East-West strike. The wall did not show signs of distress. A long section of the road retained by the wall was cracked and settled vertically by 5 to 15 cm and displaced horizontally by about 3 to 7 cm.

Figure 8.3.29. Cracked pavement due to wall movement with retaining wall on the left. (38°10'57.83"N, 20°23'9.40"E).

A case of a distressed cantilever type retaining wall is shown on Figure 8.3.30. The wall is located on the roadway between Havdata village and Lixouri. It is not known whether this wall was damaged during the Event 1 or Event 2. The wall is retaining a backfill, forming the yard of a car body shop and has variable height ranging from 0.66 m to 3.1 m. The portion of the wall with the maximum height tilted outwards and the backfill moved laterally about 12 cm and also settled, defining the sliding plane. Water drains were provided close to the base of the wall.

Figure 8.3.30. Tilted cantilever retaining wall of variable height on the roadway between Havdata and Lixouri. (38°12'21.05"N, 20°24'54.89"E).

CONCLUSIONS

There were few, if any, major retaining walls in the Cephalonia island. The main shocks of the 2014 earthquake sequence induced several mechanisms of instability (sliding, tilting, toppling, and fracture with out-of-plane collapse) to a large number of masonry earth retaining walls located in the meioseismal area of the Paliki peninsula. Most of the failures were associated with simple non-engineered walls, or walls that were part of a steep terrain and their collapse was the inevitable consequence of slope failure. The same behavior was observed, albeit to a much lesser degree, to concrete walls (gravity and cantilever type) subjected to strong horizontal (and vertical) motions. Most of the observed damage to retaining walls was caused by the strong ground shaking associated with the 2nd event of 2/3/14.

8.4 Landslides and Rock Falls

INTRODUCTION

Landslides and rock falls were observed mainly in the Paliki Peninsula west of the Argostoli Bay and along the coastal zones between the Argostoli area and Myrtos Bay. The north and east part of the island is practically free of these effects (Figs. 8.4.1). This is in accordance with general observations about seismic intensity, as derived from strong motion recordings, cemetery data, building performance, liquefaction observations, etc., as presented in the other sections of this report.

This section summarizes observations made by several reconnaissance teams, including AUTH-LSDGEE, UPatras, ITSAK, DUTH, and NTUA, following the two major events in the time period between February 8 and February 23, 2014. The areas investigated are shown in Fig. 8.4.1a and cover the meioseismal area and beyond (see also Section 2.2 with map, names and coordinates of towns). The reconnaissance teams tried to document and identify damage patterns influenced by a variety of factors, including vulnerability of materials, topographic features, presence of precarious rocks, proximity to source, near-fault earthquake directivity and site effects. It appears that most of the affected area may have been located on the hanging wall of the rupture *(pending release of fault trace by seismologists).*

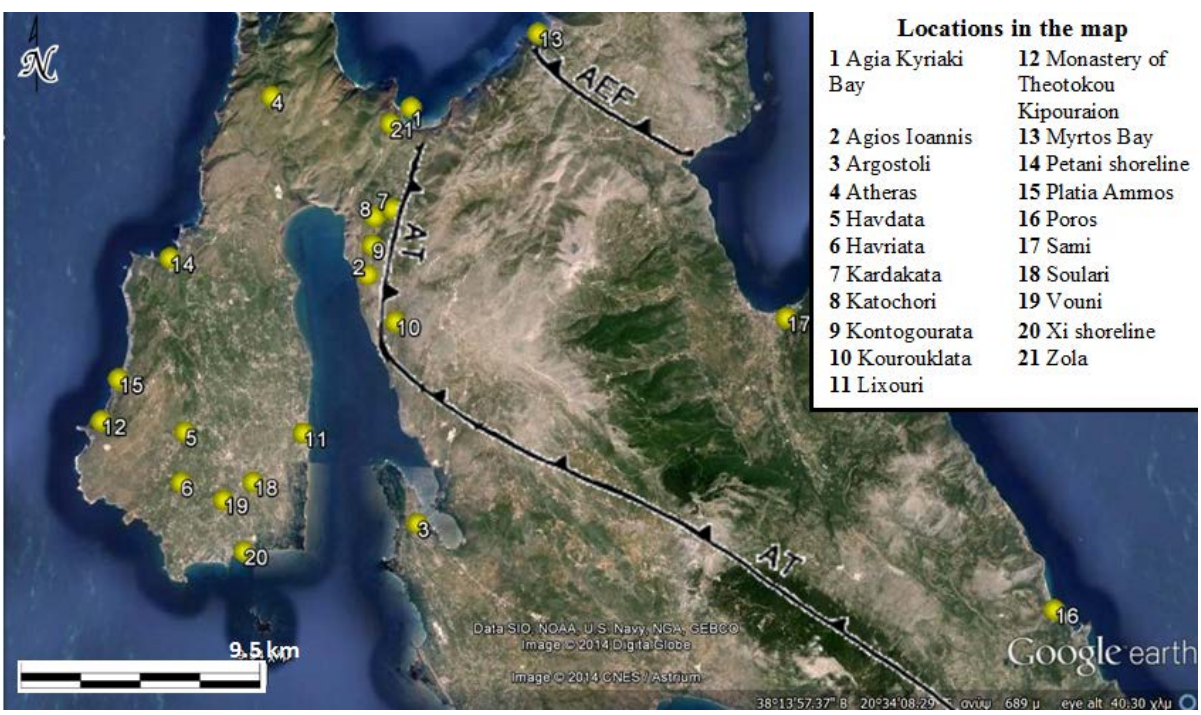

Figure 8.4.1.a Locations investigated (AT: Mt. Ainos Thrust, AEF: Aghia Ephymia Fault).

GEOLOGY ALONG THE INVESTIGATED PATHS

The western part of Cephalonia island is separated from the central part by the Mt. Ainos thrust with a NNE–SSW direction. The central part of the island is split into a northern and southern area by the Aghia Ephymia Fault with a NNW–SSE direction. Details on the geology can be found in Chapter 6 of this report.

The path from Argostoli north to Aghios Ioannis (between the villages of Kourouklata and Kontogourata), goes along Upper Cretaceous pelagic limestones. Between Kontogourata and the coast of Aghia Kyriaki, the path goes along the mount Ainos thrust which consists of successive zones of Oligocene limestones followed by well-bedded pelagic marls and marly limestones, Eocene thick-bedded limestones covered by alluvial deposits or scree. Similar geologic formations exist at the central slope of Myrtos bay, which is on the Aghia Ephymia Fault, while adjacent slopes dipping southwards and northwards consist of cretaceous pelagic limestones. The paths going through the rest of the Paliki Peninsula cross areas of conglomeratic and brecciated limestones and near Lixouri, yellowish sand, sandstones, sandy limestones and upwards blue marls, covered by sandstones and sandy marls. Figure 8.4.1a shows all locations visited by the reconnaissance teams. Figures 8.4.1c through 8.4.1d show the field investigation paths followed by the UPatras team.

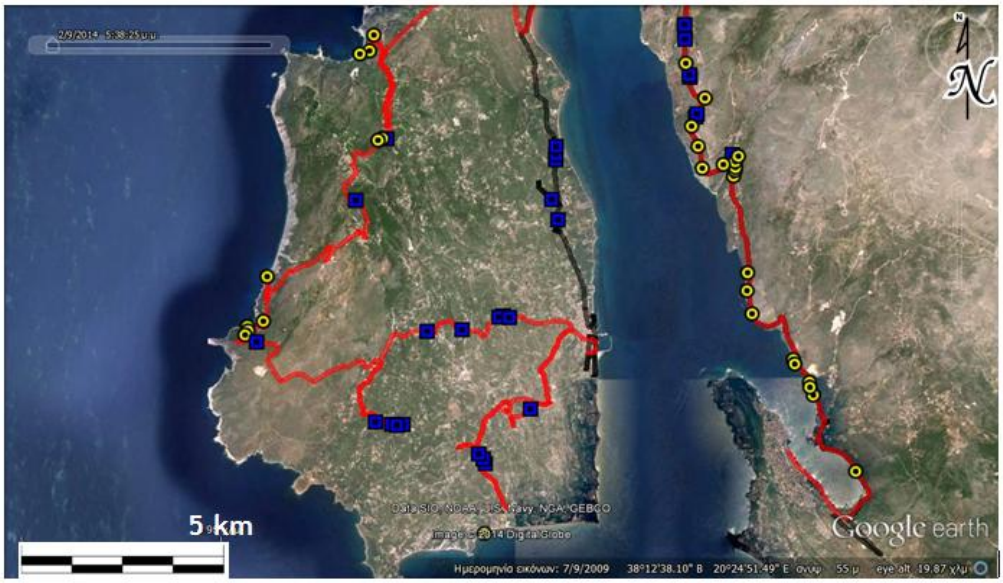

Figure 8.4.1.b Cephalonia path on 2/8/14 (black), 2/9/14 (red) of Paliki Peninsula and Argostoli Bay by UPatras team. Geographical distribution of rock falls (yellow points) and road embankment settlements (blue points).

Figure 8.4.1.c Cephalonia path on 2/8/14 (black), 2/9/14 (red) of Atheras (south of Paliki Peninsula) and Myrtos Bay by UPatras team. Geographical distribution of rock falls (yellow points) and road embankment settlements (blue points).

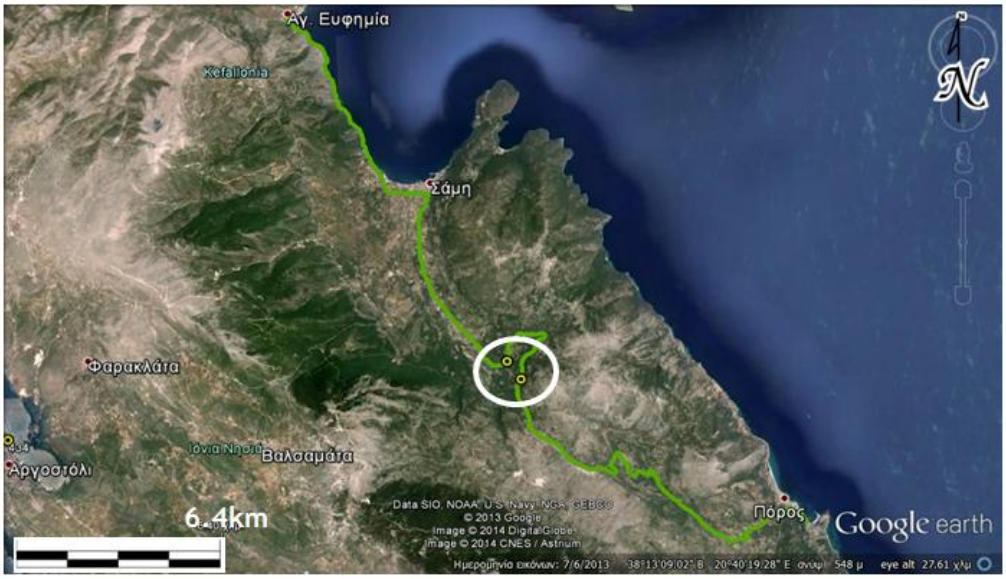

Figure 8.4.1.d Cephalonia path on 2/17/14 (green) on the eastern part of Cephalonia by UPatras team. Geographical distribution of rock falls (yellow points).

ROCK FAILURES – ROCK SLIDES

Along the paths in Figs. 8.4.1(b,c,d), the reconnaissance teams observed one major rock fall with debris slide in steep cliffs (Fig. 8.4.4) and a major deep-seated bedrock slump in a natural slope undercut by a road (Fig. 8.4.2). In addition, numerous minor rock falls were spotted along the road cuts, ranging from simple block falls to more extended rock falls within various types of limestones (blocky, fractured and/or weathered).

In total, over 30 rock falls were recorded in the Argostoli–Katochori–Myrtos Bay path, over 10 in the western part of the Paliki Peninsula and a limited quantity (possibly only 2) in the eastern part of the island (Fig. 8.4.1). Indicative cases of local rock slides in consolidated red conglomerates formations were observed north of Argostoli Bay close to Kardakata Village (38.280957°N, 20.445637°E) and along the road network connecting Argostoli and Sami village (38.205687°N, 20.607155°E), inducing damage to the road (Figs. 8.4.5, 8.4.6). In the same region of Argostoli bay, rock slides were also observed (38.287065°N, 20.448024°E) in cracked limestone formations (Fig. 8.4.7). These rock slides were significantly magnified after the 2nd event of 2/3/14.

Figure 8.4.2. Rock slope failure in limestone in Monastery of Theotokou Kipouraion (38.202517° N, 20.348083° E, (a) UPatras team, 2/9/14, (b) NTUA team, 2/10/14).

Figure 8.4.3. Numerous weathered rock landslides/rock falls along the shore near Monastery of Theotokou Kipouraion. (38.203327° N, 20.347747° E, NTUA team, 2/10/14)

Figure 8.4.4. Rock fall with debris slide in steep cliffs in Platia Ammos beach (38.213883°N, 20.353017° E, UPatras team, 2/9/14).

Figure 8.4.5. Rock failure of conglomeratic or breciatic limestone on a cut slope between Moussata & Vlachata villages on the Poros-Argostoli road axis (38.126874° N, 20.616777° E, DUTh, 2/22/14).

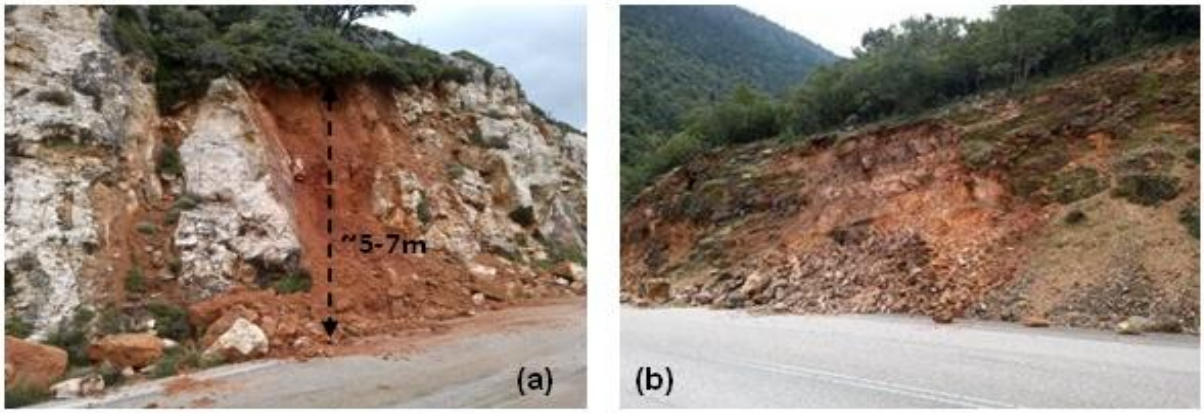

Figure 8.4.6. Rock slides in red consolidated conglomerate formations recorded at (a) Northern part of Argostoli bay close to Kardakata Village (38.280957°N, 20.445637°E) and (b) road network between Argostoli and Sami village (38.205687° N, 20.607155° E, ITSAK team, 1/28/14).

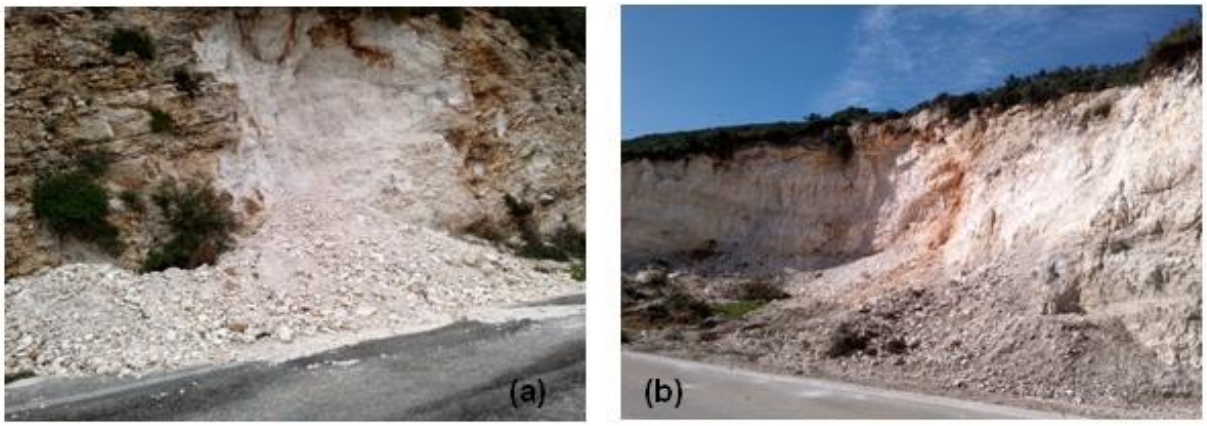

Figure 8.4.7. Rock slides in cracked limestone formations recorded at Northern part of Argostoli bay

following the (a) 1st event (38.287065° N, 20.448024° E) and (b) 2nd event (38.287018° N, 20.448027° E). Photos by ITSAK team on 1/28/14(a) and 2/10/14(b).

Many shallow rock failures, both minor and major, were observed along the steep cliffs lining the west coast of Paliki (Figure 8.4.8). The more pronounced rock failures seemed to be several disaggregated slides with debris flow observed at the Petani shoreline (38.260941°N, 20.377410°E). One of these slides resulted in the closure of the road towards the seashore. It should be mentioned that an indeterminate number of the high steep cliffs above beautiful white beaches on the west side of Paliki are in a state near limit equilibrium, most probably due to shallow decompression joints parallel to their slope and weathering. Failure of these slopes followed by debris slides does not require intense seismic accelerations, as opposed to slides - such as those shown on Figures 8.4.2 and 8.4.4 - which indicate the action of intense accelerations.

Figure 8.4.8. Disaggregated slides with debris flow observed at the Petani shoreline (38.261705° N, 20.380166° E). Photo by NTUA team, 2/9/14.

A shallow rock slide with debris flow of weathered and severely fragmented limestone was observed (Figure 8.4.9) on the local road of Argostoli between Kourouklata and Kontogourata village (38.251408°N, 20.466813°E). The local road from Kardakata to Zola village (en route to Aghia Kyriaki Bay) suffered numerous rock planar slides along the limestone's bedding. On the right side of the road, the orientation on the road cuts favored rock planar sliding (Figure 8.4.10b), while on the left side only occasional wedge failures emerged (Figure 8.4.10a) and no rock toppling or rock fragment detachments were observed.

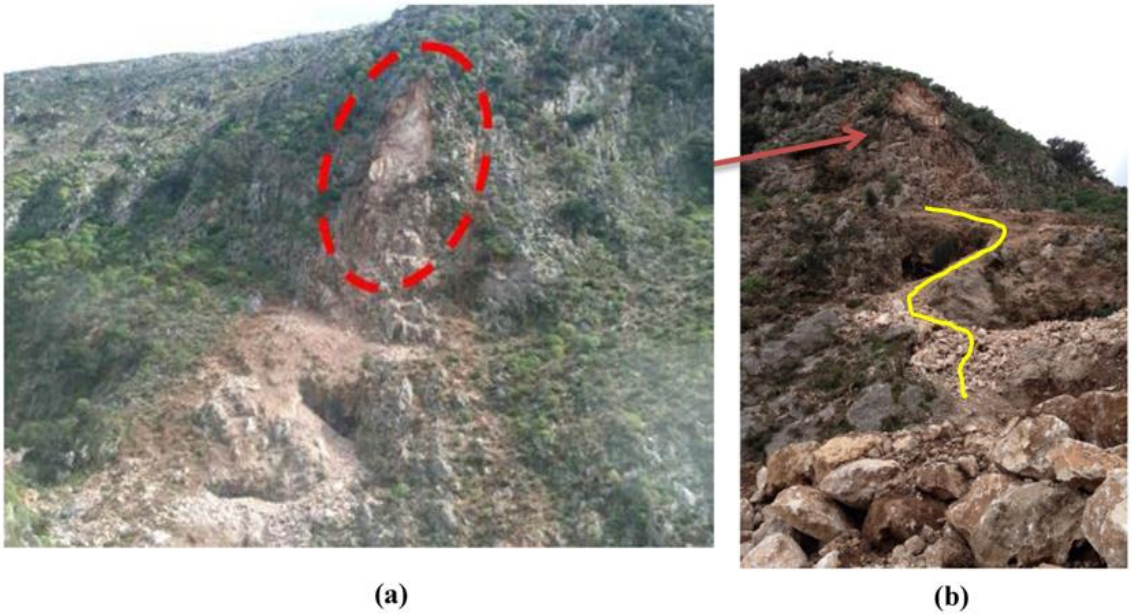

Figure 8.4.9. A shallow rock slide of a weathered and fragmented limestone with debris flow (38.251408° N, 20.466813° E, (a) Date of picture taken by DUTh team is 2/22/14, and (b) by UPatras team is 2/8/14) along the local road from Kourouklata to Kontogourata).

Figure 8.4.10. Rock failures (mostly planar slides along limestone's bedding and only occasionally wedge failures) along road cuts on the way from Kardakata to Zola village in Aghia Kyriaki bay area (from 38.287181° N, 20.457548° E to 38.310356° N, 20.469258° E, DUTH team, 2/22/14).

More important seemed to be the rock slope failures in Myrtos Bay, where four important shallow disaggregated slides with debris flow occurred at the north and south part of the Bay. On the east slope, two large blocks from the overtopping limestones rolled down westwards on soil-topped slopes, causing total destruction of the descending road at three points (38.337833°N, 20.532317°E). New movements were observed at the crest of the slope on old slide mobilization planes, likely due to blocky limestone overlaying softer material. Figure 8.4.11 shows the Myrtos bay area with debris flows at the North part (center), a wedge type failure of crashed material (top left), two major rock blocks that rolled down (bottom right) and the access road destruction from the 2nd rock block (top right). The arrows indicate the location of the details mentioned. Roll paths of the two large rock blocks are shown in Fig. 8.4.11. Interestingly, cemetery monuments at a small distance (~700 m) from Myrtos Bay had no damage at all. Similar shallow debris flows were observed in various locations along the steep cliffs on the west coast of Paliki. One such shallow debris flow was observed in Platia Ammos (Fig. 8.4.4), north of the Theotokou Kipouraion Monastery.

Figure 8.4.11. Northern cliffs and eastern slopes of Myrtos Bay. Major wedge failure, shallow rockslides and raveling; detachment and rolling down of the two major rock blocks with the associated road pavement damage (38.337833° N, 20.532317° E, UPatras, 2/10/14).

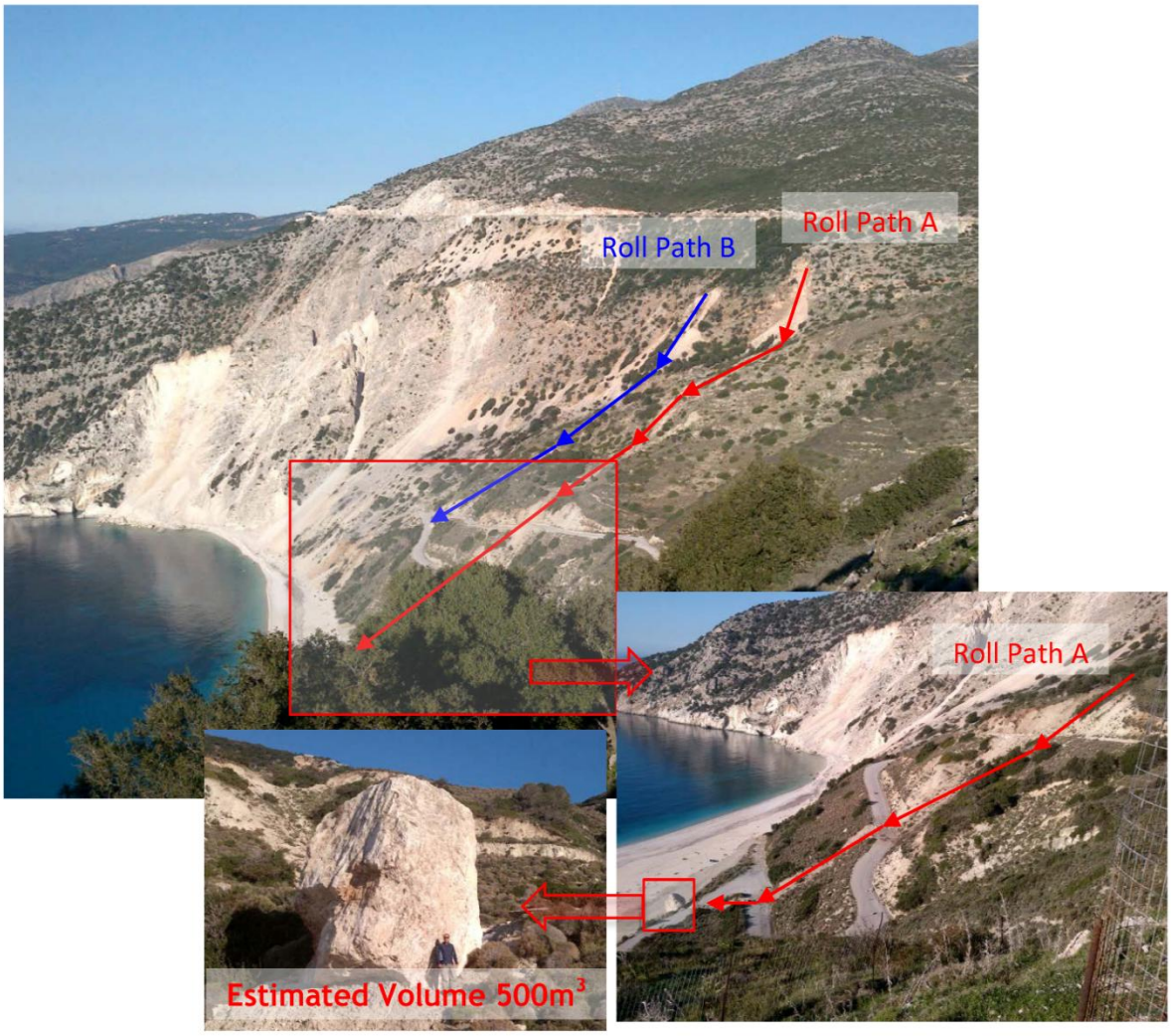

Figure 8.4.12. Roll paths A and B of the two rock blocks of estimated volume of 500 m^3 each at Myrtos Bay (38.337833°N, 20.532317°E, ITSAK team, 2/19/14).

Rock falls were observed in Atheras village (38.317350^o N, 20.418358^o E) at the northern part of the Paliki peninsula, where 7 or 8 limestone boulders ranging between 0.5 to 2.0 m^3 in volume were detected in the aforementioned village. In all these rock falls, no human injuries or deaths were reported, whereas some cases of property damage were recorded. For instance, the roof of a house, was partially destroyed by a boulder of almost 2 m^3 (Figure 8.4.13). The potential trajectory of the rolling and bouncing boulder that was detached from the upward mountain slope is roughly presented in Figure 8.4.13. In the same figure, the tracks of points where the bouncing boulder struck are also shown: the 1st and the 3rd strikes are located on limestone retaining walls.

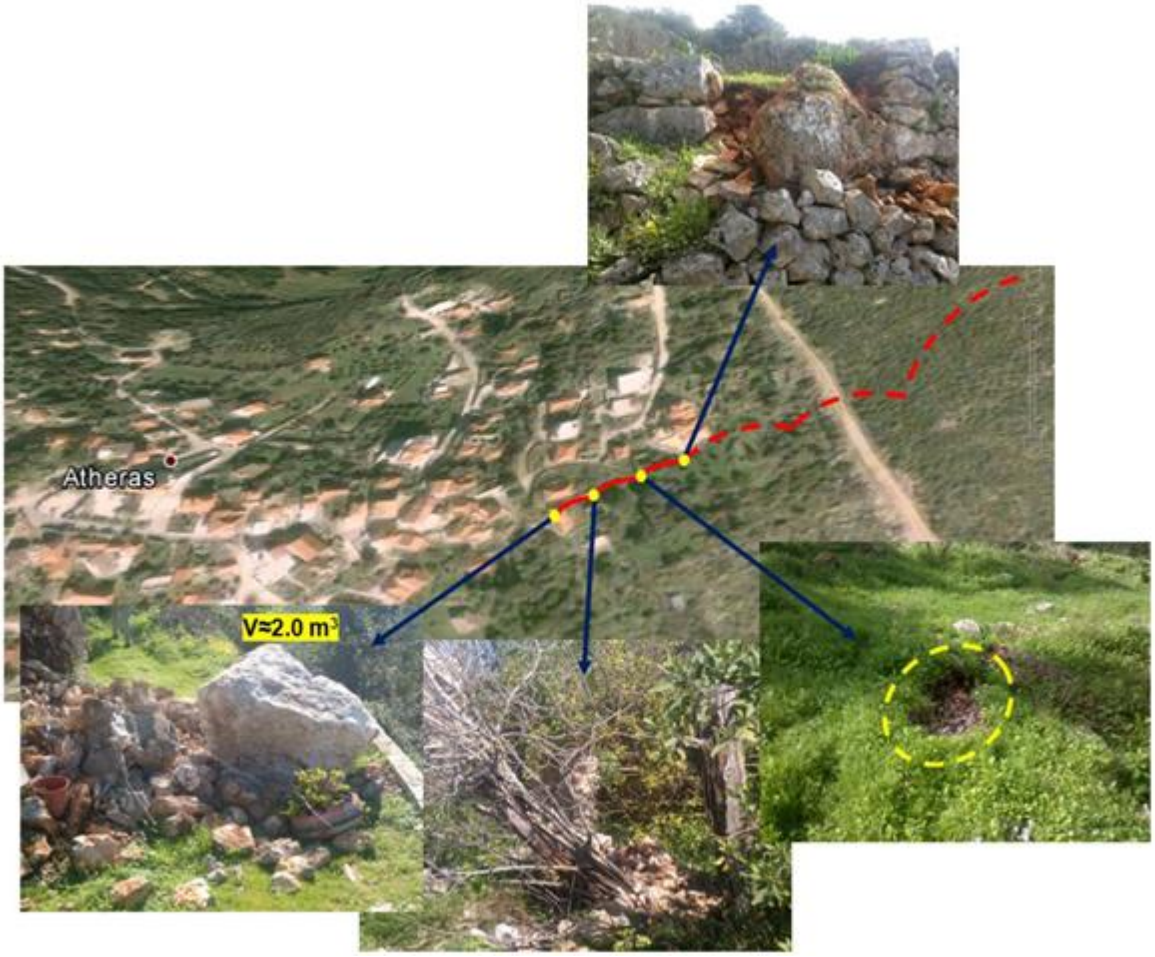

Figure 8.4.13. Possible trajectory of a limestone boulder of about 2 m^3 that rolled over a natural slope and bounced at least 3 times, passing through a tile roof of a house in Athera village. Tracks of striking points where boulder bounced also shown (38.317365° N, 20.418548° E, DUTh team, 2/22/14).

Figure 8.4.14. Shoreline of Xi area (from 38.159537° N, 20.410148° E to 38.160405° N, 20.413083° E) south of the Paliki peninsula where an extended slide (almost 250 m long) of a sandy marl escarpment was observed (ITSAK team, 02/19/2014).

An extended rock slope-type failure (almost 250 m long) of a sandy marl escarpment was observed in the Xi area shoreline (from 38.159537° N, 20.410148° E to 38.160405° N, 20.413083° E) south of the Paliki peninsula (Fig. 8.4.14). Along the local road from Sami to Poros, only two rock slides were observed with limited debris flow (Figs. 8.4.15 and 8.4.16).

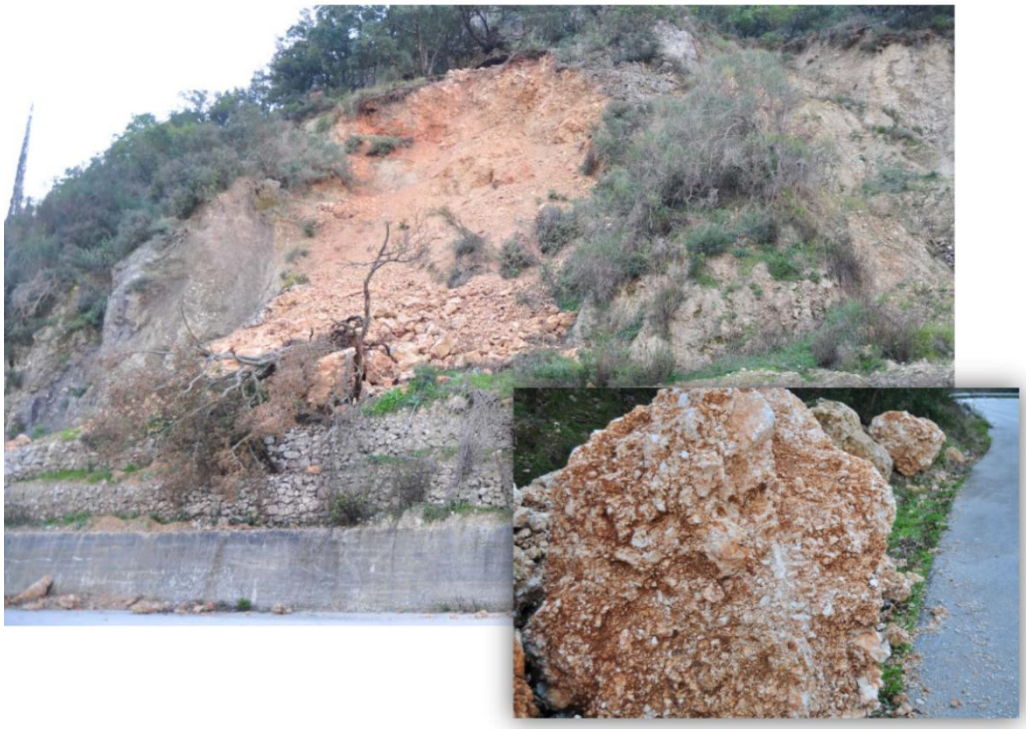

Figure 8.4.15. Rock slope failure in road cut with gabions in fractured/weathered limestone. Detached rock block crossed the road (eastern part of island: 38°11'33.51"N, 20°40'39.04"E, UPatras, 2/19/14).

Figure 8.4.16. Rock slope failure in a road cut with gabions in weathered/fractured limestones (eastern part of island, 38°11'52.99"N, 20°40'21.80"E, UPatras team, 2/19/14).

EARTH LANDSLIDES

Only two major earth landslides were observed; the first one, in the Soulari area, is more developed with an important crack formation at the crest of the slope (Fig. 8.4.17). According to locals, the specific landslide presented signs of instability due to rainfalls prior to the earthquakes and may have existed for a long time. Thus, the slope was likely near limit equilibrium and the observed patterns and displacements (~ 2.5 m) were related to the earthquakes events reactivating an older slide plane. The second is an extended incipient failure involving road embankment settlement and local stone retaining walls destruction (Figs. 8.4.18, 19). The wider area of that slope was creeping even before the earthquake, and had forced the construction of a heavy retaining wall and pavement repairs.

Figure 8.4.17. Major earth landslide in Soulari (38°11'5.66"N, 20°24'57.82"E, UPatras, 2/17/14.

Few other minor cases of slope movement were observed in the Soulari area. The first case of mild slope movements in soils was observed at an isolated 15m high clayey hill in the vicinity of the village of Soulari at the southern part of the Paliki Peninsula (Figure 8.4.20). Measurements at the crest of the slope showed horizontal displacement of 15 cm towards the East, and vertical displacement (settlement) of approximately 8 cm. Of interest in this case is the fact that the 2-story reinforced concrete building adjacent to the slide suffered no damage

(not even cracks in plaster covering the masonry infills). Another example of a small landslide in a stiff-clayey slope outside of Soulari village is presented in Figure 8.4.21.

Figure 8.4.18. Plane view of the incipient landslide failure.

Figure 8.4.19. Area showing signs of incipient earth landslide failure. (a) Cracks on upper road pavement (UPatras) and (b) stone retaining walls destruction after the 1st and 2nd events (ITSAK), and soil displacements at the toe (coordinates 38.293224°N, 20.45217°E, date 2/8/14).

Figure 8.4.20. Crest of circular type of slope movement on a 15 m high hill near Soulari village (38°11'19.73"N, 20°24'45.10"E), with slippage towards the East direction, (date 9/2/14).

Figure 8.4.21. Small landslides in stiff-clayey slopes, 400 m outside Soulari village. (38.184444° N, 20.411388° E, NTUA team, 2/10/14).

ROAD EMBANKMENT VERTICAL DISPLACEMENTS

A total of 34 vertical displacements at the shoulder of road embankments were observed mainly at the central part of the Paliki Peninsula. Figure 8.4.22 shows such major failure recorded after the two events, followed by extensive cracking of the road in Havdata (38.2028°N, 20.40445°E).

Figure 8.4.22. Road embankment settlement near bridge in Havdata (38.2028°N, 20.40445°E, UPatras team, 2/9/14).

In Figure 8.4.22, the details show the kind and the extent of vertical displacements of the embankment on both sides of a concrete bridge extending over an approximately 8 m deep creek. The total length of the settled embankment was 32 m. Figure 8.4.23 shows the road embankment settlement and surface cracks in the village of Chavriata near the south of the Paliki Peninsula.

Extensive road cracking and road embankment failure (Figure 8.4.24) were also observed on the road network connecting Chavriata and Vouni villages in the south part of the Paliki peninsula (38.287065°N, 20.448024°E) after the two major events.

Figure 8.4.23. Road embankment settlement in Chavriata (38.182733°N, 20.384067°E, date 2/9/14). Measurements by UPatras team members Eva Agapaki, Elpida Katsiveli, and Costas Papantonopoulos.

Figure 8.4.24. Road network connecting Chavriata and Vouni villages at the south part of the Paliki peninsula (38.17856° N, 20.40081° E); extensive road cracking and road embankment failure observed, respectively, after the: (a) 1st and (b) 2nd events. Photos by ITSAK team on 1/28/14 (a) and 2/5/14 (b).

CONCLUSIONS

Extended rockfalls, mostly within various types of limestones, and earthslides occurred in the Paliki peninsula, many of which induced road damage, after the two major earthquake events on 1/26/14 and 2/3/14. Important rock slides were observed in the coastal zone from the Argostoli area to Myrtos Bay (with the most extensive rock slides noted in Myrtos Bay) and in the steep cliffs west of the Paliki peninsula (Platia Ammos, Monastery of Theotokou Kipouraion). Minor damage due to rock slides was observed in the eastern part of the island. Earth landslides were generally limited with minor damage, with only two exceptional landslides (the two indicative cases shown in this chapter), one in Soulari (the formation of which may have preexisted) and the other in Chavriata, which resulted in extensive road embankment settlements.

8.5 Bridges

INTRODUCTION

As in all islands of the Ionian sea of Greece, the bridge inventory of Cephalonia includes mostly single, short-span reinforced concrete bridges. Notable exception to this rule is the historic (1830) multi-span stone Debosset bridge, discussed in this section. Overall, bridges on the island responded well to two main seismic events and their aftershocks. None of the bridges collapsed or suffered severe enough damage to interrupt traffic. Among several tens of bridges inspected (Fig. 8.5.1), only one suffered relatively significant damage on the approach embankments, resulting to partial traffic interruption.

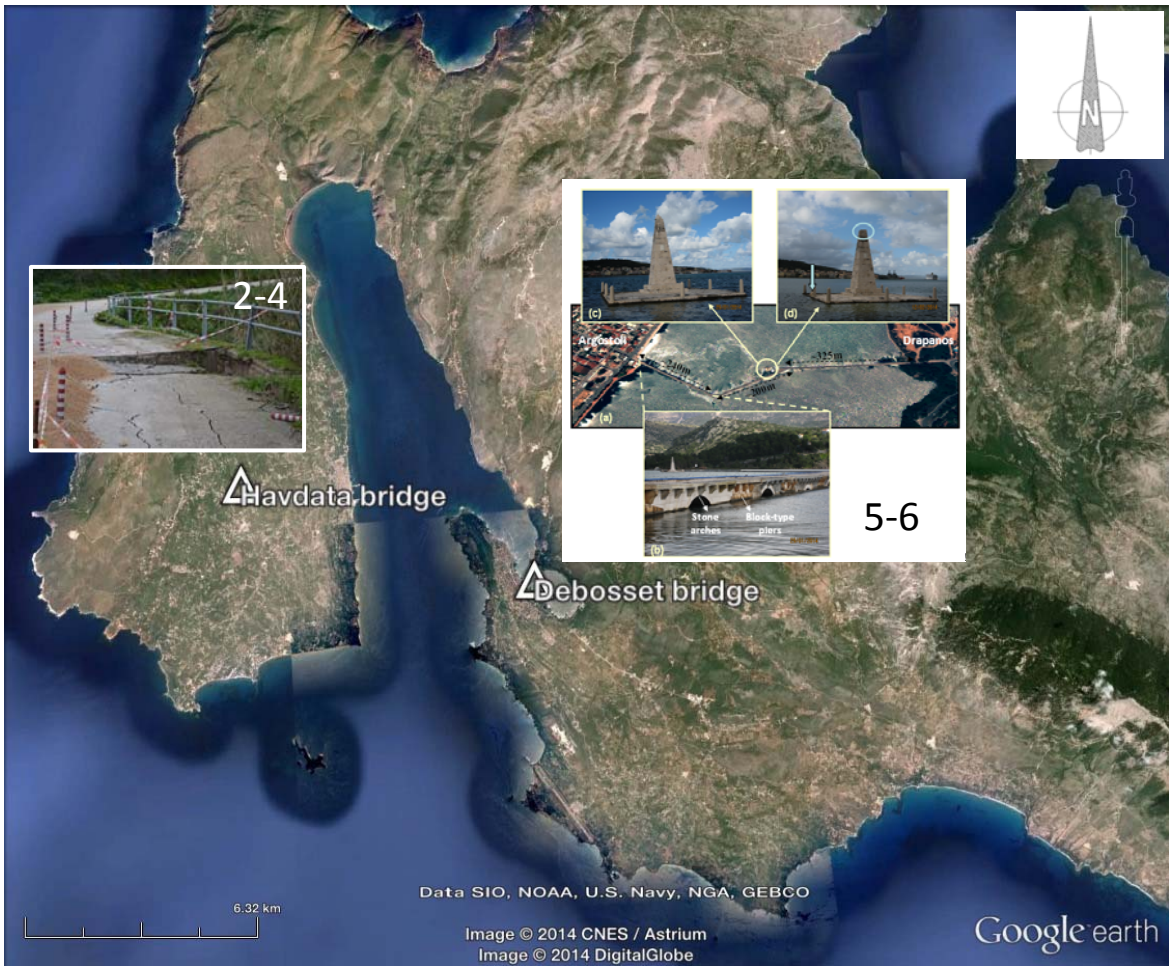

Figure 8.5.1 Locations of bridges inspected during reconnaissance and described in this section; the figures referenced correspond to the figure numbers of this section (for example, Figure 2 stands for Figure 8.5.2).

HAVDATA BRIDGE

Severe damage was observed in the reinforced concrete Havdata bridge (38°12'10.30"N, 20°24'16.05"E), only one out of the several bridges inspected during reconnaissance. This bridge is a reinforced concrete creek overpass over the asphalt country road, heading west from Lixouri city to Havdata village (approximately 3.6 km from Lixouri and 2 km from Havdata). It is 4-m long, spanning a 6-m deep creek, and is connected to the asphalt country road by 12-m long access embankments on either side.

Fig. 8.5.2(a) shows longitudinal pavement cracking and severe settlement at the location where the western access embankment adjoins the reinforced concrete bridge. Fig. 8.5.2(b) shows the much less settled pavement at the respective location of the eastern access embankment.

Settlements occurred at the southern side of the bridge, i.e., towards the downstream of the overpassed creek. We observed significant differential settlement of neighboring access embankments: up to 30 cm at the western embankment, versus a maximum of 8 cm at its eastern counterpart. Settlements diminish at a transverse distance of 2.5 m from the downstream side of the bridge (i.e., at the centerline of the road), whereas in the longitudinal direction they essentially diminish at the end of the access embankments (almost 12 m from the overpass edges).

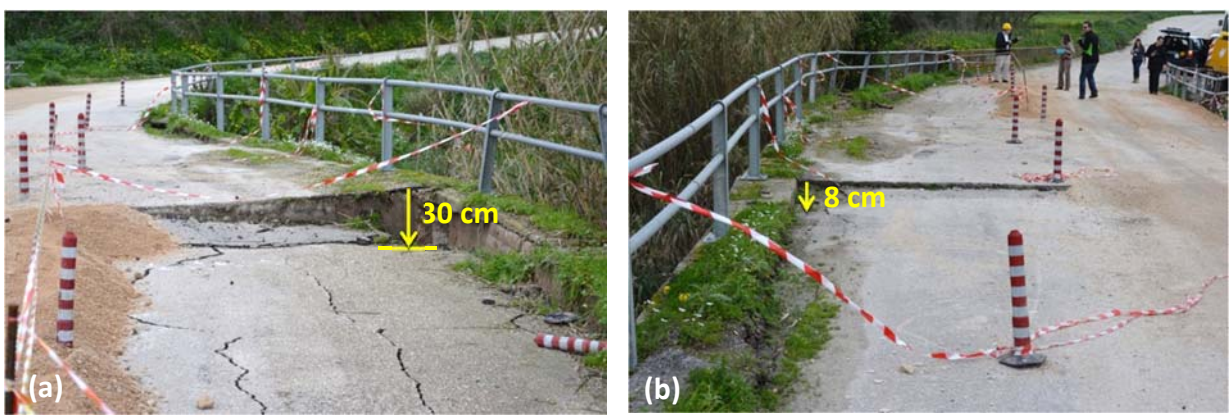

Figure 8.5.2. Havdata bridge (38°12'10.30"N, 20°24'16.05"E): (a) western access embankment and (b) eastern access embankment.

Hence, settlements and pavement cracks appeared all along the embankments, reaching maximum values at the connection to the bridge. The different settlement response in the two access embankments can be attributed to the observation that the (southern) retaining wall of the western embankment suffered downstream outward displacement of a maximum of 19 cm,

at the location where it adjoins (cold joint) the bridge (Fig. 8.5.3), whereas there was no dislocation of its counterpart at the eastern embankment.

Figure 8.5.3. Havdata bridge (38°12'10.30"N, 20°24'16.05"E): Side view of outward (downstream) displacement of southern retaining wall of western access embankment.

From a structural point of view, the reinforced concrete Havdata bridge consisted of the pier (with width equal to that of the deck) and the deck, which included a transverse beam. The deck-beam section that rested on top of the pier has undergone small permanent drift, at least in the southern embankment shown in Fig. 8.5.4. Whether there are steel studs between the two bridge sections is unknown, but there is definitely no bearing (rubber or otherwise). Also, there could have been some pounding between the retaining wall and the deck-pier and pier sections, since the edges of the reinforced concrete sections had been chipped off.

Figure 8.5.4. Havdata bridge (38°12'10.30"N, 20°24'16.05"E). Side view of connection of southern pier to deck-beam sections of the bridge.

DEBOSSET BRIDGE

The performance of the Debosset bridge following the two main events is described in this report due to the bridge's landmark status and history of retrofit. Originally constructed in 1830, the historic multi-span Debosset stone bridge (38°10'26.25"N, 20°29'45.59"E) connects the shorelines of Argostoli and Drapano at the southern side of Argostoli bay. It is comprised by successive stone arches founded on stiff block-type stone piers. The bridge has a total length of 750 m with height that varies between 2 to 4 m along its longitudinal axis (Fig. 8.5.5).

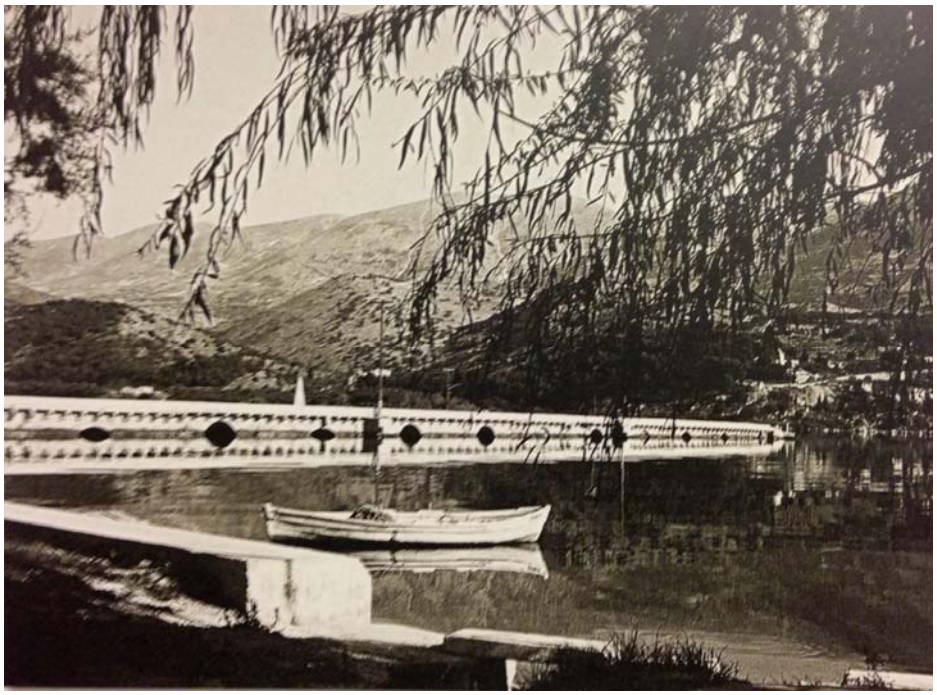

Figure 8.5.5. Debosset bridge connecting the Drapano and Argostoli shorelines (GPS coordinates 38°10'26.25"N, 20°29'45.59"E). Photo taken prior to the 1953 earthquakes (Poulaki-Katevati, 2009).

Following the severe M_s = 7.2 earthquake of 1953, the bridge sustained extensive damages, inducing differential settlement of the deck and out-of-plane collapse of the arch walls and filling material. Major parts of the bridge were reconstructed in the period 1960-70, using reinforced concrete while maintaining the original architectural pattern, but modifying substantially the material homogeneity and structural stiffness.

In 2005, a multidisciplinary research project for the seismic assessment and restoration of the Debosset bridge was undertaken by the Laboratory of Soil Mechanics, Foundation and Geotechnical Earthquake Engineering (LSMFGEE) of AUTH, under the auspices of the Greek Ministry of Culture (Directorate for the Restoration of Byzantine and Post-byzantine Monuments).

As described in Pitilakis et al. (2006) and Rovithis & Pitilakis (2011), an extensive subsurface investigation program was conducted along the bridge, including borings with Standard Penetration Testing (SPT), and geophysical testing using the Crosshole Seismic (CS) and Microtremor array methods. Locations of the testing and geologic section showing soil stratigraphy and measurements of shear wave velocities, V_s , are presented Fig. 8.5.6. The regional sandstone encountered at a depth of about 35 m below grade was characterized as bedrock with V_s of 1 km/s, overlaid by soft surface silty clay deposit with V_s ranging between 140 and 170 m/s.

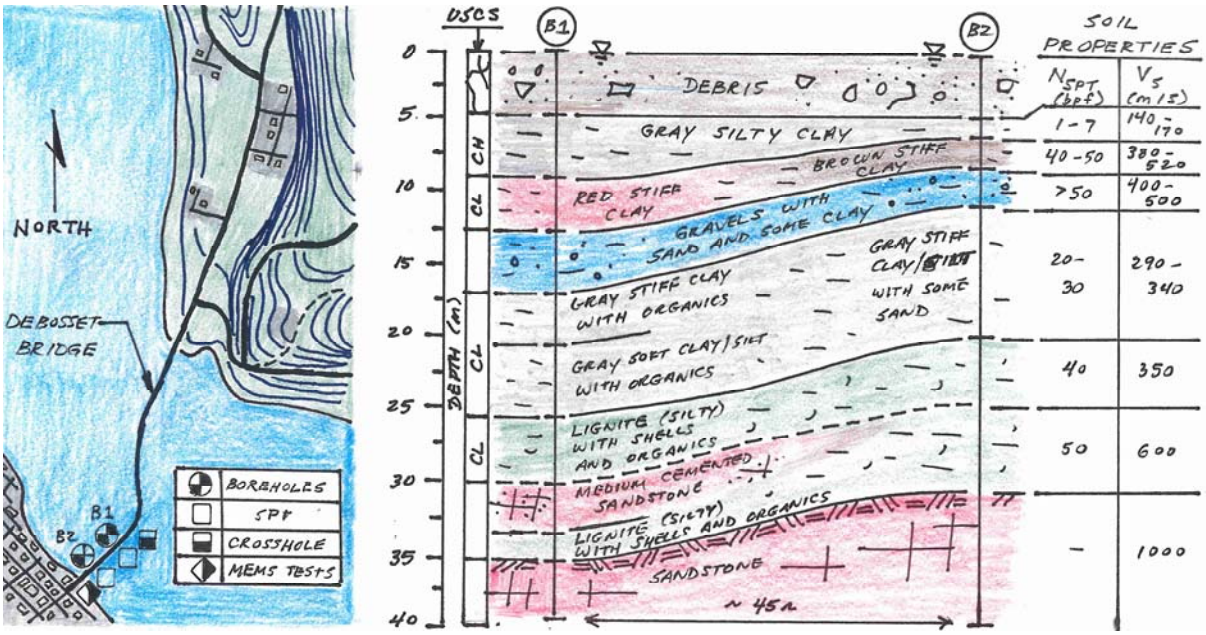

Figure 8.5.6 (a) Geotechnical and geophysical test locations along Debosset bridge, and (b) geologic section revealing soil profile along the line B1-B2 shown in (a) (sketch created by Adam Dyer of MRCE based on Pitilakis et al., 2006).

The 2005 bridge rehabilitation included use of micropile foundations to improve the soft clayey foundation soil and incorporation of lateral tendons to increase the transverse strength of the bridge, all completed before the 2014 earthquakes. Architectural restoration of the bridge facades was also partially completed at the time of structural rehabilitation (Fig. 8.5.7b). The rehabilitated Debosset bridge was inspected by ITSAK and AUTH-LSMFGEE reconnaissance teams after both major events, during the periods of January 27-30, and February 10-12 and 18-20 of 2014. The inspection revealed no damage or visible defects on the bridge structure, and overall satisfactory seismic performance, despite the high accelerations experienced in this site, indicating the benefits of the seismic rehabilitation work.

Figure 8.5.7. (a) Debosset bridge (38°10'26.25"N, 20°29'45.59"E); (b) Rehabilitated bridge with no observed damage following the major events of 2014; (c) Multi-drum obelisk (Kolona) monument intact after the 1st event; and (d) Toppling of upper drum of the obelisk induced by the 2nd event.

Figure 8.5.8. Obelisk "Kolona" monument (GPS coordinates 38°10'26.25"N, 20°29'45.59"E) in early 1900's sketch (Poulaki-Katevati, 2009). The upper drum toppled after the 2nd 2014 event (Fig. 8.5.7d).

The only damage within the opening of the bridge was observed at the multi-drum stone obelisk monument locally known as "Kolona." The monument was erected in 1813 in appreciation of Great Britain by the local Cephalonian government (see 1900's sketch of Fig. 8.5.8, modified from Poulaki-Katevati, 2009). While the monument remained intact after the 1st event of January 24, 2014, its upper drum toppled following the 2nd event of February 3, 2014 (Fig. 8.5.7d).

The quay wall adjacent to the Debosset bridge suffered permanent horizontal displacement of 10 cm towards the shoreline with an approximate backfill settlement of 15 cm measured at following the 1st event (Fig. 8.5.9a). The observed lateral movement of the quay wall and settlement of the backfill were further increased, almost doubled at some points, following the 2nd event (Fig. 8.5.9b).

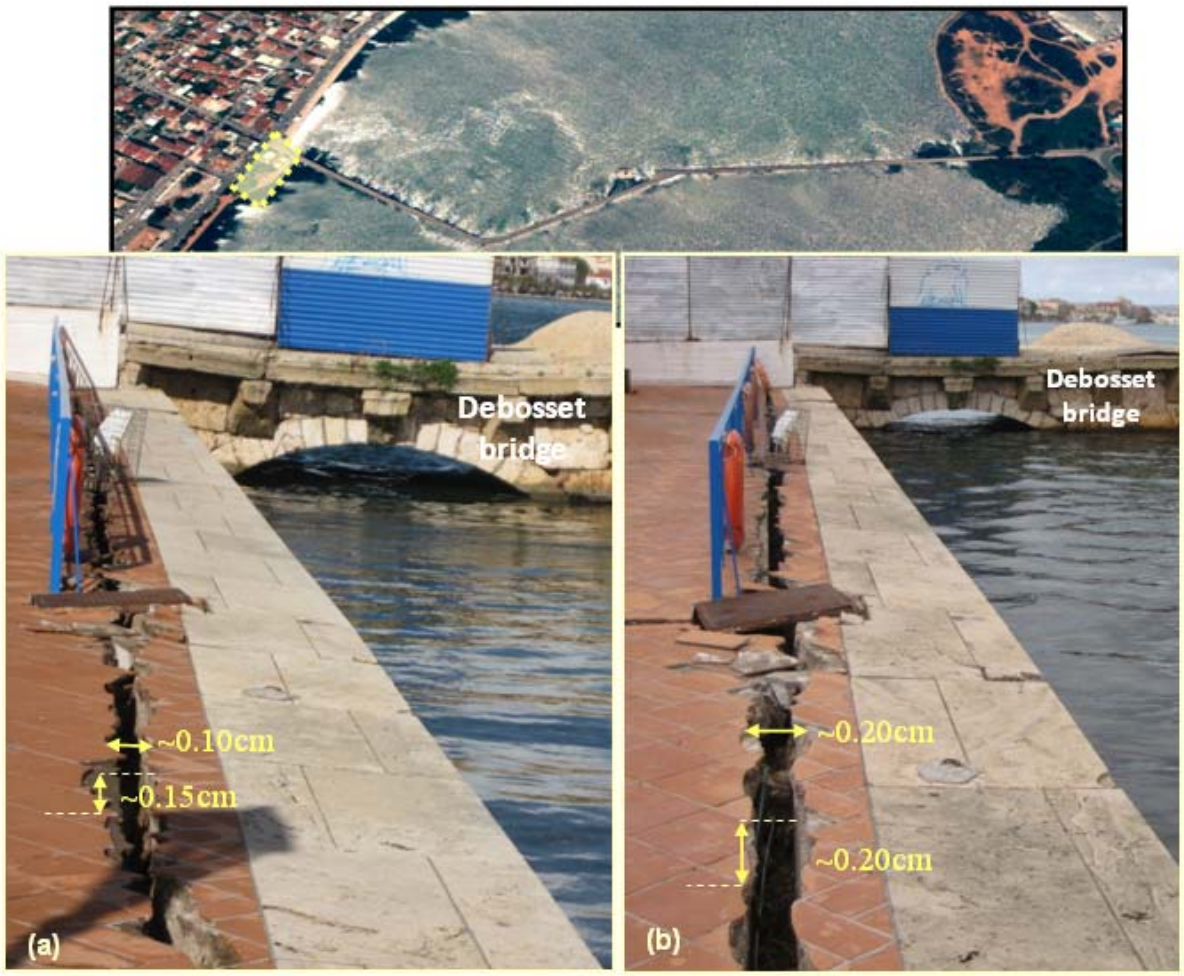

Figure 8.5.9. Observed failures adjacent to the Debosset bridge: permanent lateral displacement of the quay wall and settlement of the backfill induced by: (a) 1st event, and (b) 2nd event.

8.6 Embankments and Landfills

INTRODUCTION

This section is divided into two parts; the first part describes effects of the first and the second event on road embankments, and the second part describes both event's effects on other types of embankments such as landfills and reservoirs. Overall, road embankments performed relatively well, with very few instances of severe and moderate damage leading to complete or partial obstruction of traffic. The majority of embankments suffered minor damage, most frequently in the form of asphalt cracking near the embankment edges due to either slope stability or masonry retaining wall failures. Other types of embankments such as landfills and dams performed remarkably well with no reported damage, although arguably the former were of relatively small height, and the latter were located at large epicentral distance from both events. In the ensuing, we use the term "severe" damage for road embankment performance that completely interrupted traffic; and term "moderate" damage for road embankment performance that resulted in traffic obstruction across half or more of the road width.

ROAD EMBANKMENTS

The road embankment inventory of Cephalonia includes many (rather short) road embankments. This characteristic design stems from the intense topography, which usually prevents the construction of asphalt roads by mere cuts into steepened slopes. Typically, these roadway embankments are retained by masonry walls (typically made of natural limestone) and, to a lesser extent, by reinforced concrete walls. Figure 8.6.1 shows locations of road embankments inspected during reconnaissance surveys. Overall, the response of road embankments to two main events and their aftershocks was satisfactory. The term "satisfactory" reflects a performance of partial roadway traffic operation immediately following the two events since the road embankments damage was in general far from collapse. Some notable exceptions with severe damage observations are described in this section.

Locations with severe damage

We use the term "severe" damage for road embankment performance that completely interrupted traffic. Such locations were very few, including: (a) destruction (not only blockage) of the access road to Myrtos beach due to major rockfalls (38°20'16.20"N, 20°31'56.34"E); see also Section 8.4, and (b) extensive cracking of the embankment that affected the whole width

of the road connecting the Chavriata and Vouni villages, at two neighboring locations depicted in Figs. 8.6.2 and 8.6.3, respectively. These locations are referred to as Locations A and B, for lack of a more descriptive distinction between them.

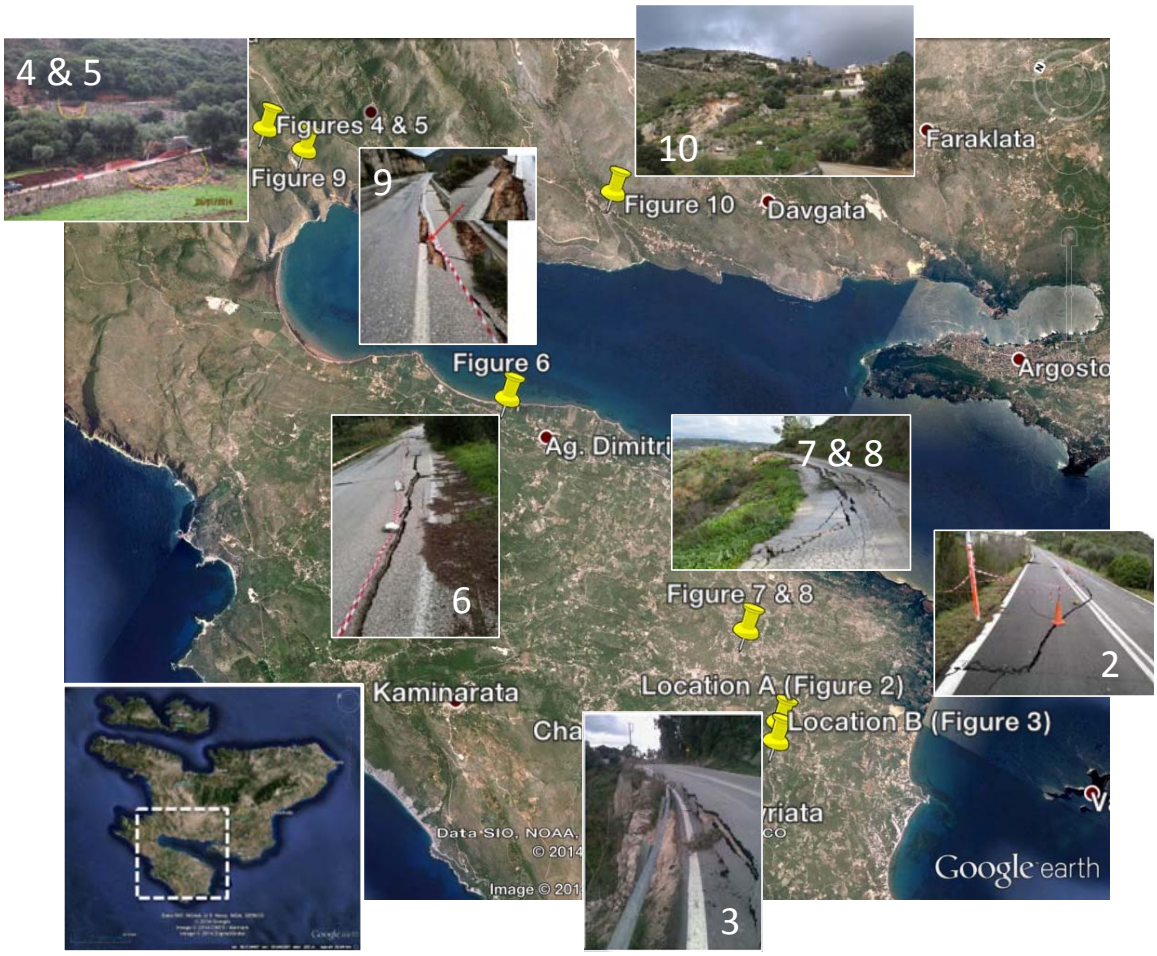

Figure 8.6.1. Locations of road embankments inspected during reconnaissance and described in this section. Figures referenced correspond to section figure numbers (e.g., Fig. 2 stands for Fig. 8.6.2).

Figure 8.6.2 shows the road embankment at location A (38°10'42.84"N, 20°24'2.96"E) after: (a) the 1st event and (b) the 2nd event. It appears that initiation of slope stability failure after the 1st event set the ground for failure of the paved road observed after the 2nd event. Similarly, severe damage was observed at Location B along the road connecting Chavriata and Vouni villages (38°10'39.79"N, 20°23'50.90"E), just 320 m away from Location A (Fig. 8.6.3). The severe damage at Location B could be attributed to failure or total collapse of the masonry walls on both the SE and NW sides of the embankment. The estimated height of the retaining walls ranged from 6 to 8 m. These wall failures induced failures on both sides of the road embankment. Intensive horizontal cracks along the roadway, 20 to 80 m in length, with horizontal and vertical displacements from 5 to 30 cm were observed. Interestingly, no damage was observed at an adjacent reinforced concrete retaining wall.

Figure 8.6.2. Location A (38°10'42.84"N, 20°24'2.96"E) on the road connecting the Chavriata and Vouni villages. (a) Circular type of sliding observed after the 1st event. (b) Embankment failure that affected the whole width of the road after the 2nd event.

Figure 8.6.3. Location B (38°10'39.79"N, 20°23'50.90"E) on the road connecting the Chavriata and Vouni villages. Severe road embankment damage was observed. Photos taken after the 2nd event.

The investigators noted that the road embankment bridges two opposite hills, where a mild natural slope (estimated 10° to 15°) trends towards the NW direction. The geomorphology, in

conjunction with the damage concentration at the embankments, may be indicative of topographic amplification of ground motion at the site, although more evidence is necessary to support this hypothesis.

Locations with moderate damage

We use the term "moderate" damage for road embankment performance that resulted in traffic obstruction across half or more of the road width. There were quite a few such locations on the island. Moderate damage typically involves major longitudinal cracks and large settlements on the asphalt pavement, as a result of large downslope displacements of sliding masses within the embankment material, or (for relatively high embankments) the total collapse of typically old masonry retaining walls mad of natural local limestone. These intermediate damages led local authorities to close down half the width of the road, such that the roads remained only partially open but traffic was maintained.

An example of moderate roadway embankment damage location was recorded along the main asphalt road connecting Argostoli to Lixouri, and to the NW of the village of Kardakata. Figure 8.6.4a shows the collapsed masonry wall which had supported the road embankment, as seen from the downhill side. Figure 8.6.4b shows the effects on the pavement of a similarly collapsed masonry wall for the same road embankment (just 160 m apart).

Figure 8.6.4. Off-Kardakata road embankments at an inter-distance of 160 m after 2nd event: a) masonry wall collapse in NS direction (38°17'34.61"N, 20°27'8.16"E), b) masonry wall collapse in EW direction (38°17'30.81"N, 20°27'11.80"E).

The GEER investigators noted that the former wall collapsed in an NS direction, while the latter wall collapsed in an EW direction, both following the downhill direction of the surface topography. The wall section in between the two failed walls suffered no damage, possibly due to height or construction quality differences. Figure 8.6.5 compares the state of the latter failed

masonry wall (that failed in an EW direction) after the 1st event (1-26-14) in subplot (a) and after the 2nd event (2-3-14) in subplot (b). Observe in this figure that the 2nd event increased considerably the length of the failed masonry wall at this location, and also deteriorated the state of the road embankment just uphill from the failed masonry wall section. Just 30 m up the road from the failed masonry wall section (Figs 8.6.4b and 8.6.5), the same road embankment was retained satisfactorily by reinforced concrete walls that suffered no damage and practically zero displacement (the undamaged reinforced concrete wall can be observed to the right of the failed masonry wall section in Fig. 8.6.5b).

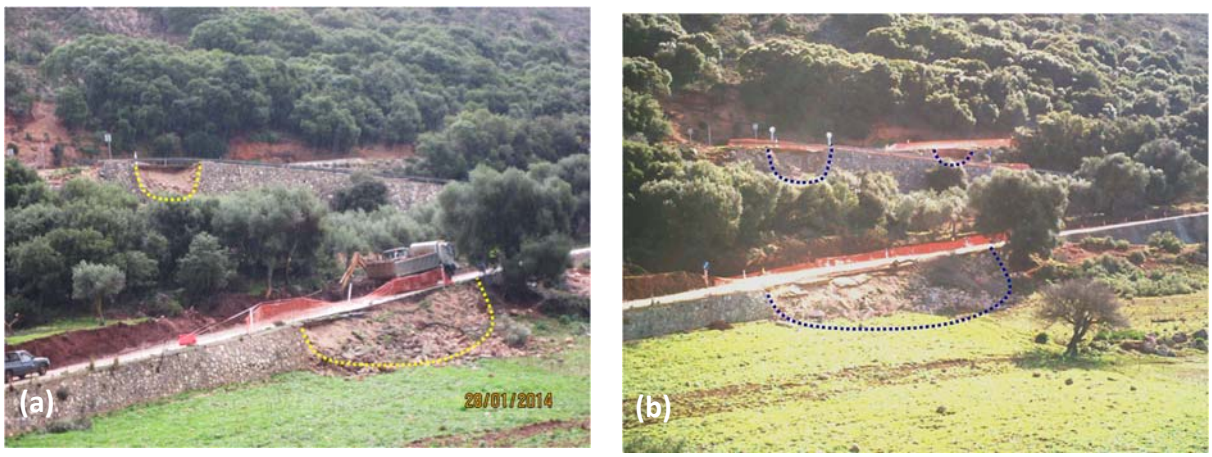

Figure 8.6.5. Overview of the broader area of the off-Kardakata road embankment failure of Figure 8.6.3b (38°17'30.81"N, 20°27'11.80"E): a) after the 1st event and, b) after the 2nd event.

Moderate damage also occurred at road embankments on the Paliki peninsula. Pertinent examples include the excessive settlements (on the order of 25 cm) in the access embankments of the (so-called) Havdata bridge, mainly due to the outward movement of the reinforced concrete wall adjoining the bridge pier (at: 38°12'10.30"N, 20°24'16.05"E, see Section 8.5). Similar damage was observed as cracks and settlements in the asphalt road (at: 38°14'17.17"N, 20°25'44.30"E) joining the Aghios Dimitrios and Livadi villages (Fig. 8.6.6). Both examples are located in areas where several reinforced concrete buildings suffered significant damage (see Section 11). Figure 8.6.6 shows the pavement cracks and the embankment settlements after the 1st (Fig. 8.6.6a) and the after the 2nd event (Fig. 8.6.6b).

Figure 8.6.6. Cracks and settlements on the road embankment between Aghios Dimitrios and Livadi villages (38°14'17.17"N, 20°25'44.30"E): (a) after the 1st (left) and (b) the 2nd (right) event.

Figure 8.6.7 presents the large downslope displacement of a circular sliding mass in clayey soil that affected a country road embankment in the vicinity (north) of Soularoi village in Paliki peninsula. The sliding occurred in an approximately NS direction, and the maximum vertical settlement of the pavement was on the order of 40 cm.

Figure 8.6.7. North of Soularoi road embankment sliding, as viewed from the pavement (38°11'21.51"N, 20°24'45.80"E).

Figure 8.6.8 presents a road embankment failure on the local road axis from Soularoi going south towards Megas Lakkos (southeastern part of Paliki peninsula) at a site called Xontiches (38°10'43.69"N, 20°25'13.87"E). This road embankment failure is the larger among others of less importance along this road. The damaged embankment is roughly 5 to 6 m tall, with slope inclination estimated at (Vertical to Horizontal) V:H = 2:3. The failure presents as longitudinal horse shoe shaped tensile crack almost 50 m long with horizontal displacements of 30 to 35 cm and vertical displacements from 40 to 50 cm near the central part (around 15 m) and significantly less movement close to the failure edges (Figure 8.6.8). Damage could be attributed to poor compaction of the embankment soil.

Figure 8.6.8. South of Soularoi road embankment failure due to slope sliding (38°10'43.69"N, 20°25'13.87"E).

Locations with minor damage

In addition to the moderately and severely damaged embankments described above, there were numerous locations where the road embankments suffered minor longitudinal cracks and small settlements of the asphalt pavement; several of these embankments were found on the Paliki peninsula in western Cephalonia and along the eastern leg of the main asphalt road connecting Argostoli to Lixouri, where the topography is steep. These cracks appear to be due to small downslope displacements of shallow surficial sliding masses within the embankment material, or the partial collapse of (typically old) masonry walls made of limestone. In many cases, the masonry walls failure left the pavement cantilevered.

Although these roads remained open to traffic, local authorities use road safety cones and “do not cross” lines to locally divert traffic. An example of typical minor road embankment

damage was observed on the eastern leg of the main asphalt road connecting Argostoli to Lixouri, just north of Katochori village (38°17'8.28"N, 20°27'8.25"E) and is presented in Figure 8.6.9. The GEER investigators observed that pavement cracks affected just the edge of the embankment material, and allowed traffic in almost the full width of the road.

Figure 8.6.9. Pavement cracks and settlement at the edge of the road embankment located at 38°17'8.28"N, 20°27'8.25"E close to Katochori village. Photo was taken after the 1st event.

A typical example of minor damage involving a masonry wall was observed on the eastern leg of the main asphalt road connecting Argostoli to Lixouri at the village of Kourouklata in the north of the island (Fig. 8.6.10). In particular, Fig. 8.6.10a shows the collapsed masonry wall in the foreground, while it also shows in the background, another similar (partial) collapse at a higher altitude on the same winding road, whose detail is presented in Fig. 8.6.10b. Both of the two collapses occurred along the NS direction (moving downslope towards the south), and neighboring locations showed no damage, possibly due to height or construction quality differences. Similar minor damage was observed in this area (e.g., at 38°14'26.29"N, 20°28'35.14"E), where this type of road embankment construction is common.

Minor damage was observed in the mountainous unpaved road from Kourouklata to Kontogourata, just uphill from the asphalt road joining Argostoli to Lixouri, between 38°14'19.81"N, 20°28'7.77"E and 38°14'48.76"N, 20°27'54.79"E in a direction almost parallel

to NS axis. At this location, intense longitudinal cracks with mean width 2 to 3 cm were observed along the western edge of the unpaved (dirt) road. The entire cross section of the unpaved road is on a cut and the depth of the displaced material at the edge of the road was very shallow. Similar minor damage to road embankments was observed on the road connecting Lixouri to Havdata, at 38°12'21.05"N, 20°24'54.89"E). In addition, a considerable number of minor to intermediate road embankment damage was observed on the local road from Mantzavinata village to Xi beach, in the south part of the Paliki peninsula.

Figure 8.6.10. Kourouklata road embankments: a) lower altitude masonry wall collapse (38°14'23.77"N, 20°28'30.29"E), b) higher altitude masonry wall collapse (38°14'28.20"N, 20°28'24.87"E) (also visible in a, is the failed bell tower of Kourouklata.)

Few road embankments supported by reinforced concrete retaining walls experienced minor damage. Damages consist of longitudinal cracks and settlements (on the order of a few cm, at most) near the displaced wall. Similar relatively good and easily repairable road embankment behavior was observed on the Chavriata main road (38°10'57.84"N, 20°23'2.64"E, but also 38°10'57.52"N, 20°23'13.61"E), and the Kourouklata church plaza, at least at the locations where the wall was not of masonry-type (38°14'31.72"N, 20°28'25.40"E).

Other (non-roadway) types of embankments did not suffer damage. Among those, the short embankments retaining the reservoirs at Aghia Eirini in eastern Cephalonia (38°07'58.44"N, 20°45'20.13"E) suffered no damage mainly due to their large distance from the epicenter.

LANDFILLS

Two landfills, located next to each other as shown on Fig. 8.6.11, were investigated as part of the reconnaissance studies. The old unlined landfill (38°18'35.26"N, 20°26'24.86"E) is now closed. The new lined landfill (38°18'34.82"N, 20°26'35.17"E) is currently receiving Municipal Solid Waste generated in the islands of Cephalonia and Ithaki.

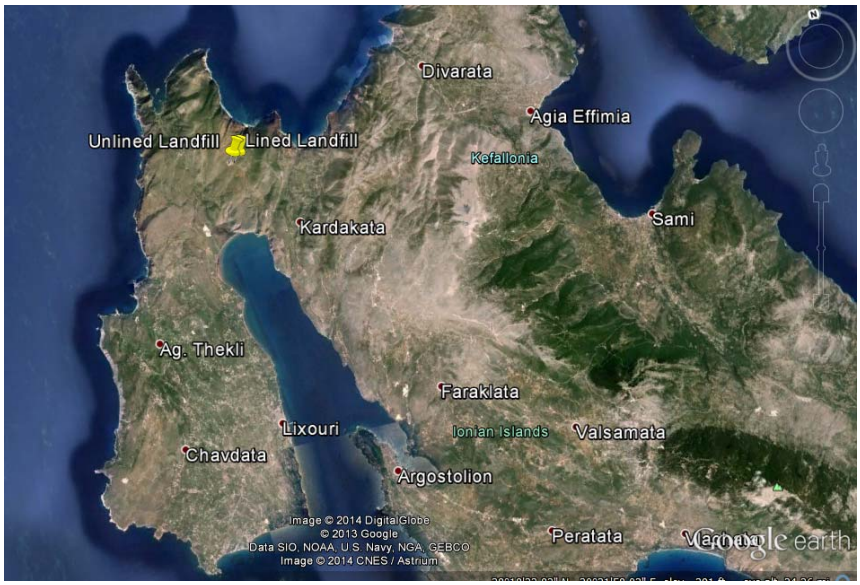

Figure 8.6.11. The location of the two adjacent Cephalonia landfills (38°10'57.52"N, 20°23'13.61"E).

The old landfill was in operation from 1981 until approximately 2004 when disposal operations switched to the new, lined landfill. Although the containment system details of the new landfill are not known, it appears to be a composite system of a compacted clay liner and a geomembrane liner overlain by a gravel layer used as leachate collection and removal system.

Fig. 8.6.12a presents the presently well vegetated old landfill and Fig. 8.6.12b shows the new landfill. According to the landfill operator and an on-site GEER visit on 2/10/14, the landfills performed well with no cracking, displacements or any other damage observed following the earthquakes. However, the investigators note that the height of the lined landfill was on the order of 10 m (30 ft), which, compared to typical modern landfills of height 60 m (200 ft) or more, is relatively short and thus likely to be resilient against slope stability failures.

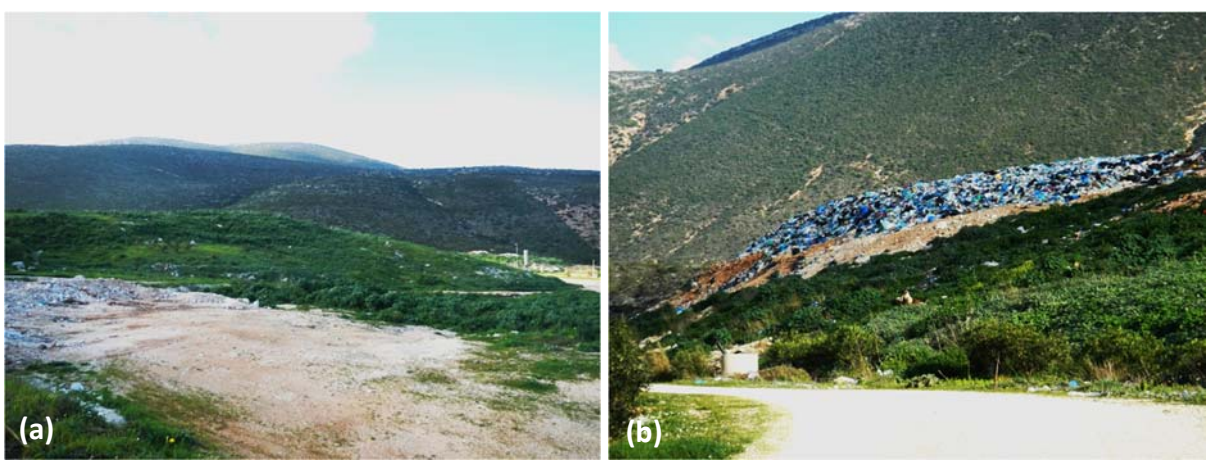

Figure 8.6.12. View of the (a) unlined landfill (vegetated, in the background; 38°18'33.15"N, 20°26'30.44"E) and (b) lined landfill (38°18'36.94"N, 20°26'29.02"E).

8.7 Settlement and Soil-Structure Interaction

INTRODUCTION

Dynamic Soil-Structure Interaction (SSI) phenomena are difficult to identify in post-earthquake investigations, since the associated kinematic and inertial effects that develop in the foundation and the superstructure are inherent in the structural response and cannot be separated from the observed residual deformations without performing detailed analyses. In presence of soil liquefaction (often manifested at the soil surface) and other soil softening phenomena, significant SSI effects can develop due to compliance of the liquefied/softened material. The results presented in this section summarize observations from 10 structures documented by AUTH, UPATRAS, UTH and MRCE reconnaissance teams regarding performance of structures with reference to settlements and SSI effects. The data were gathered from two investigations during the periods 8-10 and 18-19 of February 2014. Additional detailed documented cases of structural damage are presented in the Chapter 11.

Figure 8.7.1. Locations of the 10 structures inspected during reconnaissance for SSI and settlement effects. Additional cases documenting structural damage are presented in the Chapter 11.

A number of structures in the meioseismal area, especially in Lixouri, experienced vertical and horizontal permanent displacements. Most of the damage was concentrated near the coastline, directly inland from the port of Lixouri, built on reclaimed land generated by demolition material from the 1953 earthquake that spread laterally. Horizontal displacements were recorded with emphasis on the first row of buildings adjacent and parallel to the port. In many cases, it appears that the ground surrounding the structure has moved, while the structure has remained in place, especially for pile-supported structures.

In general, structures in this area rocked, punched through, tilted, settled and displaced. Relative permanent displacements between structures and the surrounding ground were less than 3 cm. Lack of sand boil observation and displacement patterns suggest that liquefaction did not occur and the structures in the first row of buildings next to the port may have been affected by lateral spreading or differential displacement of the uncontrolled fill that reclaimed the sea. The significant rainfall in the days preceding the reconnaissance may have erased evidence that could shed some light in this aspect. Locals refer to “clayey soils” beneath the structures that may indicate phenomena of cyclic softening due to seismic excitation. In some other cases, dynamic densification seems to be the reason for ground failure. At the moment, there is no definite conclusion for the reason behind ground failure at the port of Lixouri. Indicative examples of permanent displacement are presented in this section.

CASE 1: 3-STORY STRUCTURE AT CORNER OF NESTOROS & MEGALOU ALEXANDROU STREETS (38°11'45.50''N, 20°26'18.84''E)

The pavement surrounding the 3-story residential structure at the corner of Nestoros & Megalou Alexandrou Streets (GPS Coordinates 38°11'45.50"N, 20°26'18.84"E), as well as the structure’s porch appear to have settled without causing damage to the remaining structure (Fig. 8.7.1). Measured settlements were 11 cm on the SE corner, 1 cm in the southwest corner, and 8.5 cm in the NW corner of the porch.

CASE 2: 2-STORY STRUCTURE AT THE CORNER OF MARATHONOS & DIGENI LASKARATOU STREETS (38°12'7.47''N, 20°26'12.99''E)

The 2-story residential building (Fig. 8.7.2) at the corner of Marathonos and Digeni Laskaratou Streets (GPS Coordinates 38°12'7.47"N, 20°26'12.99"E) had no obvious signs of cracking due to differential settlements. The reconnaissance teams consider this to be a typical case of buildings with no obvious settlement-related structural damage.

Figure 8.7.2. Case 1: 3-story structure at the corner of Nestoros and Megalou Alexandrou Streets (GPS Coordinates 38°11’45.50”N, 20°26’18.84”E, 2/18/2014).

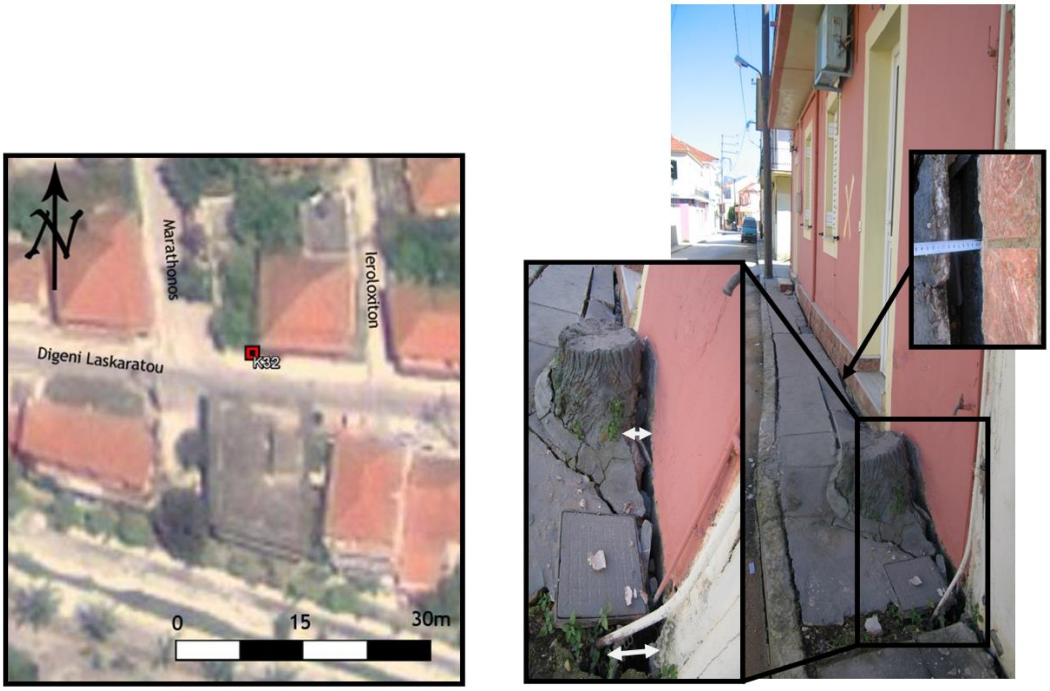

Figure 8.7.3. Typical 2-story building with no damages due to settlements. The pavement suffered significant displacements (GPS Coordinates: 38°12’7.47”N, 20°26’12.99”E, 2/18/14).

However, in the particular structure of Fig. 8.7.2, the pavements in the perimeter subsided, most likely due to lack of compaction or uncontrolled nature of the subsurface material, as this area is built on reclaimed land generated by debris of the 1953 earthquake. The unusually shaped pipes deformation and the position of the tree trunk indicate deformations of the pavement, rather than of the building itself. Horizontal and vertical displacements of about 7 cm were measured. No liquefaction ejecta were observed in the perimeter of the building.

CASE 3: PIRAEUS BANK, LIXOURI BRANCH (38°12'7.65''N, 20°26'19.70'E)

The 2-story structure (GPS Coordinated 38°12’7.65”N, 20°26’19.70”E) is supported by a grid of 20 steel piles, 1 m in diameter and 15 m in length. The structure appears to have stayed in place without any displacement at two of the corners. Measured settlements reached 2.4 cm at the entrance of the building, and 4.2 cm settlement at one corner (Fig. 8.7.4). Although it seems that the ground has settled, the structure remained in place. Observations of non-structural components damage in several bank structures are presented in the Chapter 11.

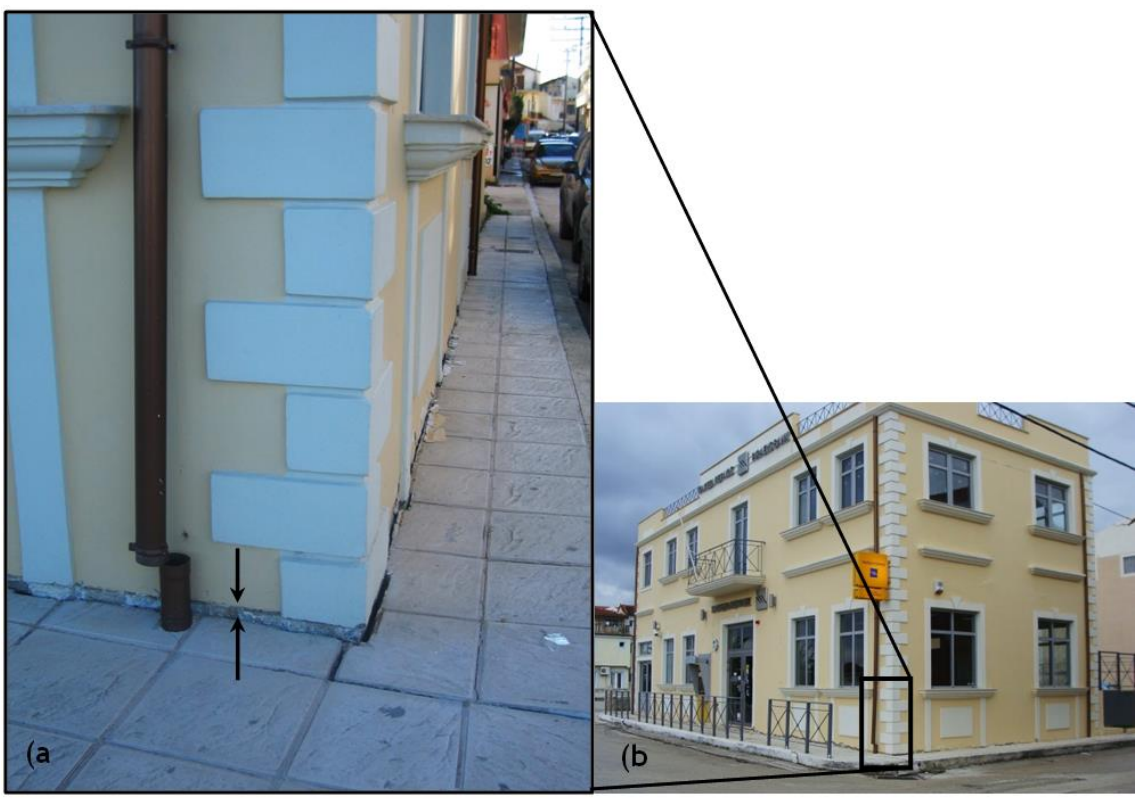

Figure 8.7.4. Case 3: Lixouri Branch of Piraeus Bank (38°12’7.65”N, 20°26’19.70”E, 2/18/14).

CASE 4: ST. NICHOLAS CHURCH BELL TOWER (38°12'9.43''N, 20°26'17.63''E)

The bell tower of St. Nicholas church (GPS coordinates 38°12’9.43”N, 20°26’17.63”E; see Fig. 8.7.5) appears to have suffered differential settlement. Settlement at the west side and uplift at the east side of the building resulted in the tower tilting toward the church (Figs. 8.7.6b,c).

It can also be seen that the bell tower has leaned against the church structure adjacent to it (Fig. 8.7.6c, insert), damaging the church roof. Settlements of 2 cm were measured at the SE and NE corner. No settlements were observed at the perimeter of the church.

Figure 8.7.5. Case 4: St. Nicholas Church Bell tower location (GPS coordinates 38°12'9.43"N, 20°26'17.63"E, 2/18/2014).

Figure 8.7.6. Case 4: St. Nicholas Church Bell Tower differential settlement (38°12'9.43"N, 20°26'17.63"E, 2/18/14).

CASE 5: POWER TRANSFORMER PILLAR (38°11'55.63"N, 20°26'20.56"E)

A power transformer pillar in Lixouri (38°11'55.63"N, 20°26'20.56"E) suffered differential settlement. One of the support columns appeared to have punched in the ground for 1.7 cm, while the other one remained in place. This behavior could be attributed to structural response influenced by SSI, with verification by site specific studies.

Figure 8.7.7. Case 5: Power transformer pillar differential settlement (38°11'55.63"N, 20°26'20.56"E, 2/19/14).

CASE 6: CAFÉ "AEN PLO" (GPS COORDINATES: 38°12'3.52"N, 20°26'20.00"E)

Café "Aen Plo" is located in the first row of residential buildings in Lixouri (GPS Coordinate: 38°12'3.52"N, 20°26'20.00"E), approximately 45 m from the quay walls (Fig. 8.7.8). It is founded on steel piles (Fig. 8.7.8.). It appears that the structure suffered minor damage, although a detailed structural assessment has not been performed.

Figure 8.7.8. Case 6: Café "Aen Plo" location and street view (38°12'3.52"N, 20°26'20" E, 2/19/14).

Figure 8.7.9. NE corner of Café "Aen Plo" NE corner ground failure (2/19/14).

In the NE corner of the structure, 3.8 cm of vertical and 1.9 cm of horizontal displacements were measured (Fig. 8.7.9). It appears that the structure remained in place, but the ground moved towards the seafront as the result of liquefaction. The owner confirmed that no sand boils were observed during or after the earthquakes near the structure and on the road in front of it.

However, the settlements at Café "Aen Plo" could be attributed to liquefaction occurring deep below the ground surface, which did not lead to bearing capacity failure or excessive settlements due to the existence of a "protective cap" of unsaturated fill on top of the liquefied ground at some depth. This layer of non-liquefiable material may exist due the topography of the area, which has a mild inclination towards the sea, thus incurring a deepening of the ground water level with distance from shore.

The difference in ground elevation from the shore is approximately 2 m at a distance of 100 m and 4 m at a distance of 170 m, where pavement cracks essentially diminish. If the topographic difference is correlated to a similar deepening of the ground water table, this condition would allow for sufficient thickness of the protective zone to prevent bearing capacity failure and excessive settlement (Karamitros et al., 2013). This "deep" liquefaction could also explain the relatively mild structural damage to the Lixouri buildings, since it could essentially act as a natural base isolator for the buildings. Although this is a credible explanation in the framework of a geotechnical reconnaissance effort, site-specific geotechnical investigations and analyses using the recorded ground motions of both main events and their aftershocks are required to substantiate this possibility.

CASE 7: 2-STORY R/C BUILDING (38°11'36.08"N, 20°26'19.90"E)

Another case of free-field soil settlement was observed at the location of a 2-story Reinforced Concrete (R/C) building located near the shore south of Lixouri (GPS coordinates 38°11'36.08"N, 20°26'19.90"E).

Although it cannot be totally ruled out, the investigators did not identify settlement of the building itself or evidence of liquefaction. The building itself had no apparent structural damage and suffered non-structural damage such as collapse of its chimneys and roof tiles.

As shown on Fig. 8.7.10, the soil around the building settled uniformly by about 3 cm. As a result, the (uncracked) mortar of the building was dislocated from the paved ground.

Drainage pipes (were also dislocated from their collective pool as the result of surrounding ground settlement. The observations could be attributed to cyclic softening and subsequent settlement of the unsaturated fill set around the building.

Figure 8.7.10. Case 7. Ground settlement in the perimeter of 2-story R/C building south of Lixouri. Location at the top part of this figure (GPS Coordinates 38°11'36.08"N, 20°26'19.90"E, 2/19/14).

CASE 8: MONASTERY OF VIRGIN KECHRIONOS (38°13'26.19''N, 20°25'43.36''E)

The 200-year old Monastery of Kechrionos located 2.5 km north of Lixouri, 900m from the sea shore, on the road between Aghios Dimitrios and Loukerata (38°13’26.19”N, 20°25’43.36”E) suffered significant structural damage. It is said that the Monastery was established by three former prisoners kept in Algeria who, after praying to Virgin Mary for release on the night of August 23 of 1694, they woke up next day on the site. The main building was constructed in 1826 and suffered damaged during the earthquake of 1867 and almost collapsed during the 1953 earthquake.

An interesting observation illustrated in Figures 8.7.11 – 8.7.14 is the structural and non-structural failure that occurred primarily along the E-W direction (i.e., in-plane shear cracks of the front garden gate, fall of non-structural elements and evident rotation of the main gate lights). While the NS and EW components of the earthquake motions contained potential directivity effects (see insert of Fig. 8.7.12 from the 2nd event), within the assumed structural period of interest between 0.1 and 0.3 seconds, the spectral accelerations did not vary significantly. This would make the Kechrionos Monastery an interesting future case study to study potential site effects, directivity and, possibly, SSI.

Note that additional detailed structural observations on the churches of Cephalonia are presented in the Chapter 11.

Figure 8.7.11. Case 8: Kechrionos Monastery. Shear failure on external gate (left) and rotation of exterior lights (right), both along the EW direction (38°13'26.19"N, 20°25'43.36"E, 2/8/14).

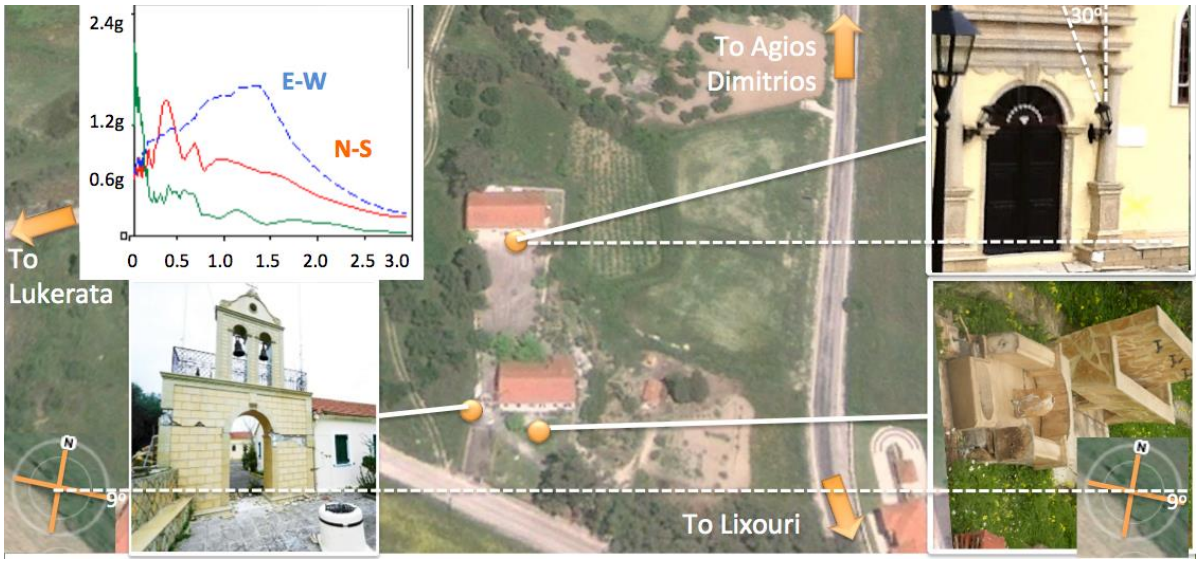

Figure 8.7.12. Orientation of structural and nonstructural damage relative to the EW direction. (38°13'26.19"N, 20°25'43.36"E, 2/8/14). Insert: the 3 components of spectral accelerations in the 2nd event.

Figure 8.7.13. Comparison of the external and main gate of the Kechrionos Monastery prior (left) and after the 2014 earthquakes (right).

Figure 8.7.14. Case 8: Kechrionos Monastery. Out-of-plane collapse of non-structural elements (left). Close view of the main gate pillar dislocation together with diagonal cracks of the external masonry.

CASE 9: NATIONAL BANK, LIXOURI BRANCH (38°12'7.8"N, 20°26'19.8"E)

The Lixouri branch of the National Bank of Greece (Fig. 8.7.15), is located in the front row of buildings parallel to the port shoreline (GPS Coordinates: 38°12'7.8"N, 20°26'19.8"E) and is adjacent to Case 3 (Piraeus Bank branch). The building experienced significant structural and non-structural damage that resulted in closing this branch. Details on these types of damage is presented in the Chapter 11.

Figure 8.7.15. Case 9: National Bank of Greece, Lixouri Branch located in the front row of buildings parallel to the shoreline (GPS Coordinates: 38°12'7.8"N, 20°26'19.8"E).

Significant ground deformations were observed towards the inland EW direction due to potential liquefaction or ground deformations of the uncontrolled fill below the pavements, most evident at the SE corner of the bank (Fig. 8.7.16a). The reconnaissance teams observed lateral and vertical deformations between the base of the structure and the sidewalk. The maximum vertical settlements (or dislocation between the base of the structure and the sidewalk) was about 4 cm (Fig. 8.7.16b), while the lateral deformations between the base and sidewalk or sidewalk and road pavement were generally 1 cm or less. A summary of the vertical deformations between the base of the building and its connection to the sidewalk along the façade of the bank is shown on Fig. 8.7.17.

Figure 8.7.16. Case 9: Observations of deformations of the: (a) ground; (b) sidewalk connection to base of building; and (c) cabinets of interior EW wall. (GPS: 38°12'7.8"N, 20°26'19.8"E, 2/9/14).

Figure 8.7.17 Case 9: Summary of vertical (exaggerated) deformations between base of building and its connection to the sidewalk along the façade of the bank. (GPS: 38°12'7.8"N, 20°26'19.8"E, 2/9/14).

CASE 10. SERIES OF STRUCTURES DESIGNED PER GREEK CODE (EAK2000)

Building damage is systematically presented in the Chapter 11 as a function of the seismic code that it was designed for. In this section, we bring the attention to a series of newly constructed structures that may be worth investigating with reference to their SSI effects, shown on Figs. 8.7.18 and 8.7.19. They are 3-story Reinforced Concrete (R/C) buildings, designed in accordance with the latest Greek Seismic Code (EAK2000).

Figure 8.7.18. Case 10. Locations of the 3-story structures designed with the latest seismic code EAK2000. (GPS coordinates 38°13'48.19"N, 20°25'53.20"E, 2/9/14).

The design base shear of these buildings was approximately equal to $V_{sd} = (a_g \times 2.5/q) \times W = 0.36g \times 2.5 \times W / 3.5 \approx 0.25\,g\,W$ (where a_g is the seismic coefficient and q is the force reduction factor as per EAK2000). The recorded spectral acceleration at the fundamental period of the structures (estimated around 0.25 sec) was about 0.7 g (for 5% damping), which generated a base shear that exceeded the design value by almost 3 times.

It appears that the lateral load resisting systems of these structures responded elastically during both the 1st and 2nd main events. Although in some cases extensive damage of the infill masonry was observed, the load bearing system remained intact. The impressive lack of damage may be attributed to different factors that either increase the available strength of the buildings (such as inherent over-strength due to the use of minimum, code-prescribed reinforcement and minimum dimensions, statistical over-strength of materials, and the beneficial, seismic energy absorbing role of the masonry walls), and/or to factors that have possibly reduced the imposed base acceleration due to site effects or SSI phenomena. The high demand-to-nominal capacity ratio, small distance from the shore (less than 500 m) and the presence of settlements in nearby structures makes these desirable case studies.

Figure 8.7.19. Cases of buildings designed to EAK2000 experienced no damage to their load bearing system due to multiple sources of over-strength. Possible beneficial effects of SSI could have played a factor and should be studied further (38°13'48.19"N, 20°25'53.20"E, 2/9/14).